



1 Secondary Organic Aerosol Production from Local Emissions Dominates the 2 Organic Aerosol Budget over Seoul, South Korea, during KORUS-AQ

3 Benjamin A. Nault^{1,2}, Pedro Campuzano-Jost^{1,2}, Douglas A. Day^{1,2}, Jason C. Schroder^{1,2}, Bruce
4 Anderson³, Andreas J. Beyersdorf^{3,*}, Donald R. Blake⁴, William H. Brune⁵, , Yonghoon Choi^{3,6},
5 Chelsea A. Corr^{3,**}, Joost A. de Gouw^{1,2}, Jack Dibb⁷, Joshua P. DiGangi³, Glenn S. Diskin³, Alan
6 Fried⁸, L. Gregory Huey⁹, Michelle J. Kim¹⁰, Christoph J. Knote¹¹, Kara D. Lamb^{2,12}, Taehyoung
7 Lee¹³, Taehyun Park¹³, Sally E. Pusede¹⁴, Eric Scheuer⁷, Kenneth L. Thornhill^{3,6}, Jung-Hun
8 Woo¹⁵, and Jose L. Jimenez^{1,2}

9 10 *Affiliations*

11 1. Department of Chemistry, University of Colorado, Boulder, CO, USA

12 2. Cooperative Institute for Research in Environmental Sciences, University of Colorado, Boulder, CO,
13 USA

14 3. NASA Langley Research Center, Hampton, Virginia, USA

15 4. Department of Chemistry, University of California, Irvine, Irvine, CA, USA

16 5. Department of Meteorology and Atmospheric Science, Pennsylvania State University, University Park,
17 Pennsylvania, USA

18 6. Science Systems and Applications, Inc., Hampton, Virginia, USA

19 7. Earth Systems Research Center, Institute for the Study of Earth, Oceans, and Space, University of New
20 Hampshire, Durham, New Hampshire, USA

21 8. Institute of Arctic and Alpine Research, University of Colorado, Boulder, CO, USA

22 9. School of Earth and Atmospheric Sciences, Georgia Institute of Technology, Atlanta, Georgia, USA

23 10. Division of Geological and Planetary Sciences, California Institute of Technology, Pasadena, CA, USA

24 11. Meteorologisches Institut, Ludwig-Maximilians-Universität München, München, Germany

25 12. Chemical Sciences Division, Earth System Research Laboratory, National Oceanic and Atmospheric
26 Administration, Boulder, CO, USA

27 13. Department of Environmental Science, Hankuk University of Foreign Studies, Republic of Korea

28 14. Department of Environmental Sciences, University of Virginia, Charlottesville, VA, USA

29 15. Department of Advanced Technology Fusion, Konkuk University, Seoul, Republic of Korea

30 * Now at: Department of Chemistry and Biochemistry, California State University, San Bernardino,
31 California

32 ** Now at: USDA UV-B Monitoring and Research Program, Natural Resource Ecology
33 Laboratory, Colorado State University, Fort Collins, CO, USA

34

35 *Correspondence to:* J. L. Jimenez (jose.jimenez@colorado.edu)

36

37 **Abstract**

38 Organic aerosol (OA) is an important fraction of submicron aerosols. However, it is challenging
39 to predict and attribute the specific organic compounds and sources that lead to observed OA
40 loadings, largely due to contributions from secondary production. This is especially true for
41 megacities surrounded by numerous regional sources that create an OA background. Here, we
42 utilize *in-situ* gas and aerosol observations collected on-board the NASA DC-8 during the
43 NASA/NIER KORUS-AQ (KORea United States-Air Quality) campaign to investigate the
44 sources and hydrocarbon precursors that led to the secondary OA (SOA) production observed over
45 Seoul. First, we investigate the contribution of transported OA to total loadings observed over
46 Seoul, by using observations over the West Sea coupled to FLEXPART Lagrangian simulations.
47 During KORUS-AQ, the average OA loading advected into Seoul was $\sim 1 - 3 \mu\text{g sm}^{-3}$. Second,
48 taking this background into account, the dilution-corrected SOA concentration observed over
49 Seoul was $\sim 140 \mu\text{g sm}^{-3} \text{ppmv}^{-1}$ at 0.5 equivalent photochemical days. This value is at the high
50 end of what has been observed in other megacities around the world ($20-70 \mu\text{g sm}^{-3} \text{ppmv}^{-1}$ at 0.5
51 equivalent days). For the average OA concentration observed over Seoul ($13 \mu\text{g sm}^{-3}$), it is clear
52 that production of SOA from locally emitted precursors is the major source in the region. The
53 importance of local SOA production was supported by the following observations: (1)
54 FLEXPART source contribution calculations indicate any hydrocarbons with a lifetime less than
55 1 day, which are shown to dominate the observed SOA production, mainly originate from South
56 Korea. (2) SOA correlated strongly with other secondary photochemical species, including short-
57 lived species (formaldehyde, peroxy acetyl nitrate, sum of acyl peroxy nitrates, dihydroxy toluene,
58 and nitrate aerosol). (3) Results from an airborne oxidation flow reactor (OFR), flown for the first
59 time, show a factor of 4.5 increase in potential SOA concentrations over Seoul versus over the
60 West Sea, a region where background air masses that are advected into Seoul can be measured. (4)
61 Box model simulations reproduce SOA observed over Seoul within 15% on average, and suggest
62 that short-lived hydrocarbons (i.e., xylenes, trimethylbenzenes, semi- and intermediate volatility
63 compounds) were the main SOA precursors over Seoul. Toluene, alone, contributes 9% of the
64 modeled SOA over Seoul. Finally, along with these results, we use the metric $\Delta\text{OA}/\Delta\text{CO}_2$ to
65 examine the amount of OA produced per fuel consumed in a megacity, which shows less variability
66 across the world than $\Delta\text{OA}/\Delta\text{CO}$.



67 1. Introduction

68 Prior to 1950, 30% of the human population resided in urban areas (UNDESA, 2015). In
69 2007, the human population living in urban areas had increased to over 50% (making it the first
70 time in human history that more people reside in urban than rural areas), and it is predicted that
71 nearly 2/3 of the human population will be living in urban areas by 2050 (Monks et al., 2009;
72 UNDESA, 2015; Baklanov et al., 2016). Urban areas are large sources of anthropogenic emissions
73 to the atmosphere (from sources including transportation, industry, cooking, personal care
74 products, and power produced from fossil fuels), and these emissions have important impacts on
75 local, regional, and global air pollution, climate, and human and ecological health (Hallquist et al.,
76 2009; Monks et al., 2009; Myhre et al., 2013; Baklanov et al., 2016; WHO, 2016; Cohen et al.,
77 2017; Landrigan et al., 2018; McDonald et al., 2018). Effects from urban emissions are strongly
78 modulated by the chemical evolution of the primary emissions (e.g., nitrogen oxides,
79 hydrocarbons, and primary organic aerosols) to secondary pollutants, including secondary organic
80 aerosols (SOA, produced from atmospheric reactions) and other aerosol (Monks et al., 2009).
81 These emissions and their chemical by-products significantly influence hemispheric climate and
82 air quality. They increase mortality in polluted urban areas, leading to over 3 million premature
83 deaths annually (Lelieveld et al., 2015; Baklanov et al., 2016; WHO, 2016). Finally, the emissions
84 and production of anthropogenic aerosol may strongly regulate cloud nucleation (Peng et al.,
85 2014), which impacts the aerosols' direct and indirect effects on climate (Myhre et al., 2013).

86 Production of SOA is poorly understood (Hallquist et al., 2009; Shrivastava et al., 2017;
87 Tsimpidi et al., 2017), including in large urban environments (Volkamer et al., 2006; de Gouw et
88 al., 2008, 2009; Hayes et al., 2015; Woody et al., 2016; Janssen et al., 2017; Ma et al., 2017). It
89 has been shown that a large fraction (35 – 85%) of urban fine aerosol is composed of OA (Zhang



90 et al., 2007; Jimenez et al., 2009), and a substantial fraction of this OA is typically SOA produced
91 through the chemical processing of urban hydrocarbon emissions (Kleinman et al., 2007, 2008;
92 Dzepina et al., 2009; Kleinman et al., 2009; DeCarlo et al., 2010; Hodzic et al., 2010; Dzepina et
93 al., 2011; Hersey et al., 2013; Freney et al., 2014; Zhao et al., 2014; Hayes et al., 2015; Kleinman
94 et al., 2016; Zhao et al., 2016; Ma et al., 2017). Also, observations indicate the majority of urban
95 SOA production is rapid and is nearly completed within 24 equivalent photochemical hours (a
96 measure of OH exposure, assuming interactions in a volume with 1.5×10^6 molecules/cm³ OH
97 throughout a 24 h period; equivalent age enables comparison of chemistry rates across different
98 events or studies) (DeCarlo et al., 2010; Hayes et al., 2013; Freney et al., 2014; Hu et al., 2016;
99 Ortega et al., 2016; Ma et al., 2017), even during winter (Schroder et al., 2018). This consistently
100 rapid SOA production over urban areas around the world may be due to the short lifetime (less
101 than one day) of urban semi- and intermediate-volatile organic compounds (S/IVOCs), that
102 numerous studies suggest to be a major SOA precursors, along with aromatics (Robinson et al.,
103 2007; Zhao et al., 2014, 2016; Hayes et al., 2015; Ma et al., 2017; McDonald et al., 2018). S/IVOCs
104 and low volatility organic compounds (LVOCs—compounds produced from the photooxidation
105 of hydrocarbons (Robinson et al., 2007; Kroll and Seinfeld, 2008; Murphy et al., 2011; Palm et
106 al., 2016)) are challenging to measure due to strong interaction with inlet and instrument surfaces
107 (e.g., Pagonis et al., 2017), limiting our knowledge of the emission rates and concentrations of
108 these species in the atmosphere (Zhao et al., 2014; Hunter et al., 2017). It has also been recently
109 shown that historical chamber SOA yields are biased low due to unaccounted-for partitioning of
110 S/IVOCs to walls (Matsunaga and Ziemann, 2010; Zhang et al., 2014; Krechmer et al., 2016,
111 2017). These missing or under-represented compounds and low-biased yields, along with uncertain
112 emission inventories for SOA precursors (Shrivastava et al., 2008; Woody et al., 2016; Murphy et



113 al., 2017), led SOA modeling efforts over urban areas using pre-2007 models to under-predict
114 observed SOA concentrations (de Gouw et al., 2005, 2009; Volkamer et al., 2006; Dzepina et al.,
115 2009; Freney et al., 2014; Woody et al., 2016). More recent modeling efforts have achieved closure
116 (and sometimes over-prediction) of the observed SOA, but with some controversy about the real
117 causes of the increased modeled SOA (Dzepina et al., 2009; Hodzic et al., 2010; Tsimpidi et al.,
118 2010; Hayes et al., 2015; Cappa et al., 2016; Ma et al., 2017; McDonald et al., 2018).

119 Another complexity in understanding SOA production over urban areas is addressing the
120 contributions of transport of SOA and its gas-phase precursors. Airborne observations of SOA and
121 SOA precursors upwind, over, and downwind of megacities around the world (Kleinman et al.,
122 2007, 2008, 2009, 2016, DeCarlo et al., 2008, 2010; Bahreini et al., 2009; McMeeking et al., 2012;
123 Craven et al., 2013; Freney et al., 2014; Schroder et al., 2018) have constrained the role of regional
124 transport versus megacity emissions. In general, these studies show that there is often regional
125 background SOA, often due to biogenic compounds and regional pollution, transported into
126 megacities, but that rapid SOA production is always observed and is generally dominated by the
127 anthropogenic emissions from the urban area being studied.

128 The Seoul Metropolitan Area (SMA), as considered here, is a densely populated megacity,
129 extending beyond Seoul proper into the large Incheon and Gyeonggi cities. SMA has ~24 million
130 people, or ~50% of the South Korean population, living on ~12,000 km² of land (Park et al., 2017).
131 SMA has large anthropogenic emissions but is also often downwind of China, presenting the
132 challenge of separating local emissions and production of SOA versus transport of SOA and its
133 precursors from regions upwind (H. S. Kim et al., 2007; Heo et al., 2009; Kim et al., 2009, 2016,
134 2018; H. C. Kim et al., 2017; H. Kim et al., 2017; Jeong et al., 2017; Lee et al., 2017; Seo et al.,
135 2017). Most of the studies in this region have used ground-based observations and/or 3D models



136 to characterize the amount of aerosol, and aerosol precursors, transported to SMA and South
137 Korea, finding 50 to 80% of the aerosol load due to international transport in the seasons with
138 favorable synoptic conditions (winter and spring). Though satellites are starting to be used to
139 investigate transport of aerosols into SMA and South Korea (Lee et al., 2013; Park et al., 2014;
140 Jeong et al., 2017), retrievals typically do not provide any chemical characterization or vertical
141 location of the aerosol (boundary layer versus free troposphere), and are typically strongly
142 influenced by larger aerosols (e.g., mineral dust). Airborne observations of the upwind transport
143 and local production of aerosol and aerosol precursors have the potential to directly assess the
144 impact of transport versus local emissions in this region.

145 In this study, we use observations collected on board the NASA DC-8 research aircraft
146 during the NASA/NIER (South Korean National Institute of Environmental Research) KOREan
147 United States Air Quality (KORUS-AQ) field campaign. These data provided the opportunity to
148 investigate SOA production; as well as, the role of OA and SOA precursor transport on the OA
149 concentration and SOA production over Seoul during the campaign. We evaluate the observed
150 SOA production over the SMA with source analysis models, correlation of secondary gas-phase
151 species with SOA, an oxidation flow reactor, and box modeling to constrain local versus transport
152 contributions. These results are discussed and placed into context of improving our knowledge
153 about SOA production and sources in urban environments.

154 **2. Methods**

155 Here, we introduce the KORUS-AQ campaign (Sect. 2.1), the key instrument for this study
156 (2.2), additional measurements used in the analyses (2.3), and the airborne oxidation flow reactor
157 (2.4). All linear fits, unless otherwise noted, use the least orthogonal distance regression fitting
158 method (ODR).



159 **2.1 KORUS-AQ brief overview**

160 KORUS-AQ was conducted over South Korea and the West Sea during May – June, 2016.
161 This study focuses on the NASA DC-8 (Aknan and Chen, 2018) observations; however, there were
162 numerous other measurement platforms in operation (Al-Saadi et al., 2015). The DC-8 was
163 stationed in the Songtan area of Pyeongtaek, South Korea, approximately 60 km south of Seoul.
164 The DC-8 flew 20 research flights (RF) (Figure 1; Table S1). For each RF, the DC-8 would take-
165 off from near Seoul, typically at 8:00 local time (LT), which is Korean Standard Time, and perform
166 a missed approach over Seoul Air Base, which is less than 15 km from the Seoul city center. This
167 pattern was typically conducted 2 more times during each flight, around 12:00 LT and prior to
168 landing (~15:00 LT), leading to 55 missed approaches over Seoul during the campaign. Each
169 missed approach involved flying near Seoul below 1000 m (above ground) for 15 – 45 minutes,
170 providing a large number of observations of the Seoul boundary layer. The observations collected
171 during this pattern, along with any other flights conducted within the coordinates defined as Seoul
172 (Table S2, Fig. S1) are referred to as “Seoul” below.

173 Briefly, the SMA is bordered by the West Sea (i.e., the Yellow Sea) and Gyeonggi Bay to
174 the west and forests and mountainous regions to the north, south, and east (Park et al., 2017).
175 Within this region, nearly 30% of the land is used for human activities, ~21% is used for cropland,
176 pasture, and grassland, and ~36% is forested (Park et al., 2017). During the time period of KORUS-
177 AQ, the wind is typically from the west to northwest, meaning that observations over the West Sea
178 represent typical background (inflow) air mass observations for Seoul (H. C. Kim et al., 2017).
179 May and June are typically characterized by low precipitation and rising temperatures prior to the
180 summer monsoon (Hong and Hong, 2016; H. C. Kim et al., 2017).



181 Besides the Seoul missed approaches, the DC-8 would fly either over the West Sea, the
182 Jeju jetway, or the Busan jetway at four different altitudes (nominally ~300 m, ~1000 m, ~1500
183 m, and ~7500 m above ground, depending on the height of the boundary layer, clouds, and
184 chemical forecasts). Many of the 3 lower elevation sampling legs also encountered significant
185 pollution in all regions. The approximate coordinates for these regions are also included in Table
186 S2. For this study, the observations over the West Sea have been split into 2 categories: “clean,”
187 referring to the typical conditions observed during KORUS-AQ, and “transport/polluted,”
188 referring to one RF (RF12, 24/May/2016) that had direct transport of pollution from the Shanghai
189 region over the West Sea. Also, RF11 (21/May/2016) is not included in the West Sea category, as
190 this flight was sampling outflow from the SMA (prevailing winds from the east).

191 **2.2 CU-AMS sampling and analysis**

192 A highly customized, high-resolution time-of-flight aerosol mass spectrometer (HR-ToF-
193 AMS, Aerodyne Research, Inc.) was flown on the NASA DC-8 during KORUS-AQ. Hereafter,
194 this instrument will be referred to as CU-AMS since there were two high-resolution AMSs on the
195 DC-8 during KORUS-AQ (see Sect. 2.4). Both AMSs measured non-refractory composition of
196 PM₁ (particulate matter with aerodynamic diameters less than 1 μm) (DeCarlo et al., 2006;
197 Canagaratna et al., 2007). The key differences between the two AMSs was the type of vaporizer
198 (standard for CU-AMS versus capture for the other AMS), which has been described in prior
199 publications (Jayne and Worsnop, 2015; Hu et al., 2017a, 2017b, 2018a, 2018b; Xu et al., 2017)
200 and below and in Sect. 2.4. The basic concept, and operation, of the CU-AMS for aircraft sampling
201 has been described elsewhere (DeCarlo et al., 2006, 2008, 2010; Dunlea et al., 2009; Cubison et
202 al., 2011; Kimmel et al., 2011; Schroder et al., 2018), and a brief description of other important



203 details follow. For detailed information on field AMS calibrations, positive matrix factorization,
204 photochemical clock calculations, and model setups, see Supplemental Sect. S2 – S7.

205 Ambient particles were drawn into the airplane through an NCAR High-Performance
206 Instrumented Airborne Platform for Environmental Research Modular Inlet (HIMIL; Stith et al.,
207 2009) at a constant standard ($T = 273$ K and $P = 1013$ hPa) flow rate of 9 L min^{-1} . The ram heating
208 of the inlet dried the aerosol prior to entering the airplane, and the temperature of the cabin
209 (typically $\sim 10^\circ\text{C}$ higher than ambient) maintained the sampling line RH to less than 40%, ensuring
210 the aerosol remained dry prior to entering the AMS. The sample was introduced into the AMS
211 aerodynamic focusing lens (Zhang et al., 2002, 2004), operated at 1.5 Torr, through a pressure-
212 controlled inlet, which was operated at 433 hPa (325 Torr) (Bahreini et al., 2008). The focused
213 particles were then introduced after several differential pumping stages into a detection chamber,
214 where they impacted on an inverted cone porous tungsten vaporizer (“standard” vaporizer) held at
215 600°C . The non-refractory species were flash-vaporized and the vapors were ionized by 70 eV
216 electron ionization. Finally, the ions were extracted, and analyzed by a high-resolution time-of-
217 flight mass spectrometer (HTOF, ToFwerk AG). The residence time from outside the inlet to the
218 vaporizer was ~ 0.4 s in the boundary layer and ~ 1.0 s at 7500 m during KORUS-AQ. Unless
219 otherwise noted, all aerosol data reported here is at standard temperature (273 K) and pressure
220 (1013 hPa) (STP), leading to the notation $\mu\text{g sm}^{-3}$ (sm^{-3} is the standard volume, in m^3 , at STP).
221 Notation in scm^{-3} is also at STP.

222 For KORUS-AQ, the CU-AMS was operated in the Fast Mass Spectrum (FMS) mode
223 (Kimmel et al., 2011), in order to obtain high-time resolution measurements (1 Hz) continuously.
224 Each FMS 1 s “run” is either collected as chopper closed (background with particle beam blocked)
225 or chopper open (background plus ambient particles and air) position. For KORUS-AQ, the CU-



226 AMS sampled with chopper closed for 6 s and chopper open for 46 s. For the remaining 8 s of the
227 1 min cycle, it sampled with the efficient particle time-of-flight (ePToF) mode which provides
228 particle sizing but with reduced sensitivity (Fig. S2). Also, once every 20 – 30 min, rapid sampling
229 (20 s) of outside air through a particle filter was used to ensure quality control of the instrument
230 background and detection limits. The average of the two background signal periods (chopper
231 closed) before and after the open signal was subtracted from each 1 s open measurement. In
232 addition to the 1 s data, we reported a 1 min data product, in which we averaged raw mass spectra
233 prior to fitting the high-resolution ions, leading to improved signal-to-noise (SNR) from reduced
234 nonlinear fitting noise (beyond the expected increased SNR from averaging in an ion-counting
235 noise regime). For this study, the 1 min data product is used since the additional spatial resolution
236 provided by the 1 s product was not required for the analysis of regional plumes. The software
237 packages Squirrel V1.60 and PIKA V1.20 within Igor Pro 7 (Wavemetrics) (DeCarlo et al., 2006;
238 Sueper, 2018) were used to analyze all AMS data.

239 The CU-AMS always used the “V-mode” ion path (DeCarlo et al., 2006), with a spectral
240 resolution ($m/\Delta m$) of 2500 at m/z 44 and 2800 at m/z 184. The collection efficiency (CE) for the
241 CU-AMS was estimated per Middlebrook et al. (2012). Calibrations of the CU-AMS are discussed
242 in the supplement (Sect. S2), and detection limits for the 1 min data were 26, 12, 4, 10, and 115
243 ng sm^{-3} for SO_4 (sulfate), NO_3 (nitrate), NH_4 (ammonium), Chl (chloride), and OA, respectively
244 (Note that the charge symbol is not included for the nominally inorganic species, as organic
245 compounds may make (typically small) contributions to these species (e.g., organonitrates,
246 organosulfates, and reduced organic nitrogen species) (Huffman et al., 2009; Farmer et al., 2010).
247 pNO_3 will be used throughout the rest of the paper to represent aerosol NO_3 and to ensure it is not
248 confused with radical NO_3 . These detection limits are estimated for every data point per Drewnick



249 et al. (2009) and remained nearly constant during each flight and throughout the campaign. It was
250 scaled by $\sim \times 0.8$ based on comparison with periodic filter blanks (Campuzano-Jost et al., 2016). It
251 was found that the scaling with the period blanks from the filters were not impacted by the length
252 of sampling outside air through the filter. The low limit of detection for these species remained
253 nearly constant during the flight by using a cryogenic pump that lowered the temperature of a
254 surface surrounding the vaporizer region to 90 K. This freezes out most background gases, and
255 provided consistently low detection limits during the flight, when other AMSs may suffer from
256 much increased detection limits for several hours into a flight due to pumping out of large initial
257 backgrounds. The 2σ accuracy for the CU-AMS of inorganic and organic species is estimated to
258 be 35% and 38%, respectively (Bahreini et al., 2009). The O/C and H/C ratios were determined
259 using the improved-ambient method (Canagaratna et al., 2015). The CU-AMS was fully
260 operational during KORUS-AQ, except for 2 hours in RF01, leading to nearly 99% data collection
261 coverage. Additional information on AMS data interpretation can be found in Jimenez et al. (2018)
262 as well as the datafile headers for the KORUS-AQ AMS data (Aknan and Chen, 2018).

263 **2.3 Oxidation flow reactor sampling and analysis**

264 The Potential Aerosol Mass (PAM) oxidation flow reactor (OFR) allows the measurement
265 of the aerosol mass that can be formed from the precursors that are present in ambient or laboratory
266 air (Kang et al., 2007; Lambe et al., 2011). The OFR has been successfully deployed in multiple
267 urban and forested locations to quantify potential SOA (Ortega et al., 2016; Palm et al., 2016,
268 2017, 2018; Kang et al., 2018). The chemical regimes and comparability to ambient results of the
269 OFR have been characterized extensively by modeling, which indicate that SOA formation
270 proceeds by chemistry similar to the atmosphere, dominated by OH oxidation under low-NO
271 conditions (Li et al., 2015; Peng et al., 2015, 2016). The sampling schematic of the OFR during



272 KORUS-AQ is shown in Fig. S12. Briefly, it is a 13 L (45.7 cm length OD × 19.7 cm ID)
273 cylindrical aluminum tubular vessel that uses two low-pressure mercury 185 and 254 nm lamps
274 (BHK, Inc., model no. 82-904-03) to produce OH radical through the photolysis of ambient H₂O,
275 O₂, and O₃ (R1 – R5). This mode of operation is referred to as “OFR185.”



281 The KORUS-AQ study represents the first airborne operation of an OFR to our knowledge.
282 Unlike prior ground-based field studies (Ortega et al., 2016; Palm et al., 2016, 2017, 2018), the
283 UV lamps were typically maintained at one constant light setting since the OFR was sampling
284 more rapidly varying air masses. Since external OH reactivity (OHR) and water vapor
285 concentrations changed with air mass, a range of OH exposures (OH_{exp}) were reached inside the
286 OFR despite the constant photolytic flux (Peng et al., 2015). The OFR OH_{exp} was calibrated using
287 two different methods: (1) Using the removal of ambient CO in the OFR during flight (on-line
288 calibration in Fig. S14a). (2) While on the ground, injecting known amounts of humidified
289 (multichannel Nafion drier) CO from a zero air cylinder spiked with ~2 ppmv of CO (Scott
290 Marrin), and varying the light intensity to produce different amounts of OH (off-line calibration in
291 Fig. S14b) and thus CO reactive removal. Both the off- and on-line approach yielded a calibration
292 factor of ×0.4 for the OH_{exp}, calculated using the parameterization of Peng et al. (2015), similar to
293 Palm et al. (2016). The OH_{exp} calculated with the calibrated equation is used for periods in which
294 the Picarro was not sampling the OFR output. A histogram of the other key parameters used to
295 calculate OH_{exp} with the Peng et al. (2015) equation—H₂O(g) (measured by DLH) and ambient



296 OH reactivity (measured by ATHOS)—are shown in Fig. S15. The OFR operating conditions were
297 in the “Safe” zone (Peng et al., 2015, 2016), meaning that they were consistent with tropospheric
298 chemistry.

299 A key difference between the operation of this OFR during KORUS-AQ and previous field
300 studies (which did not use any inlet (Ortega et al., 2016; Palm et al., 2016, 2017, 2018)) was that
301 the gas and aerosol passed through ~1.8 m of ~4.6 mm ID stainless steel tubing at 5 vlp
302 (residence time ~1.4 s through tubing). The residence time in the OFR was ~150 s. The gas and
303 aerosol sample entered the OFR through a ½” press fitted stainless steel inlet that was coated in
304 SilcoNert (SilcoTek Co, Bellefonte, PA) and had 18 evenly spaced holes (Fig. S13), to promote
305 more even injection of the sample into the OFR flow cross-section (Ortega et al., 2016; Palm et
306 al., 2017; Mitroo et al., 2018). The gas-phase output of the OFR was sampled by an 8.25 cm
307 diameter Teflon ring inside the OFR connected to 1/8” Teflon tubing, and sampled by two gas
308 analyzers for O₃ (Model 205, 2B Technologies, Boulder, CO, USA) and CO (Picarro, see above).
309 The aerosol was sampled by a 2 mm ID stainless steel tube. A constant flow through the OFR at
310 all times was maintained with a bypass flow (when the CU-AMS or CO instrument were not
311 sampling from the OFR) to always maintain a constant residence time in the OFR. The CU-AMS
312 sampled from the OFR for 12 – 15 seconds every three minutes (Fig. S2). This sampling scheme
313 was chosen to ensure the CU-AMS had a high sampling frequency for ambient aerosol, while also
314 sampling the OFR once each time the air inside it was replaced (given its residence time of ~150
315 s).

316 In prior ground-based studies the OFR was placed outside, leading to the ambient and OFR
317 temperature being within 1 – 2°C (Ortega et al., 2016; Palm et al., 2016, 2017, 2018). During
318 KORUS-AQ the OFR was housed inside the DC-8 cabin, which was typically ~10°C (range 0 –



319 20°C) warmer than ambient air (Fig. S16). Since (NH₄)₂SO₄ is nonvolatile, there was little impact
320 on the amount of SO₄ entering and exiting the OFR (as confirmed when the UV lights were off
321 and OH_{exp} was zero) (Fig. S17). For OA, which is typically a mixture of semivolatile and
322 nonvolatile compounds, and for pNO₃, which can be quite semivolatile (Huffman et al., 2009;
323 Cappa and Jimenez, 2010), the mass concentration exiting the OFR was significantly lower than
324 when entering, with lights off. This is due to evaporation of OA and pNO₃ at the warmer cabin
325 temperatures and longer residence times (~150 s). Thus, the average ratio of OA transmitted
326 through the OFR versus bypassing the OFR with lights off is used (slope in Fig. S17) as an
327 approximate correction for the amount of OA that should have exited the OFR without chemistry
328 when the OFR was in oxidation mode. These values were highly correlated (R² = 0.94) and did
329 not vary for the entire campaign, leading to confidence in the correction. This corrects for the semi-
330 volatile nature of ambient OA, but it does not correct for any temperature dependence of SOA
331 formation.

332 The average aerosol condensation sink (CS) inside the OFR is needed for the LVOC fate
333 model described in Palm et al. (2016) to compute the amount of condensable vapors that do not
334 form SOA in the OFR (due to residence-time limitations and surface losses), but that would be
335 expected to form SOA in the atmosphere. Since there were no particle sizers available to estimate
336 the changes in the aerosol surface area after the OFR (Palm et al., 2016), we used Eq. (1) to estimate
337 the average aerosol surface area in the OFR and estimated condensational sink (CS_{est}).

$$338 \quad CS_{est} = CS_{amb} \times \left(\frac{AMS \text{ Tot Mass Out} + AMS \text{ Tot Mass In}}{2 \times AMS \text{ Tot Mass In}} \right)^{2/3} \times 2 \quad (1)$$

339 The CS_{amb} (ambient condensational sink) is calculated using the LAS and SMPS measurements.
340 The second term is a scaling factor to account for the observed increase in mass in OFR (with a
341 power of 2/3 for approximate conversion to relative surface area). The third term is a scaling factor



342 for relative increase in surface area due to strong nanoparticle formation in the OFR, as observed
343 in Los Angeles during CalNex (Ortega et al., 2016). A hygroscopic growth factor is not included
344 in the CS_{est} (Palm et al., 2016) as the aerosol in the OFR was dry (Sect. 2.1).

345 One simple way to confirm the validity of the OH exposures derived from the in-field
346 calibrations and measurements, is to compare the observed versus modeled sulfate enhancements
347 in the OFR while traversing SO_2 plumes (Palm et al., 2016) (Fig. S18 and S19). Albeit the point-
348 to-point comparison is noisy as expected, we find good agreement on average between the modeled
349 and measured SO_4 enhancement (slope = 0.94), validating the quantification of the OFR for this
350 study. We obtained results from the OFR for all flights except RF12 (24/May/2016), when a valve
351 malfunction prevented measurements of O_3 and thus the ability to quantify OFR OH_{exp} . During
352 this flight, the Picarro was also not sampling from the OFR.

353 **2.4 Co-located supporting measurements used in this study**

354 In addition, the CU-AMS measurements, this study utilizes several co-located gas- and
355 aerosol-phase measurements collected on-board the DC-8.

356 **2.4.1 Gas-phase measurements**

357 NO , NO_2 , NO_y , and O_3 were measured by the NCAR chemiluminescence instrument
358 (Weinheimer et al., 1994). For CO , the ambient measurements were made with the NASA Langley
359 tunable diode laser absorption spectroscopy (DACOM) (Sachse et al., 1987) while the
360 measurements for CO exiting the oxidation flow reactor (Sect. 2.3) were made with a Picarro
361 G2401-m. The Picarro was calibrated in flight with a WMO traceable gas standard. Gas-phase
362 H_2O was measured with the NASA Langley open-path tunable diode laser hygrometer (DLH)
363 (Diskin et al., 2002). The Pennsylvania State University Airborne Tropospheric Hydrogen Oxides
364 Sensor (ATHOS), based on laser-induced fluorescence, measured OH , HO_2 , and OH reactivity



365 (Faloona et al., 2004; Mao et al., 2009). Hydrocarbons were measured by the University of
366 California-Irvine whole air sampler (WAS), followed by analysis with a gas-chromatography
367 followed by either a flame ionization detector or mass spectrometer (Blake et al., 2003), and also
368 by the University of Oslo proton transfer reaction time-of-flight mass spectrometer (PTR-MS)
369 (Wisthaler et al., 2002; Müller et al., 2014). SO₂ and speciated acyl peroxy nitrates (e.g., PAN and
370 PPN) were measured by the Georgia Institute of Technology chemical ionization mass
371 spectrometer (GT-CIMS) (Huey et al., 2004; Slusher et al., 2004; S. Kim et al., 2007) The sum of
372 the total peroxy nitrates (ΣROONO_2) and total alkyl and multifunctional nitrates (ΣRONO_2) were
373 measured by the University of California-Berkeley thermal-dissociation laser-induced
374 fluorescence (TD-LIF) technique (Day et al., 2002; Wooldridge et al., 2010). Formaldehyde was
375 measured with the University of Colorado-Boulder difference frequency absorption spectrometer
376 (CAMS, or Compact Atmospheric Multi-species Spectrometer) (Weibring et al., 2010; Richter et
377 al., 2015). Finally, HCN, HNO₃, and dihydroxy-toluene were measured by the California Institute
378 of Technology chemical ionization mass spectrometer (CIT-CIMS) (Crouse et al., 2006;
379 Schwantes et al., 2017).

380 **2.4.2 Supporting aerosol measurements**

381 Refractory Black carbon (BC) mass concentrations in the accumulation mode size range
382 measured by the NOAA Single Particle Soot Photometer (SP2) (Schwarz et al., 2013). SO₄²⁻ was
383 measured both by the University of New Hampshire mist-chamber ion-chromatograph (MC/IC,
384 fine mode only) (Talbot et al., 1997) and total particulate filters, analyzed off-line with ion
385 chromatography (fine and coarse mode with an estimated size cut of 4 μm) (Dibb et al., 2003;
386 McNaughton et al., 2007; Heim et al., 2018). Besides the CU-AMS, the Hankuk University of
387 Foreign Studies operated an AMS onboard as well (hereinafter referred to as K-AMS); however,



388 using a “capture vaporizer” (see Sect. 2.2 above). Briefly, the geometry and material of the
389 vaporizer has been modified to reduce the amount of particle bounce, and this leads to a CE of ~1
390 for all ambient species, albeit with more thermal decomposition (Jayne and Worsnop, 2015; Hu et
391 al., 2017a, 2017b, 2018a, 2018b; Xu et al., 2017).

392 Finally, the physical concentration and properties of the aerosol were measured by the
393 NASA Langley Aerosol Research Group (LARGE). These included: (1) Size-resolved particle
394 number concentrations (values used to estimate surface area and volume) were measured by a TSI
395 Laser Aerosol Spectrometer (LAS, model 3340; TSI Inc., St. Paul, MN; calibrated with a range of
396 NIST traceable polystyrene latex spheres (PSL), size range 100 – 5000 nm PSL mobility diameter),
397 a scanning mobility particle sizer (SMPS, composed of a differential mobility analyzer, TSI model
398 3081 long column with custom flow system and SMPS operated using TSI software) and a CPC
399 (TSI model 3010, size range 10 – 200 nm PSL mobility diameter). (2) Scattering coefficients at
400 450, 550 and 700 nm were measured with an integrating nephelometer (TSI, Inc. model 3563) and
401 corrected for truncation errors per Anderson and Ogren (1998). (3) Absorption coefficients at 470,
402 532 and 660 nm were measured with a Particle Soot Absorption Photometer (PSAP, Radiance
403 Research) and corrected for filter scattering per Virkkula (2010). In order to calculate extinction,
404 which is used in this study, the measured Angstrom exponent was used to adjust the scattering at
405 550 nm to 532 nm (Ziemba et al., 2013).

406 **3. PM₁ comparisons, composition, and transport during KORUS-AQ**

407 **3.1 Intercomparisons of airborne PM₁ during KORUS-AQ**

408 The intercomparison of aerosol measurements less than 1 μm are summarized here and
409 shown in Table 1, and the full detailed intercomparison is found in SI 8. The AMS and the other



410 aerosol measurements agree within their combined uncertainties, similar to prior studies (DeCarlo
 411 et al., 2008; Dunlea et al., 2009; Hayes et al., 2013; Liu et al., 2017; Schroder et al., 2018).

412 **Table 1.** Overview of intercomparisons for KORUS-AQ CU-AMS versus other PM₁
 413 measurements. Uncertainties listed are 1σ.

<i>Instrument Comparison</i>	<i>What is being Compared</i>	<i>Slope</i>	<i>R²</i>	<i>Combined Uncertainty of Instruments</i>	<i>Uncertainty of Regression Slope</i>
MC/IC	SO ₄ Mass	0.95	0.76	±20%	±1%
Filters	SO ₄ Mass	0.80	0.86	±24%	±2%
AMS Scatter Plot (Total Campaign)	Total PM ₁	0.95		±27%	±1%
AMS Scatter Plot (Lower PM ₁ Sizes) ^a	Mass/CE Transmission	1.02	0.91	±27%	±1%
AMS Scatter Plot (Higher PM ₁ Sizes) ^b	Mass/ Transmission	0.84	0.82	±27%	±1%
Extinction	Total PM ₁	6.00	0.87	±31%	±3%
	Mass to 532 nm Extinction				
LAS (all data)	PM ₁ Volume	1.56	0.86	±43%	±1%
LAS (Conc. Filter) ^c	PM ₁ Volume	1.19	0.91	±43%	±1%
LAS (Mass Filter) ^c	PM ₁ Volume	1.00	0.79	±43%	±1%

414 ^aComparison of K-AMS and CU-AMS for RFs 1 – 9, 11, 15, 19. ^bComparison of K-AMS and CU-
 415 AMS for RFs 10, 12 – 14, 16 – 18, 20. ^cUsing the lower concentration and mass filter. See SI 8
 416 and Fig. S27.

417
 418 There are two comparisons that show lower agreement. The slope between AMS SO₄
 419 versus filter SO₄ is 20% lower than unity. As previously mentioned, the filters collect aerosols
 420 with diameters up to 4 μm, and Heim et al. (2018) concluded that the difference was due to
 421 supermicron SO₄²⁻ throughout the campaign from the transport of dust from continental Asia to
 422 South Korea. Thus, the differences in the diameter cut-off between the AMS and filters and
 423 observations of supermicron SO₄²⁻ are the likely cause of the lower slope. The comparison of
 424 calculated volume from AMS plus BC versus calculated volume from LAS indicate that the AMS
 425 and BC calculated volume is higher. Part of the reason could be that LAS vaporizes BC (Kupc et
 426 al., 2018); however, as shown in Figure 1, BC accounts for a small fraction of PM₁. As discussed
 427 in SI 8, the LAS detector saturated at high particle number concentrations/high mass
 428 concentrations. This has also been observed by Liu et al. (2017) in a prior airborne campaign with



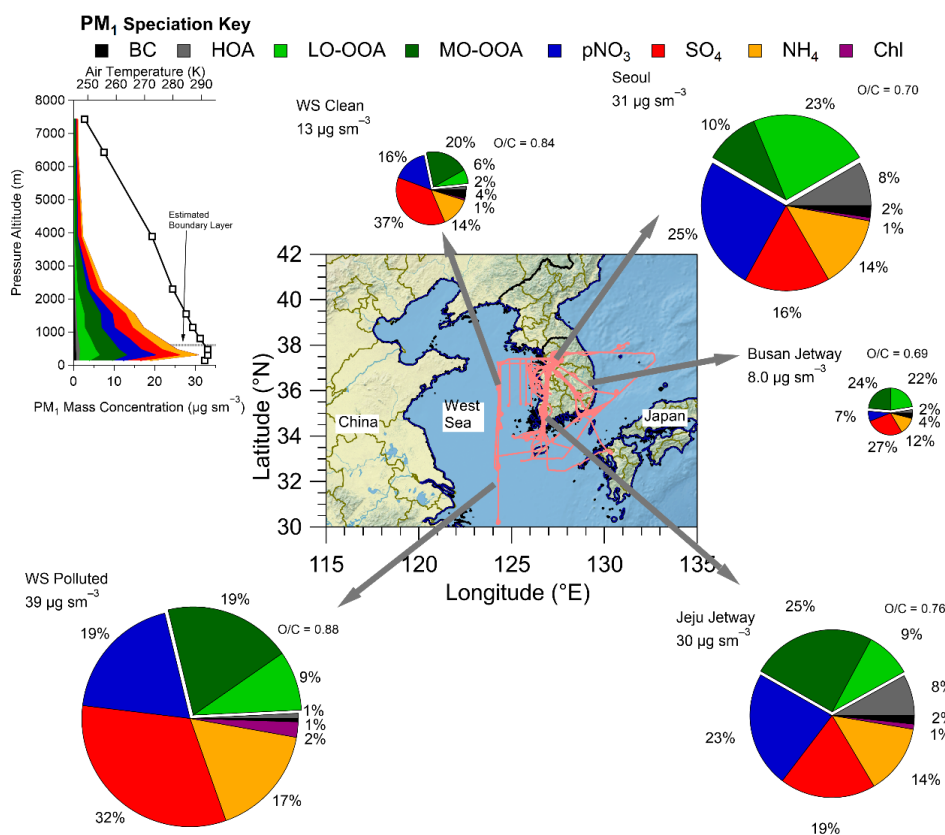
429 the same instruments. Comparing the LAS and AMS plus BC volume at lower total mass
430 concentrations/particle number concentrations, the difference is reduced to ~10%, which is well
431 within the combined uncertainties.

432 **3.2 PM₁ concentration and composition over South Korea during KORUS-AQ**

433 We briefly describe the PM₁ composition observed over South Korea during the campaign
434 and compare it to prior observations in the same region and for other large urban areas around the
435 world. First, the comparison of PM₁ in the boundary layer (estimated to be ~600 m from
436 temperature profiles measured on the DC-8 during the entire campaign, as shown in Figure 1) in
437 the KORUS-AQ domain is discussed. As shown in Figure 1, the highest average PM₁ during
438 KORUS-AQ were observed over the West Sea during the “transport/polluted” research flight
439 (RF12, 24/May/2016), at 39 $\mu\text{g sm}^{-3}$, and over Seoul, at 31 $\mu\text{g sm}^{-3}$ (average of all flights over
440 Seoul). However, during the latter half of the mission, PM₁ was regularly greater than 60 $\mu\text{g sm}^{-3}$,
441 and as high as 100 $\mu\text{g sm}^{-3}$, over Seoul. During the rest of the flights, the average mass
442 concentration over the West Sea was a factor of 3 lower (13 $\mu\text{g sm}^{-3}$). Also, the Seoul and West
443 Sea PM₁ composition was different, where SO₄ and more-oxidized oxidized organic aerosol (MO-
444 OOA) dominated the West Sea PM₁ budget, indicative of transported, aged chemistry (Dunlea et
445 al., 2009; Lee et al., 2015). Also, the O/C ratio for the West Sea was 0.84 (WS Clean) to 0.88 (WS
446 polluted). Seoul showed higher fractions of less-oxidized OOA (LO-OOA) than MO-OOA, and
447 higher pNO₃ than SO₄, which is more typical of fresher, urban chemistry, with an average O/C
448 ratio of 0.70 (DeCarlo et al., 2008; Hennigan et al., 2008; Hayes et al., 2013; H. Kim et al., 2017;
449 Kim et al., 2018). The eastern side of South Korea had lower average PM₁ than observed over
450 Seoul. This region of South Korea is not as highly populated as around Seoul, reducing the sources
451 and production of PM₁ and is more representative of PM₁ background pollution/transport across



452 the country. The average PM_{10} observed over the Jeju jetway was similar to what was observed
 453 over Seoul. Also, this area had similar contributions from hydrocarbon-like organic aerosol (HOA)
 454 and pNO_3 as Seoul, indicating local emissions, including industry, along with
 455 transport/background, are impacting the PM_{10} composition (e.g., Hayes et al., 2013). This part of
 456 South Korea has some large population centers (e.g., Gwangju and Jeonju) and power plants (e.g.,
 457 Boryeong Power Station), which are consistent with the observed impact.



458

459 **Figure 1.** Pie charts of the average boundary layer PM_{10} composition by the different regions
 460 (defined in Table S2) sampled over South Korea during the campaign. The flight paths are shown
 461 in light red. The Busan jetway had no measurable Chl; therefore, Chl is not included in the pie
 462 chart. The pie charts area is proportional to PM_{10} in each region. The average O/C for the OA is
 463 shown by each OA section in the pie charts. The map shows the DC-8 flight paths throughout



464 KORUS-AQ. The average vertical profile of PM₁ species (along with temperature and continental
465 PBL height) over all of South Korea is shown in the upper left.

466 The average PM₁ observed over Seoul during KORUS-AQ was similar to the mass
467 concentration measured in Seoul in previous years (37, 38, 37, 27, and 22 μg m⁻³ for Choi et al.,
468 2012, Kim et al., 2007, H. C. Kim et al., 2016, Park et al., 2012, and Kim and Zhang, 2017,
469 respectively). Also, the average PM₁ over the West Sea during clean conditions (13 μg sm⁻³) is in
470 line with what has been reported over Baengnyeong Island (Lee et al., 2015), located west of South
471 Korea in the West Sea (37°58'00" N, 124°37'04" S). Finally, the PM_{2.5} mass concentrations have
472 remained nearly constant for the last ~20 years (OECD, 2018).

473 The PM₁ composition over Seoul is dominated by pNO₃ and SOA, similar to what was
474 observed on the ground during the same time period (Kim et al., 2018). The composition over
475 Seoul is more similar to what has been observed over Mexico City during MILAGRO (DeCarlo
476 et al., 2008), and in Los Angeles during CalNex (Hayes et al., 2013) than observed over large
477 urban areas in Asia (Hu et al., 2016).

478 As the differences in PM₁ composition for the different regions mostly occurred in the
479 boundary layer, we show the average PM₁ profile observed during all of KORUS-AQ in the inset
480 of Figure 1, and the fractional contribution to the profile in Fig. S32. At low altitudes, the PM₁
481 mass is dominated by secondary PM₁ species that compose the largest fractions in the pie charts
482 in Figure 1 (LO-OOA, MO-OOA, pNO₃, and SO₄). The fractional contributions of SO₄ and MO-
483 OOA to PM₁ mass increase with altitude and become dominant above ~4 km, representative of
484 more aged aerosol, away from sources (e.g., Dunlea et al., 2009).



485 3.3 Analysis of background and transport influence on PM₁

486 Transport of aerosols and aerosol precursors from distant sources creates a larger-scale
487 background that needs to be quantified in order to understand the impact of local emissions on
488 aerosol production. Prior studies have shown the potential impact of long-distance transport in
489 creating a background aerosol mass over Seoul (H. S. Kim et al., 2007; Heo et al., 2009; Kim et
490 al., 2009, 2016, 2018; H. C. Kim et al., 2017; H. Kim et al., 2017; Jeong et al., 2017; Lee et al.,
491 2017; Seo et al., 2017). To investigate the influence of background and transported air to Seoul,
492 the FLEXPART Lagrangian model with WRF winds and meteorology is used. The application of
493 FLEXPART to this study is described in SI 7. Briefly, the model uses back trajectories from the
494 point where the DC-8 was sampling and calculates the amount of CO and NO₂ contributed by
495 different emission regions for each sampled air parcel.

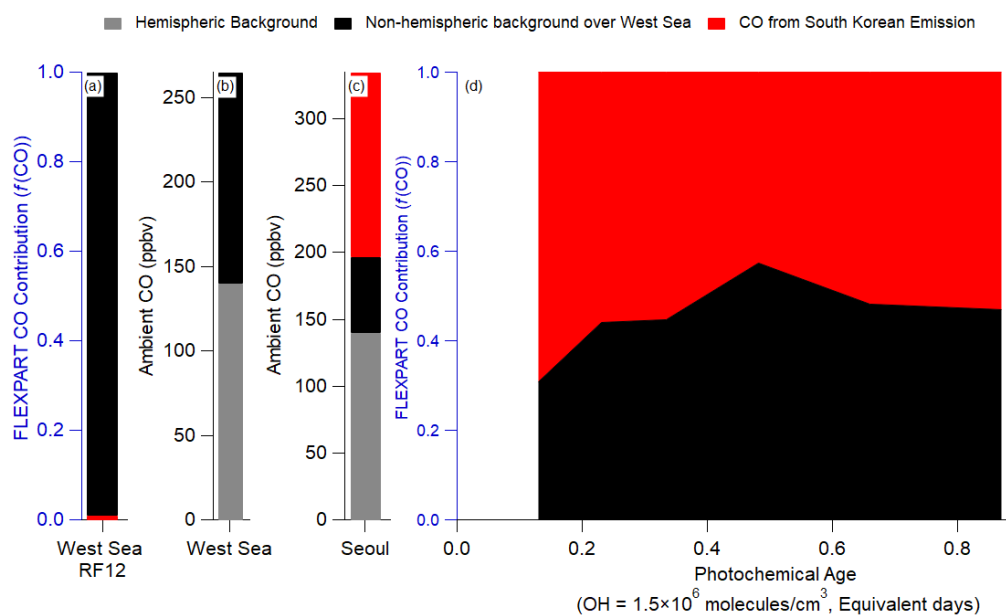
496 The CO concentration measured during KORUS-AQ can be described by Eq. (2). The
497 average CO mixing ratios observed during the campaign are used.

$$498 \quad \text{CO}_{\text{ambient}} = \text{CO}_{\text{hem. bckg.}} + \text{CO}_{\text{foreign}} + \text{CO}_{\text{South Korean}} \quad (2)$$

499 Here, CO_{hem. bckg.} is the hemispheric background of CO. In FLEXPART, the foreign emissions are
500 from China, Hong Kong, Japan, Laos, Macau, Myanmar, Mongolia, North Korea, Russia, Taiwan
501 and Vietnam. FLEXPART does not include the CO hemispheric background; therefore, that term
502 is estimated from upwind sites (Mt. Waliguan, China and Ulan Uul, Mongolia) (Novelli et al.,
503 2017) to be 140 ppbv CO. The West Sea is the simplest case, as FLEXPART predicted that all the
504 CO originated from the foreign sources listed above (Figure 2a). Thus, CO_{ambient} in the West Sea
505 can be attributed to 140 ppbv CO_{hem. bckg.} and 125 ppbv CO_{foreign} (Figure 2b). The advection of CO
506 from the West Sea to Seoul will lead to dilution and mixing of the CO_{foreign} with air containing
507 only the CO_{hem. bckg.}. With an average wind speed of 4 m/s over the West Sea, and a distance of



508 ~300 km, the air takes ~1 actual day to move from where the DC-8 sampled over the West Sea to
509 Seoul. The results from FLEXPART are used to estimate the dilution rate, $\sim 0.7 \text{ day}^{-1}$, comparable
510 to the values determined in prior studies (McKeen et al., 1996; Price et al., 2004; Arnold et al.,
511 2007; Dzepina et al., 2011; Fried et al., 2011). Thus, after 1 day of advection, $\sim 60 \text{ ppbv CO}_{\text{foreign}}$
512 is expected over Seoul (Figure 2c); thus, with Eq. (2), the total CO background ($\text{CO}_{\text{foreign}} + \text{CO}_{\text{hem.}}$
513 bckg.) is 200 ppbv, and the remainder of the observed ambient CO is attributed to local South Korean
514 emissions (on average, 165 ppbv CO). Finally, results from FLEXPART show that the $\text{CO}_{\text{foreign}}$
515 contribution (Figure 2d) remained nearly constant throughout the campaign at all observed
516 photochemical ages. Therefore, 200 ppbv CO background for observations over Seoul will be used
517 throughout this study.



518

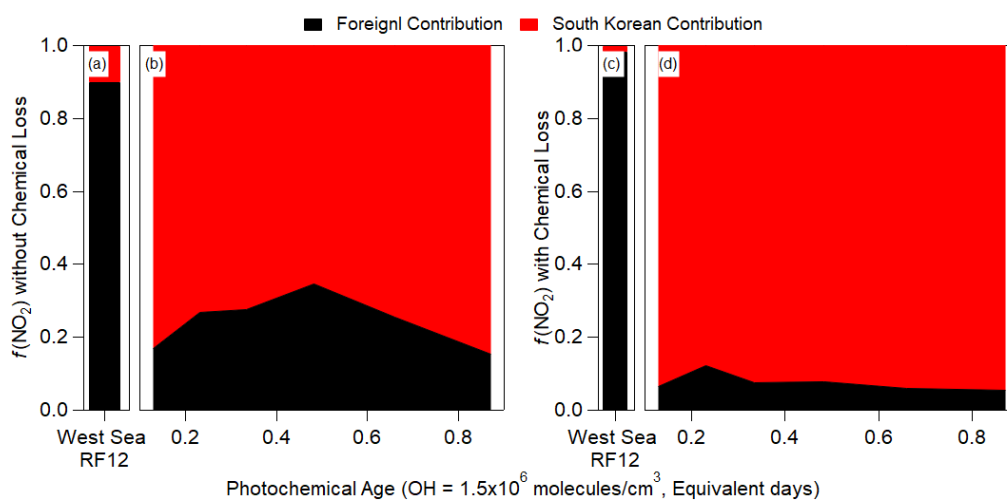
519 **Figure 2.** Note differences in labels and values for each y-axis. Also, note that FLEXPART does
520 not include hemispheric background; therefore, it is not included in the figure. (a) Fractional
521 contribution of foreign versus South Korean CO emission over the West Sea from FLEXPART.
522 (b) Estimated measured partitioning of the average CO observed over the West Sea. (c) Same as
523 (b), but for over Seoul. (d) Same as (a), but for over Seoul. For all panels, CO does not include any
524 chemical losses or production.



525 From the observed dilution-corrected OA concentrations (OA concentration divided by
 526 background subtracted CO mixing ratios) over the West Sea (13 and $40 \mu\text{g sm}^{-3} \text{ppmv}^{-1}$ for clean
 527 West Sea and RF12 West Sea, respectively), the $\text{CO}_{\text{foreign}}$ over Seoul would correspond to $1 - 3$
 528 $\mu\text{g sm}^{-3}$ OA background (Eq. (3)).

$$529 \quad \text{OA}_{\text{background}} = \text{CO}_{\text{foreign}} \times \left(\frac{\text{OA}}{\text{CO}} \right)_{\text{foreign}} \quad (3)$$

530 The upper limit will be used for the remainder of the study. The corresponding observed
 531 background values for HOA, LO-OOA, and MO-OOA are 0 , 1 ± 1 , and $2 \pm 2 \mu\text{g sm}^{-3}$, respectively.
 532 Finally, the background for key gas-phase and aerosol species (which are discussed below) are
 533 1.05 ± 0.28 (CH_2O), 69 ± 5 (O_x), 0.25 ± 0.06 (PAN), and 0.30 ± 0.10 (ΣROONO_2) ppbv, 0.44 ± 0.34
 534 (Dihydroxy toluene) pptv, and $2 \pm 2 \mu\text{g sm}^{-3}$ (pNO_3). Thus, the increase in OA mass concentration
 535 from the background values ($3 \mu\text{g sm}^{-3}$) to average Seoul values ($13 \mu\text{g sm}^{-3}$) must be due to South
 536 Korean emissions of POA and production of SOA.



537

538 **Figure 3.** Binned fractional contribution (South Korea/(South Korea + Foreign)) of the
 539 FLEXPART, sampled from aircraft position for contributions to (a and b) NO_2 (without any
 540 chemical losses) and (c and d) NO_2 (with chemical losses ($\tau = 1$ day)) versus the observed (aircraft)
 541 photochemical age. For (a) and (c), the West Sea bars are the average fractional contributions for
 542 RF12.



543 The contribution of foreign versus South Korean emissions of NO₂ from FLEXPART over
544 Seoul and West Sea (Figure 3) is analyzed next. NO₂ is investigated since it has a photochemical
545 lifetime of ~1 day (at OH ≈ 1.5×10⁶ molecules/cm³). This lifetime is similar to short-lived
546 hydrocarbons (e.g., xylene, S/IVOC, etc.) that are thought to dominate urban SOA production in
547 this campaign and other megacities (de Gouw et al., 2005; Kleinman et al., 2007, 2008; DeCarlo
548 et al., 2010; Wood et al., 2010; Hayes et al., 2013, 2015, Hu et al., 2013, 2016; Ortega et al., 2016;
549 Ma et al., 2017; Schroder et al., 2018). In general, $f(\text{NO}_2)_{\text{foreign}}$ and $f(\text{NO}_2)_{\text{local}}$ (with and without
550 photochemical loss included in the FLEXPART model runs) is quite constant with photochemical
551 age (Figure 3), like CO. Unlike CO, the contribution of local NO₂ is ~70% (if photochemical
552 removal is not included) and ~90% (if photochemical removal is included). This strongly suggests
553 that most short-lived hydrocarbons over Seoul, which are believed to dominate urban SOA
554 production, are dominated by South Korean emissions and not transport from foreign sources.

555 **4. SOA production over the Seoul Metropolitan Area**

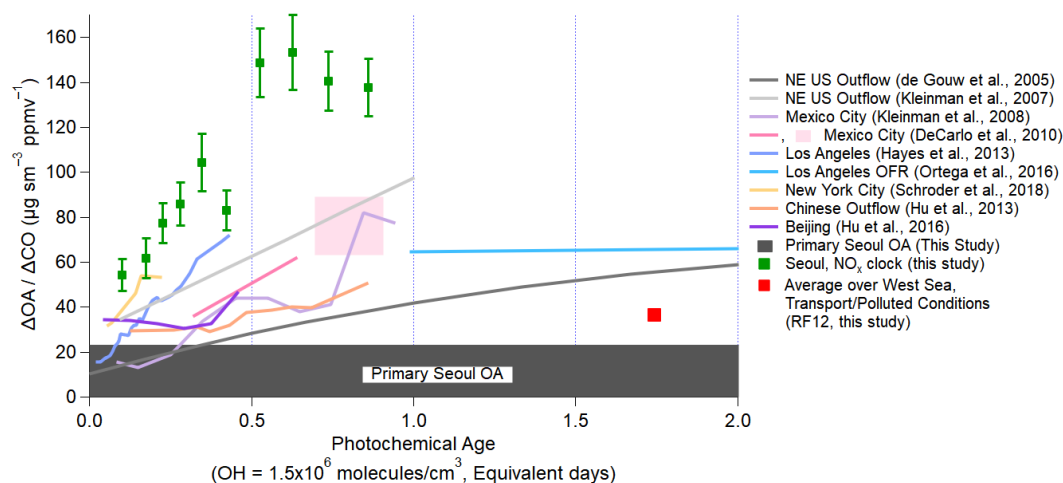
556 **4.1 SOA production over Seoul during KORUS-AQ**

557 The conceptual model for analysis of photochemical SOA production over and downwind
558 of megacities has been discussed in detail in de Gouw (2005) and DeCarlo et al. (2010) and
559 subsequent studies (Hayes et al., 2013; Hu et al., 2013, 2016; Freney et al., 2014; Schroder et al.,
560 2018). An air mass with “background” values of OA and CO is advected over a megacity area,
561 where fresh emissions of POA, SOA precursors, and CO are emitted into the air mass. The SOA
562 precursors will oxidize to produce SOA and undergo dilution with the surrounding background air
563 masses. To correct for this dilution effect, the change of OA over background OA ($\Delta\text{OA} = \text{OA} -$
564 background OA) is divided by the change of CO over background CO ($\Delta\text{CO} = \text{CO} -$ background
565 CO), and this term is the dilution-corrected concentration. CO has been used in prior studies as a



566 surrogate for primary pollution emissions as this compound has high signal-to-noise between
567 urban plumes and background and a long photochemical lifetime (meaning minimal CO is lost due
568 to chemistry or produced from VOC oxidation over a ~1 day timescale (Griffin et al., 2007)) (de
569 Gouw et al., 2005; DeCarlo et al., 2010). Finally, $\Delta\text{OA}/\Delta\text{CO}$ is plotted versus estimated
570 photochemical age. The photochemical age approximately accounts for the chemical evolution of
571 precursors either into products which can be estimated from the time evolution of NO_x/NO_y , or the
572 differences in removal rates of two hydrocarbons (o-xylene or m+p-xylene to ethylbenzene). See
573 SI 5 for more information about the calculation of the photochemical age. The potential impact of
574 SOA precursors being advected into Seoul is addressed in Sect. 4.4.

575 Throughout the paper, the estimated photochemical age from NO_x/NO_y will be used as this
576 measurement has higher temporal coverage, and an emissions ratio is not needed to calculate the
577 photochemical age (SI 5), but note that ages estimated from hydrocarbon-based clocks are
578 consistent. For photochemical ages greater than 1 day (measurements over the West Sea), the
579 aromatic photochemical clock is used (SI 5) as the NO_x/NO_y clock does not work well past 1
580 equivalent day (SI 5). As discussed in Parrish et al. (2007), compounds used to calculate
581 photochemical ages should have lifetimes on the order of the range in ages to be quantified. For
582 example, photochemical age over Seoul is less than 1 equivalent day, which is equivalent to the
583 NO_x lifetime; whereas, the photochemical age over the West Sea is expected to be a few equivalent
584 days, which is bracketed by the lifetimes of benzene and toluene.



585

586 **Figure 4.** Evolution of dilution-corrected OA versus equivalent photochemical age (days), where
587 $\Delta\text{OA} = \text{OA} - \text{background OA}$ and $\Delta\text{CO} = \text{CO} - \text{background CO}$, during KORUS-AQ. Over Seoul
588 and the West Sea, the CO background is 200 (hemispheric plus foreign) and 140 ppbv (hemispheric
589 only), respectively. The vertical error bars for the observations during KORUS-AQ are the
590 standard error of $\Delta\text{OA}/\Delta\text{CO}$ for each bin. Photochemical age is determined by the NO_x/NO_y . The
591 dark grey bar at the bottom ($22 \mu\text{g sm}^{-3} \text{ppmv}^{-1}$) is the observed POA over Seoul during the
592 campaign. Observations from other megacities (de Gouw et al., 2005; Kleinman et al., 2007, 2008;
593 DeCarlo et al., 2010; Hayes et al., 2013; Hu et al., 2013, 2016; Ortega et al., 2016; Schroder et al.,
594 2018) are also shown, as lines, for comparison, and have been updated, as described in Schroder
595 et al. (2018).

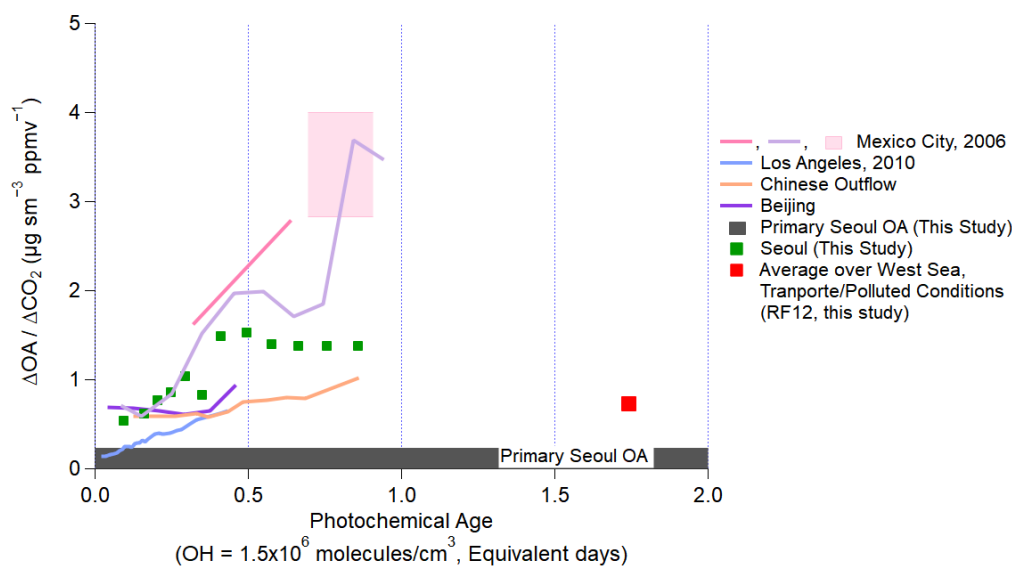
596 Similar to prior studies, OA over Seoul increased rapidly within the first photochemical
597 equivalent day from the emission source (Figure 4). The dilution-corrected SOA production is very
598 rapid for photochemical ages less than 0.7 equivalent days (note that this would be only 4 actual
599 hours of exposure for average OH concentration of 6×10^6 molecules/cm³ observed during this
600 campaign). After that time, the dilution-corrected OA plateaus and remains nearly constant.
601 George et al. (2008) and Ortega et al. (2016) found that after ~4 – 5 equivalent days, OH
602 heterogeneous reactions start fragmenting the compounds in SOA, leading to a reduction in the
603 dilution-corrected OA mass with age. Compared to prior megacity studies, the dilution-corrected
604 OA produced over Seoul is between $40 - 80 \mu\text{g sm}^{-3} \text{ppmv}^{-1}$ higher at ~0.5 equivalent days of
605 photochemical aging and $\sim 70 \mu\text{g sm}^{-3} \text{ppmv}^{-1}$ higher than in Chinese megacities (Hu et al., 2013,



606 2016). The strong SOA production over Seoul is similar to that observed in other relatively isolated
607 megacities (e.g., Los Angeles and Mexico City). It also appears not to be significantly influenced
608 by the outflow of upwind Chinese megacities, since Seoul SOA formation is very rapid and occurs
609 much faster than air mass transport from those megacities, and since the dilution-corrected
610 production is much larger in Seoul than in Chinese megacities.

611 Finally, these results do not depend on the assumed CO background. As shown in Fig. S34,
612 the OA mass concentration increases versus CO mixing ratios as photochemical age increase, and
613 in Fig. S35, even assuming a lower CO background (140 ppbv), the dilution-corrected OA
614 concentration is still $\sim 100 \mu\text{g sm}^{-3} \text{ppmv}^{-1}$. This value is still higher than what has been observed
615 in prior cities (Figure 4). If the CO background is higher than assumed here (200 ppbv), the OA
616 production would be even higher.

617 To further investigate the potential influence from upwind megacities, we compare
618 $\Delta\text{OA}/\Delta\text{CO}$ over the West Sea versus that over Seoul (Figure 4). The average $\Delta\text{OA}/\Delta\text{CO}$ over the
619 West Sea during the “transport/polluted” conditions (RF12, 24/May/2016) is $\sim 40 \mu\text{g sm}^{-3} \text{ppmv}^{-1}$.
620 This value is similar to the upper limit values observed in Beijing (Hu et al., 2016) and Changdao
621 (Chinese outflow) (Hu et al., 2013). This suggests that for Chinese outflow, the maximum dilution-
622 corrected OA concentration is $\sim 40 \mu\text{g sm}^{-3} \text{ppmv}^{-1}$. This value has already been subtracted from
623 the observations over Seoul. Finding OA concentrations greater than POA concentrations at the
624 youngest photochemical ages may be due to (1) very rapid SOA production; (2) sunrise occurring
625 3 – 4 hours (sunrise between 5:10 – 5:30 LT) prior to sampling air over Seoul in the morning; and,
626 (3) the imperfect characterization provided by the average photochemical age when fresh
627 emissions have been recently injected into an air parcel.



628

629 **Figure 5.** Same as Figure 4, but normalized by ΔCO_2 . The ratios to CO_2 are calculated using
630 $\Delta\text{CO}/\Delta\text{CO}_2$ emissions ratios from prior studies in each megacity that occur during the same
631 campaign or for the same time of year, since direct measurements of the CO_2 enhancements above
632 background during the aircraft studies of each megacity are very challenging. (Table S4).

633 Here, we introduce another dilution-correction method to investigate SOA production over
634 a megacity— $\Delta\text{OA}/\Delta\text{CO}_2$ (Figure 5). $\Delta\text{OA}/\Delta\text{CO}_2$ is a way to investigate the amount of OA
635 produced per unit mass of fuel burned in each megacity. Note that although some SOA precursors
636 are not emitted from combustion sources, such as volatile consumer products (McDonald et al.,
637 2018), one can still define this ratio in an average sense for each megacity. It has been used
638 previously for laboratory experiments (e.g., Gordon et al., 2013; Platt et al., 2013, 2017) and
639 biomass burning (e.g., Akagi et al., 2012; Collier et al., 2016); however, to the best of the authors'
640 knowledge, it has not been used for SOA production over a megacity. As noted above, CO has
641 been typically used instead, given that it is always measured in pollution studies, and it typically
642 has a higher signal-to-background ratio than CO_2 in urban areas. Also, during spring and summer,
643 CO_2 is taken up by plants, which can reduce its signal-to-background ratio. However, the ratio of



644 other gases to CO can vary between urban areas depending on the average combustion efficiency
645 of the dominant sources (Silva et al., 2013). CO₂ better accounts for fuel consumption in an urban
646 area (Vay et al., 2009; Tang et al., 2018). Multiple recent studies have reported average emissions
647 ratios for different megacities based on high precision measurements of $\Delta\text{CO}/\Delta\text{CO}_2$ (Vay et al.,
648 2009; Wang et al., 2010; Peischl et al., 2013; Silva et al., 2013; Tohjima et al., 2014; Tang et al.,
649 2018). These results provide an ability to convert the $\Delta\text{OA}/\Delta\text{CO}$ determined in prior studies to
650 $\Delta\text{OA}/\Delta\text{CO}_2$ (Table S4). We find that for most of the megacities studied, $\Delta\text{OA}/\Delta\text{CO}_2$ is very
651 similar, though Mexico City and Seoul show higher values (approximately factor of 2). The range
652 of observed $\Delta\text{OA}/\Delta\text{CO}_2$ versus photochemical age is narrower, compared to the spread for all
653 megacities observed for $\Delta\text{OA}/\Delta\text{CO}$. Both analyses suggest that Seoul has larger relative emissions
654 of SOA precursors compared to other megacities, which could be targeted for air quality
655 improvement. However, more observations across other megacities and additional comparative
656 analyses would be beneficial.

657 **4.2 Composition-based analysis of the foreign versus South Korean contribution to SOA** 658 **precursors and SOA over Seoul**

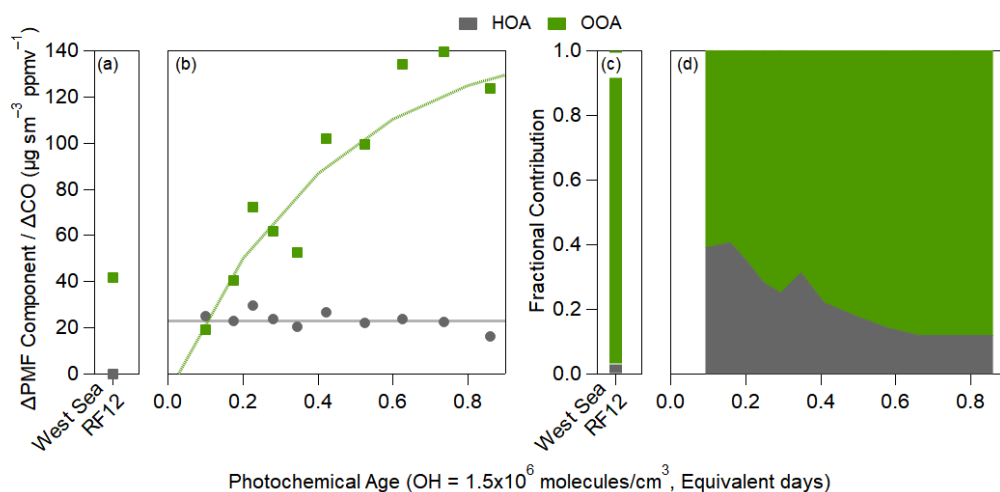
659 **4.2.1 Evolution of oxygenated organic aerosol over Seoul**

660 Here, we focus on the positive matrix factorization (PMF) (Ulbrich et al., 2009) factors for
661 OA resolved during KORUS-AQ, whose evolution over Seoul is shown in Figure 6. Total OOA
662 (LO-OOA plus MO-OOA) is used as a surrogate of total SOA. The fractional contribution of these
663 two factors can be found in Fig. S36. Rapid production of OOA is observed, accounting for all of
664 the observed growth in total OA over Seoul. LO-OOA, overall, is slightly more abundant than
665 MO-OOA (Fig. S36). LO-OOA has lower O/C compared to MO-OOA (Fig. S10); thus, the faster
666 production of LO-OOA likely represents the less oxidized OOA produced from the photooxidation



667 of SOA precursors (Hayes et al., 2013; Freney et al., 2014; Hu et al., 2016; Kim et al., 2018), while
 668 MO-OOA may represent the more oxidized species or those formed from later generations of
 669 oxidation (Robinson et al., 2007; Miracolo et al., 2010; Tritscher et al., 2011; Ortega et al., 2016;
 670 Sato et al., 2017; Schwantes et al., 2017).

671 The PMF factors have very different dilution-corrected concentrations over the West Sea
 672 during the “transport/polluted” event (Figure 6a). All Δ PMF factors/ Δ CO show much lower values
 673 than for aged air over Seoul. The discontinuity between the three factors between Seoul and West
 674 Sea indicate that transported OA, and transported SOA production, has limited impact on the OA
 675 over Seoul.



676

677 **Figure 6.** Same as Figure 4, but for the PMF results of the OA evolution over (a) West Sea during
 678 the polluted event (West Sea RF12 at ~1.75 equivalent days) and (b) over Seoul. For (b), fit to
 679 HOA and OOA are $23 \mu\text{g sm}^{-3} \text{ppmv}^{-1}$ and $150 \times (1 - \exp(-2.3 \times \text{eq. day}))$, respectively. For the OOA
 680 equation, 150 equals the max SOA. Fractional contribution of the PMF factors over (c) West Sea
 681 (RF12) and (d) over Seoul.

682 The slope of Δ HOA/ Δ CO versus age was nearly zero $\mu\text{g sm}^{-3} \text{ppmv}^{-1}$ equivalent day⁻¹,
 683 indicating minimal evolution within these timescales. There are mixed results on whether HOA
 684 changes with photochemical age (DeCarlo et al., 2010; Hayes et al., 2013; Hu et al., 2013, 2016;



685 Freney et al., 2014; Schroder et al., 2018); however, due to the uncertainty that comes from the
686 CO background, it is difficult to determine whether these changes are real or not.

687 At the lowest photochemical ages, HOA is ~35% of the total $\Delta\text{OA}/\Delta\text{CO}$ (Figure 6d). Since
688 HOA remains approximately constant with age while OOA rapidly increases (Figure 6b), the HOA
689 contribution to total $\Delta\text{OA}/\Delta\text{CO}$ decreases to ~10% after ~1 equivalent day. It has been observed
690 in prior urban campaigns that HOA contributes 10 – 50% and total POA (HOA + other primary
691 OA factors in AMS) contributes 30 – 60% (Aiken et al., 2009; DeCarlo et al., 2010; Hayes et al.,
692 2013; Crippa et al., 2014; Hu et al., 2016; H. Kim et al., 2017; Kim et al., 2018). The fractional
693 contribution of HOA in Seoul is within this range.

694 A more detailed discussion of the behavior of AMS OA source tracers can be found in SI
695 11. In general, the AMS OA source tracers behave similarly to other urban campaigns (e.g., Hayes
696 et al., 2013; Freney et al., 2014). Some dilute biomass burning OA was evident, but this source
697 was not major most of the KORUS-AQ. Similarly, isoprene oxidation chemistry was not a major
698 contributor to SOA during this campaign.

699 **4.2.2 Correlation of SOA versus other fast photochemical products**

700 Results above support that a major fraction of the SOA observed over Seoul is rapidly
701 produced through photooxidation of South Korean SOA precursors. To further evaluate this result,
702 we analyze the correlation of OOA with other secondary species known to be rapidly produced
703 through photooxidation of organic precursors.

704 The other secondary species used in this study are odd oxygen (O_x), formaldehyde (CH_2O),
705 peroxy acetyl nitrate (PAN), the sum of all acyl peroxy nitrates (ΣROONO_2), and pNO_3 . O_x
706 (approximated as $\text{NO}_2 + \text{O}_3$) is used instead of O_3 to account for titration of O_3 in the presence of
707 fresh NO emissions. Prior studies have used O_x to provide insights into SOA production (Herndon



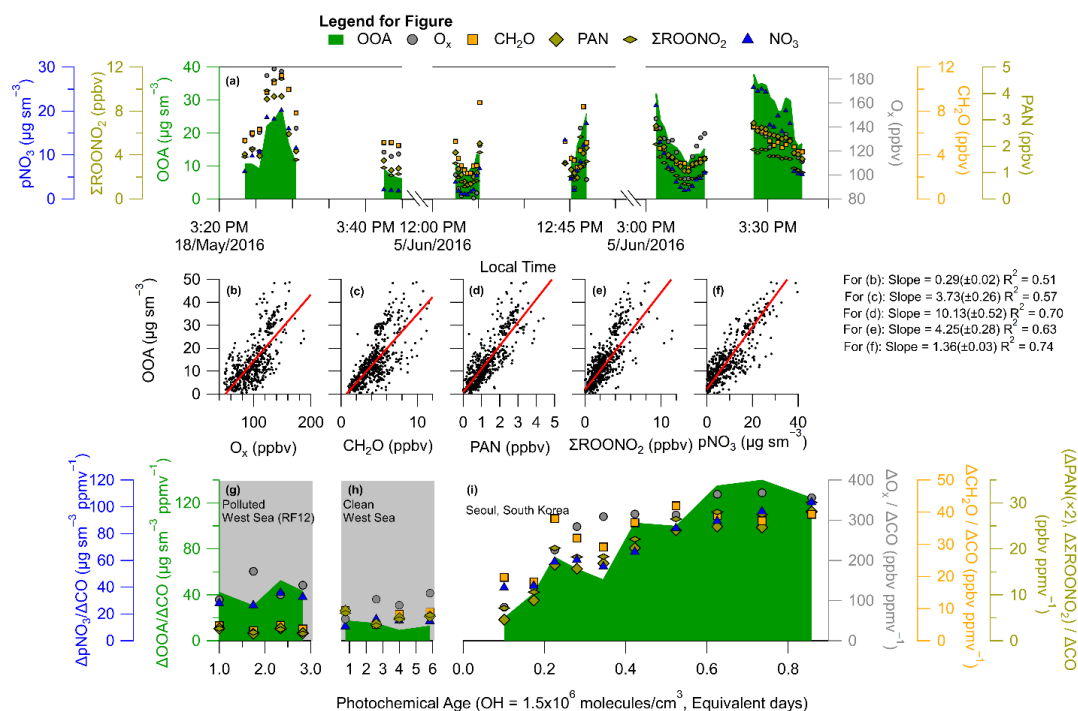
708 et al., 2008; Wood et al., 2010; Hayes et al., 2013; Morino et al., 2014; Zhang et al., 2015; Hu et
709 al., 2016) since O_x has a similar lifetime to SOA (~1 week) (Jacob, 2000; Goldberg et al., 2015;
710 Hodzic et al., 2015; Ortega et al., 2016), and O_x is also produced through the photooxidation of
711 organic compounds. However, since both O_x and SOA have longer lifetimes, the correlation
712 observed between these two species may have a contribution from transport of polluted air masses.
713 To reduce the influence of transport on this analysis, the correlation of OOA with CH_2O , PAN,
714 and $\Sigma ROONO_2$ is also investigated. The benefit of these species is that they have estimated
715 lifetimes of less than 3 hours during daytime in KORUS-AQ (typical temperature for transported
716 air 17°C). Also, it has been shown that dilution-corrected pNO_3 decreases rapidly from urban
717 centers, possibly due to dilution with surrounding air low in HNO_3 and NH_3 and irreversible uptake
718 of HNO_3 onto coarser particles (e.g., DeCarlo et al., 2008).

719 Example time series of OOA with O_x , CH_2O , PAN, $\Sigma ROONO_2$, and pNO_3 during three
720 different afternoon Seoul overpasses are shown in Figure 7a. All gas and aerosol species exhibit
721 similar behavior, indicating that these species are undergoing photochemical production during
722 these afternoon passes, similar to what has been observed in other urban environments during the
723 afternoon (Perring et al., 2010; Fried et al., 2011; Parrish et al., 2012; Hayes et al., 2013; Zhang et
724 al., 2015). OOA also tracks the evolution of these species, consistent with OOA also being a
725 secondary product from hydrocarbon photooxidation.

726 Analyzing the entire KORUS-AQ campaign, correlations with $R^2 > 0.50$ are observed
727 between OOA and O_x , CH_2O , PAN, $\Sigma ROONO_2$, and pNO_3 for the overpass observations after
728 12:00 LT (Figure 7b-f). These correlations for these secondary species produced through the
729 oxidation of hydrocarbons, in the afternoon, when photochemical production dominates over



730 mixing and losses, further supports that the OOA production observed in Figure 4 and 6 is
 731 dominated by the photochemistry of locally emitted hydrocarbons.



732

733 **Figure 7.** (a) Time series of OOA (OOA = LO-OOA + MO-OOA), O_x, CH₂O, PAN, ΣROONO₂,
 734 and pNO₃ during RF09 (18/May/2016), and RF18 (05/June/2016) noon and afternoon overpasses.
 735 Gaps in time series correspond to climbing out of the boundary layer. OOA versus (b) O_x (O_x =
 736 O₃ + NO₂), (c) CH₂O, (d) PAN, (e) ΣROONO₂, and (f) pNO₃ over Seoul, South Korea, during
 737 KORUS-AQ. For panels (b) – (f), the observations are after 12:00 local time (03:00 UTC), the
 738 black dots are all data, and the slopes (red line) is an ODR fit to the data. (g – i) Same as Figure 6
 739 for ΔOOA/ΔCO versus photochemical age, and including the dilution-corrected production of O_x,
 740 CH₂O, PAN, ΣROONO₂, and pNO₃. (g) is over the West Sea (RF12), (h) is over the West Sea
 741 (normal conditions) and (i) is over Seoul. Similar to Figure 4, the Δ corresponds to subtracting the
 742 background values for the respective species.

743 O_x, CH₂O, PAN, ΣROONO₂, and pNO₃, when dilution-corrected with ΔCO, show a similar
 744 trend as OOA (Figure 7i). From the lowest observed photochemical age (~0.1 equivalent day) to
 745 the highest (~0.85 equivalent day), O_x, CH₂O, PAN, ΣROONO₂, and pNO₃ increase by factors of
 746 4, 2, 7, 4, and 2, respectively. Over Mexico City, increases of factors of ~2 (CH₂O) (Fried et al.,



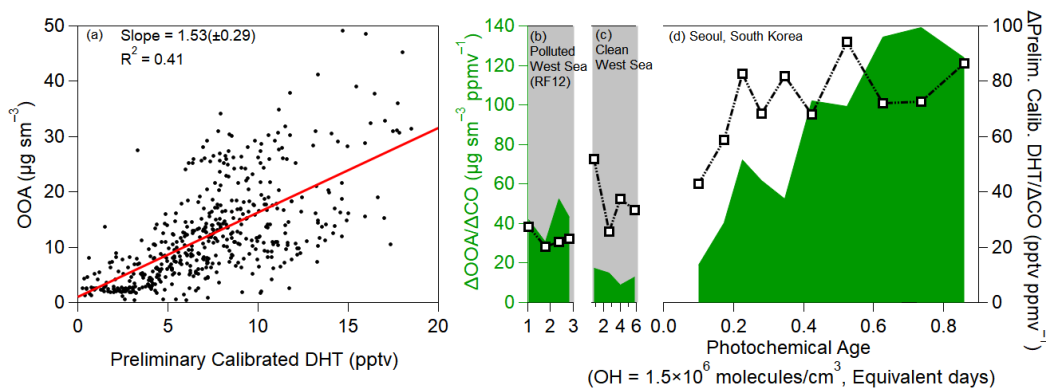
747 2011) and ~ 3 (ΣROONO_2) (Perring et al., 2010) were observed, which are comparable to the Seoul
748 observations. These rapid increases can only be explained by photooxidation of South Korean
749 primary emissions (hydrocarbons and NO_x).

750 The influence of the upwind, background air masses over the West Sea are investigated
751 and shown in Figure 7g and h. Over the West Sea, the dilution-corrected concentration of SOA,
752 O_x , CH_2O , PAN, ΣROONO_2 , and pNO_3 were all nearly constant. This indicates that the secondary
753 short-lived gas-phase species have reached steady state. Also, since dilution-corrected SOA
754 concentration is flat, this suggests that the SOA precursors have been depleted, and the SOA
755 production has ended, with SOA concentration reaching the plateau that is typically observed after
756 ~ 1 equivalent day (Ortega et al., 2016). The low PAN concentration and influence from transport
757 over the West Sea was also observed by Lee et al. (2012) over Baengyeoung Island, a regional
758 background monitoring location for Seoul and South Korea, during August 2010 and March –
759 April 2011. This further indicates low amounts of PAN are transported due to its thermal
760 decomposition and very short lifetime, and any production, and correlation, of PAN with OOA
761 would suggest local, photochemical production.

762 Besides the ubiquitous (but less specific) secondary species from organic compound
763 oxidation, OOA shows a robust correlation with dihydroxy toluene (DHT) (Figure 8), a known
764 SOA precursor from toluene photooxidation (Schwantes et al., 2017). DHT is very short lived,
765 with a photochemical lifetime of less than 1 hour, and it is formed under both low and high NO
766 conditions (Schwantes et al., 2017). The lower correlation, compared to the ubiquitous secondary
767 species, is possibly due to DHT forming from one precursor (toluene) instead of the broad range
768 of precursors that form OOA and O_x , PAN, and CH_2O . The correlation of OOA with a known
769 SOA precursor, that is very short-lived, again supports that OOA production is dominated by



770 photooxidation of locally emitted hydrocarbons, including toluene. The increasing ratio of OOA
771 to DHT also suggests that SOA production is fastest at low equivalent ages and is starting to
772 plateau at higher ages.



773

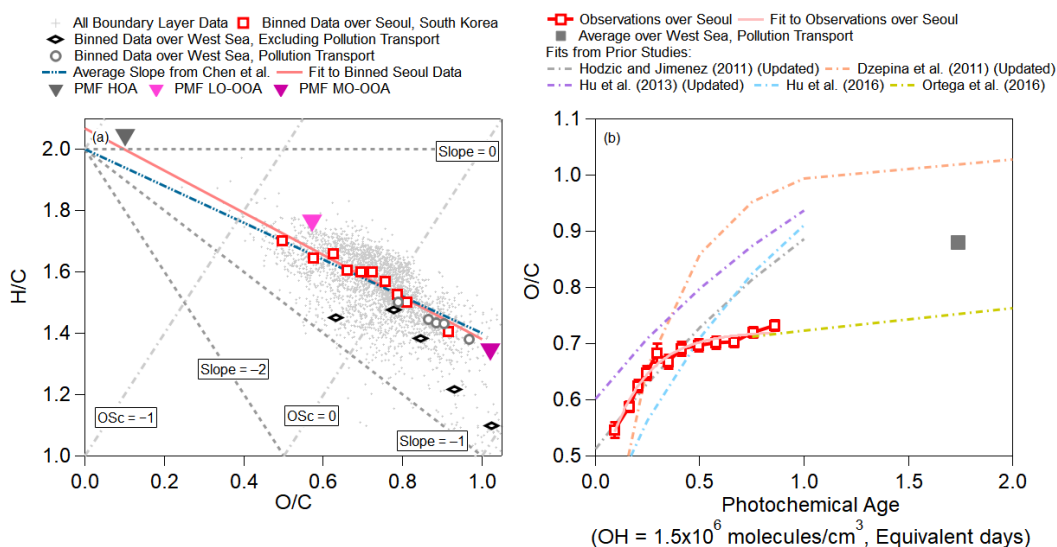
774 **Figure 8.** (a) Scatter plot of OOA versus DHT over Seoul, South Korea, during KORUS-AQ, after
775 12:00 local time (03:00 UTC). (b) Same as Figure 7f, but for DHT over the West Sea (RF12). (c)
776 Same as Figure 7g, but for DHT over the West Sea. (d) Same as Figure 7i, but for DHT over Seoul.
777 As an important note, concentrations of DHT are based on a preliminary calibration; however, any
778 further calibrations are not expected to impact the relative trend and general correlation.

779 The correlation between OOA and secondary species that have very short lifetimes further
780 suggest that the observed OOA is dominantly due to photooxidation of local emissions to produce
781 SOA and the other secondary species and not transport. This is due to the fact that the short
782 photochemical lifetimes of PAN, CH₂O, DHT, and ΣROONO₂ would cause the secondary species
783 to be in steady state. The observations over the West Sea, which is mainly upwind of Seoul and
784 thus background air, show much lower ratios. These two observations further suggest that local
785 SMA emissions are the precursors that undergo the rapid photooxidation to produce SOA, pNO₃,
786 and the other secondary species.



787 4.2.3 Oxidation state of SOA

788 We investigate the oxidation state of the observed OA with the van Krevelen diagram
 789 (Heald et al., 2010) in Figure 9a. The slope over Seoul (−0.69) is close to the average slope for
 790 numerous studies summarized by Chen et al. (2015) (−0.60) and similar to the range of slopes
 791 (−0.7 to −1.0) for studies impacted by urban pollution (Aiken et al., 2009; Docherty et al., 2011;
 792 Ge et al., 2012), including Los Angeles during CalNex (ranges from −0.64 to −0.68 from Hayes
 793 et al. (2013) and Ortega et al. (2016)) or chamber studies investigating the photooxidation of
 794 combustion exhausts (Heald et al., 2010; Lambe et al., 2012; Jathar et al., 2013; Presto et al., 2014;
 795 Tkacik et al., 2014; Liu et al., 2015). This generally indicates that the photochemistry controlling
 796 the production of SOA is similar in urban areas, including photooxidation of diesel and gasoline
 797 emissions, evaporative diesel and gasoline, and cooking emissions (Hayes et al., 2015; Woody et
 798 al., 2016; Janssen et al., 2017; Ma et al., 2017; Kim et al., 2018).



799

800 **Figure 9.** (a) Van Krevelen diagram for all of KORUS-AQ. $\text{OSc} = (\text{O}/\text{C} - 2 \times \text{H}/\text{C})$ (Kroll et al.,
 801 2011). The observations are binned, into deciles, for observations over Seoul, South Korea, and
 802 binned, into 5 bins, for clean West Sea, and polluted West Sea. The teal line represents the average
 803 slope reported in Chen et al. (2015) of −0.60, and the light red line represents the slope (slope =



804 $-0.69(\pm 0.15)$, y-intercept= $2.07(\pm 0.11)$) observed over Seoul, South Korea, during the campaign.
805 (b) Binned O/C from observations versus photochemical age, over Seoul, South Korea, and
806 averaged O/C versus photochemical clock over polluted West Sea. The light red line is the fit to
807 the observations over Seoul during KORUS-AQ. The values of O/C versus photochemical age
808 from Hodzic and Jimenez (2011), Dzepina et al. (2011), Hu et al. (2013), are updated with
809 calibrations of Canagaratna et al. (2015); whereas, Hu et al. (2016), and Ortega et al. (2016) did
810 not need updates.

811 The “transport/polluted” evolution of H/C versus O/C falls on the same slope as the
812 observations over Seoul; however, the values lie at higher O/C ratios, indicative of more aged
813 OOA. O/C versus H/C during the “transported/polluted” event over the West Sea is also
814 comparable to the H/C versus O/C slope (-0.63) observed in Chinese outflow at Changdao (Hu et
815 al., 2013). On the other hand, O/C versus H/C over the West Sea during “clean” events show
816 distinctly lower values and a steeper evolution (slope = -1.1).

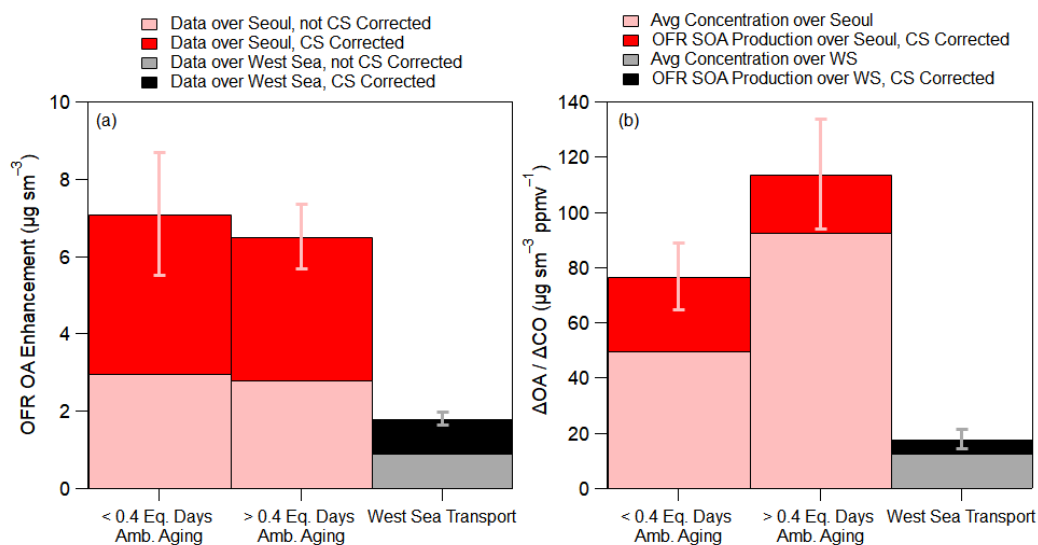
817 The evolution of O/C with photochemical age over Seoul and over the West Sea is shown
818 in Figure 9b, along with results from prior studies (Dzepina et al., 2011; Hodzic and Jimenez,
819 2011; Hu et al., 2013, 2016; Ortega et al., 2016). Note that older studies have been updated with
820 the calibration of Canagaratna et al. (2015). For the first 0.5 equivalent days, O/C is nearly identical
821 to the Mexico City observations (Hodzic and Jimenez, 2011); however, after 0.5 equivalent days,
822 the O/C ratio growth slows down. The O/C evolution then becomes more similar to that observed
823 when processing Los Angeles air in an OFR (Ortega et al., 2016). The evolution of O/C over Seoul
824 is at the low end of the range of values observed from prior megacities. The average O/C value
825 observed over the West Sea during RF12 is more similar to the values observed after 1 equivalent
826 day in two sites in China (Hu et al., 2013, 2016).

827 **4.4 Influence of local versus transported SOA precursors to SOA production over Seoul**

828 OFR results can be used to investigate the role of SOA production from South Korean and
829 Seoul emissions versus long-distance transported SOA precursors. As shown in prior studies
830 (Ortega et al., 2016; Palm et al., 2016, 2017, 2018), the SOA potential decreases drastically in the



831 daytime, as the most reactive compounds to OH have already oxidized and formed SOA. Thus,
832 these results will not directly capture the full emitted SOA potential for Seoul, South Korea. Also,
833 recent studies indicate that lower volatility species (e.g., S/IVOCs) can be lost to tubing walls, or
834 their transfer can be greatly delayed (Pagonis et al., 2017; Deming et al., 2018). Thus, it is likely
835 that the OFR inlet line on the DC-8 acted at least as a partial sink of S/IVOCs and thus reduced
836 the measured potential SOA. As a reminder, a correction is included for the condensational sink
837 (CS) of LVOC in the OFR based on Eq. (1).



838

839 **Figure 10.** (a) Comparison of OFR OA enhancement (OFR OA enhancement = OA exiting OFR
840 – ambient OA) over Seoul, South Korea, and the West Sea, corrected for evaporation losses. The
841 difference between the two stacked shaded bars is that the lighter (bottom) shade has no CS
842 correction whereas the darker shade does. (b) The lighter colored represents the average dilution-
843 corrected observed ambient OA preexisting concentration corresponding to the OFR observations
844 of the same air mass. The darker color represents the dilution-corrected SOA production in the
845 OFR. The average additional photochemical age added in the OFR is ~ 4 days ($\text{OH}_{\text{exp}} \sim 5.4 \times 10^{11}$
846 molecules/ $\text{cm}^3 \times \text{s}$) for both over Seoul and West Sea. Also, the observations for the West Sea are
847 for all flights, not including RF12, where the average $\Delta\text{OA}/\Delta\text{CO}$ was $13 \mu\text{g sm}^{-3} \text{ppmv}^{-1}$. For both
848 (a) and (b), the OFR observations over Seoul are split between lower and higher equivalent ages
849 (see x-axis). The average ambient ages for the two bars are 0.17 and 0.63 equivalent days. Error
850 bars are the standard errors of the observations.



851 The average OA enhancement in the OFR (OA Enhancement = OA in OFR – Ambient
852 OA) in Seoul is slightly greater for the less aged ambient air (7.1 ± 1.6 versus $6.5 \pm 0.8 \mu\text{g sm}^{-3}$) but
853 both values lie within the range of the measurements (Figure 10a). The less aged ambient air show
854 slightly higher OA enhancement suggests that more SOA precursors might have been present and
855 available to form SOA mass (Ortega et al., 2016; Palm et al., 2016, 2017, 2018). The OA
856 enhancement observed over Seoul was a factor of 3.5 greater than observed over the West Sea (~ 7
857 $\mu\text{g sm}^{-3}$ over Seoul versus $\sim 2 \mu\text{g sm}^{-3}$ over the West Sea). The much higher SOA formation
858 potential observed over Seoul versus the West Sea indicates that the majority of the precursors that
859 led to the observed SOA and SOA production over Seoul originated from local emissions,
860 consistent with results above.

861 Plotting the OA enhancements as $\Delta\text{OA}/\Delta\text{CO}$, similar to Figure 4, the amount of ambient
862 SOA production, not including pre-existing OA, for ambient air that has aged less than 0.4
863 equivalent days is $27(\pm 12) \mu\text{g sm}^{-3} \text{ppmv}^{-1}$, a 50% increase compared to the average $\Delta\text{OA}/\Delta\text{CO}$
864 observed over Seoul at the same ambient photochemical age (Figure 10b). For air older than 0.4
865 equivalent days, the increase is slightly smaller ($21(\pm 20) \mu\text{g sm}^{-3} \text{ppmv}^{-1}$ above ambient pre-
866 existing OA) since a large fraction of the most reactive, high aerosol producing compounds have
867 already been depleted and produced ambient SOA (Ortega et al., 2016; Palm et al., 2016, 2017,
868 2018).

869 Finally, there is still a small amount of SOA production potential in the air transported over
870 the West Sea to Seoul. The average potential, not including pre-existing OA, is $5(\pm 4) \mu\text{g sm}^{-3}$
871 ppmv^{-1} . This is a factor of 4 – 5 less than the potential SOA production observed in the OFR for
872 Seoul. Including the pre-existing dilution-corrected OA for the West Sea observation ($18 \mu\text{g sm}^{-3}$
873 ppmv^{-1}), the concentration is approximately a factor of 8.5 less than the maximum ambient



874 dilution-corrected OA concentration and a factor of 6 – 8 less than the total dilution corrected OA
875 concentration exiting the OFR. Some of this remaining production would have been further
876 consumed during transport between the West Sea and Seoul (typically 1 day); therefore, it is not
877 expected to significantly impact the SOA production over Seoul. This further indicates that, during
878 this campaign, the transported SOA precursors to Seoul from foreign sources did not contribute
879 significantly to the overall observed SOA production.

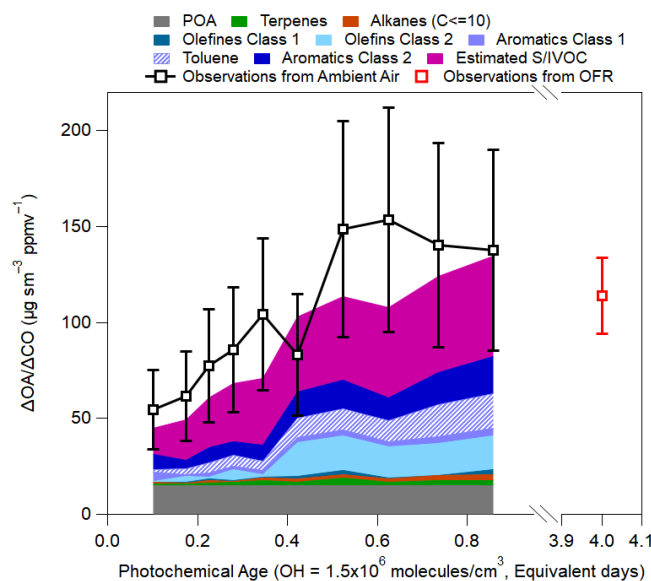
880 **4.5 Calculated precursor contributions to the SOA production over Seoul**

881 We use a simple SOA model (Dzepina et al., 2009; Zhao et al., 2014) to calculate the
882 contribution of various precursors to SOA over Seoul (Figure 11, details in Sect. SI 6). Observed
883 hydrocarbons (Table 2), from WAS, along with estimated S/IVOC (Robinson et al., 2007; Dzepina
884 et al., 2009; Hayes et al., 2015) and SOA yields updated to account for vapor wall losses (Ma et
885 al., 2017) were used to estimate (SI Eq. (S3) and (S4)) the contribution of various precursors to
886 SOA production observed over Seoul. Dzepina et al. (2009) and Hayes et al. (2015) both found
887 that the “Robinson” parameterization of SOA from S/IVOC was consistent with SOA production
888 in Mexico City and Los Angeles for observations at 1 equivalent day or less; thus, the same
889 parameterizations are used here.

890 The percent difference between the modeled and measured total OA ranged between –24
891 to 32% with an average value of the observations being 15% higher. This provides confidence that
892 the calculation described in SI 6 captures the chemical production of SOA over Seoul. Also, the
893 difference between the estimated and measured OA is comparable to, or better than, found in other
894 studies that utilized a similar modeling approaches (Dzepina et al., 2009; Zhao et al., 2014, 2016;
895 Hayes et al., 2015; Huang et al., 2015; Ma et al., 2017), and within the uncertainty of the measured
896 OA (38%, 2σ).



897 This box model does not explicitly consider volatile consumer products (VCPs) (Khare
898 and Gentner, 2018; McDonald et al., 2018), S/IVOC from cooking emissions (e.g., Hayes et al.,
899 2013; Ots et al., 2016), or glyoxal (Volkamer et al., 2006; Knote et al., 2014), although
900 contributions from these components may be partially included in the empirical estimation of
901 S/IVOC. Modeled SOA in Los Angeles, using estimates of S/IVOC from $\Delta\text{HOA}/\Delta\text{CO}$, including
902 $\sim 2/3$ of VCPs and not including glyoxal, were able to capture the observed SOA in the first 0.5
903 equivalent days (Hayes et al., 2015; McDonald et al., 2018), similar to the results here.



904

905 **Figure 11.** Calculated SOA production for KORUS-AQ. POA is from observations shown in
906 Figure 6, and the observations of $\Delta\text{OA}/\Delta\text{CO}$ are from Figure 4. The SOA precursor classes are
907 defined in Table 2. Note, Toluene is part of Aromatics Class 1 (light purple), but it is shown
908 separately for discussion. The error bars represent the uncertainty in OA ($\pm 38\%$). The OFR
909 observations, and error bars, are from Figure 10.



910 **Table 2.** Definition of classes used in Figure 11. The VOCs listed in the table were all measured
911 by WAS.

<i>Class</i>	<i>Included Compounds or Parameterization</i>
Terpenes	alpha-pinene, beta-pinene
Alkanes ($C \leq 10$)	methyl-cyclopentane, cyclohexane, methyl-cyclohexane, n-hetpane, n-octane, n-nonane, n-decane,
Olefins Class 1	1-butene, i-butene, cis-butene, trans-butene
Olefins Class 2	Styrene, 1,3-butadiene
Aromatics Class 1	benzene, toluene, isopropylbenzene, n-propylbenzene, ethylbenzene,
Aromatics Class 2	m+p-xylene, o-xylene, 3-ethyltoluene, 4-ethyltoluene, 1,2,3-trimethylbenzene, 1,2,4-trimethylbenzene, 1,3,5-trimethylbenzene
Estimated S/IVOC	$6.7^a \times \Delta HOA / \Delta CO$ ($\Delta HOA / \Delta CO = 22 \mu g \text{ sm}^{-3} \text{ ppmv}^{-1}$ from Figure 6)

912 ^aThis value is taken from Dzepina et al. (2009), which is based on partitioning calculations.

913 The most important calculated SOA precursors are S/IVOC and the most reactive
914 aromatics (Table 2). These two classes of compounds comprise ~70% of the total modeled SOA
915 over Seoul. The calculation further supports the conclusions from multiple previous studies
916 (Dzepina et al., 2009, 2011; Hodzic et al., 2010; Chen et al., 2015; Hayes et al., 2015; Ma et al.,
917 2017) that aromatics and primary S/IVOC dominate SOA formation over different urban
918 environments. A consistent feature across most species in both classes of compounds is that they
919 all have photochemical lifetimes of less than 1 equivalent day and less than 4 actual hours for the
920 average observed daytime OH (6×10^6 molecules/cm³) over Seoul. With the typical wind speeds
921 during KORUS-AQ (~4 m/s), the lifetime of these species would limit their transport
922 approximately 60 km during daytime. Since these compounds have short photochemical lifetimes,
923 and they compose the majority of the calculated SOA budget, our conclusion that the SOA
924 production over Seoul originates from local emissions is further supported.

925 Numerous prior studies have shown the importance of S/IVOC in order to explain the
926 observed SOA production (Robinson et al., 2007; Dzepina et al., 2009, 2011; Grieshop et al., 2009;
927 Pye and Seinfeld, 2010; Hodzic et al., 2010; Zhao et al., 2014; Jathar et al., 2014; Chen et al.,
928 2015; Hayes et al., 2015; Palm et al., 2016, 2017, 2018; Ortega et al., 2016; Janssen et al., 2017;



929 Ma et al., 2017). Until recently, it has been analytically challenging to measure these compounds
930 (Ait-Helal et al., 2014; Zhao et al., 2014; Hunter et al., 2017), and they can make up a small fraction
931 of the total measured, and speciated, hydrocarbons in an urban location (Ait-Helal et al., 2014;
932 Zhao et al., 2014). However, due to the higher initial molecular weight, S/IVOC already have a
933 low saturation concentration ($C^* \sim 1 - 1000 \mu\text{g m}^{-3}$ for SVOC and $\sim 1 \times 10^4 - 1 \times 10^6$ for IVOC),
934 especially compared to aromatic compounds ($C^* \sim 10^7 \mu\text{g m}^{-3}$); thus, any addition of functional
935 groups will more easily lead to the partitioning of oxidized S/IVOC to the particle phase (Robinson
936 et al., 2007; Hayes et al., 2015; Ma et al., 2017). In urban environments, S/IVOC emissions come
937 from numerous sources, including transportation, cooking, and VCPs (Robinson et al., 2007;
938 Hayes et al., 2015; Woody et al., 2016; Janssen et al., 2017; Ma et al., 2017; McDonald et al.,
939 2018).

940 The next most important compound is toluene, composing $9(\pm 3)\%$ of the estimated SOA
941 production. Though this single compound is as important as the rest of Aromatics Class 1, Olefins
942 Class 1 and 2, alkanes, and terpenes (Table 2) combined, it does not contribute the majority of the
943 calculated SOA budget, as was recently suggested in another study (Wu et al., 2016). The average
944 aerosol yield for toluene used in this study ($Y \approx 0.30$) is similar to the value used in Wu et al.
945 (2016) and recommended by Hildebrandt et al. (2015). The aerosol yield is similar for all
946 aromatics; however, the more reactive aromatics will contribute more SOA per unit precursor at
947 shorter photochemical ages. The longer photochemical lifetime (factor of 2) for toluene decreases
948 the overall amount of SOA produced compared to the very reactive aromatics.

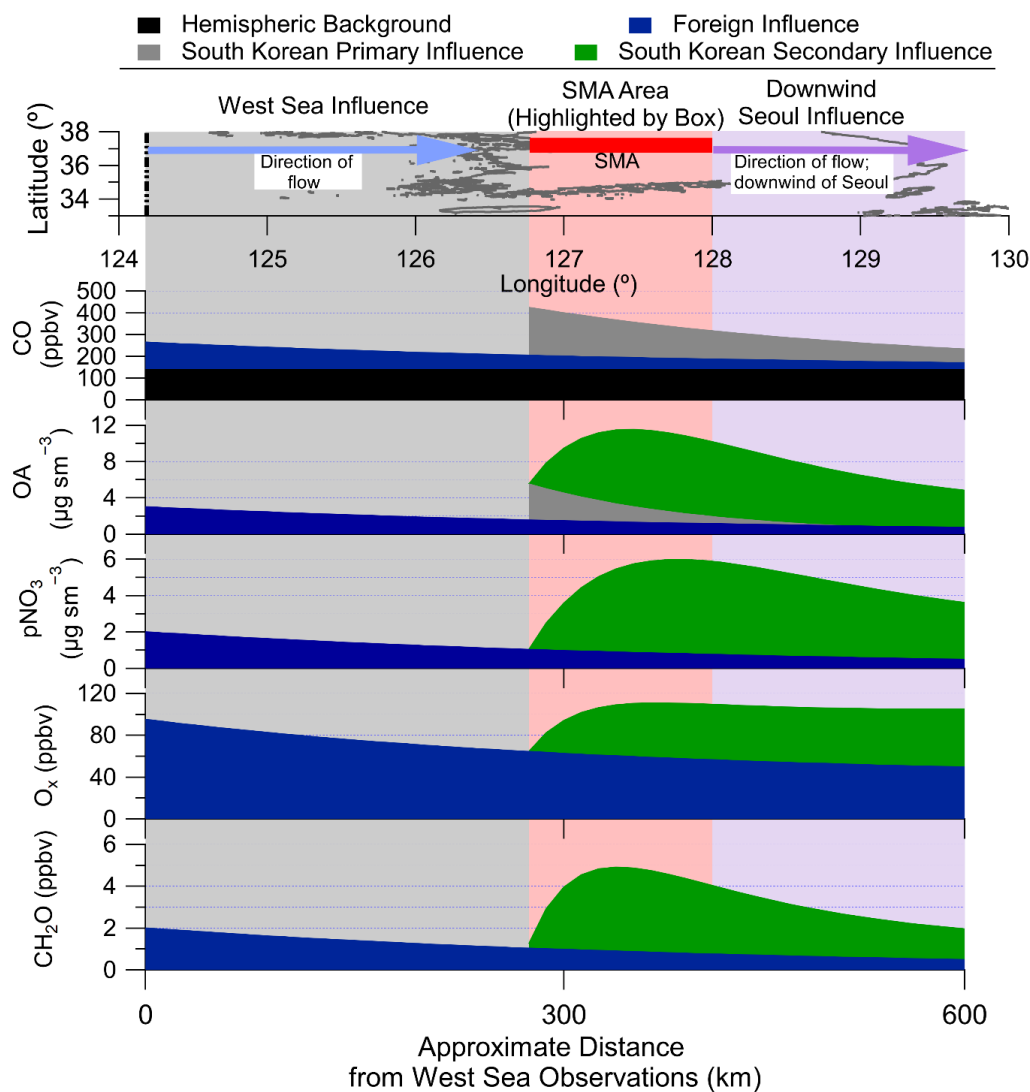
949 **4.6 Conceptual model representing rapid photochemical production**

950 A conceptual model representing rapid photochemical production of SOA, pNO₃, O_x, and
951 CH₂O is presented here. For the model, the flow is simplified to be from the west to the east. The



952 lateral and vertical dilution have been represented as the equivalent first order rate, constrained by
953 observations ($\sim 0.7 \text{ day}^{-1}$). Also, the hemispheric and foreign transport is accurate on average based
954 on observations, and is discussed in Sect. 3.3. For the production over Seoul, it is represented by
955 photochemical aging, constrained by observations (Figure 7i), as a first order rate. Thus, the
956 important processes are represented with realistic quantitative constraints, but in a simple enough
957 system to demonstrate the impact of the secondary chemistry from Seoul.

958 The results are shown in Figure 12. The figure summarizes and demonstrates the results
959 discussed throughout the paper. First, as discussed in Sect. 3.2 and 4.2, there is no clear net
960 production of the pollutants over the West Sea. Instead, they undergo dilution as the air travels
961 across the West Sea. Then, as the air enters SMA area, there are fresh injections of primary
962 emissions (CO, HOA, hydrocarbons, and NO_x). These primary emissions undergo rapid
963 photooxidation to produce SOA, pNO_3 , O_x , and CH_2O , as detailed in Sect. 4.2. As demonstrated
964 in Figure 12, most of the production occurs with SMA prior to dilution taking over. This
965 demonstrates that the emissions and subsequent chemistry from SMA are directly impacting the
966 residents of SMA. Thus, control of the primary pollutants, including the SOA precursors discussed
967 in Sect. 4.5 (aromatics and S/IVOC), and NO_x , would substantially reduce concentration of the
968 secondary photochemical products impacting SMA, even during period of higher foreign transport
969 than observed during KORUS-AQ.



970

971 **Figure 12.** Conceptual model representing the transport of background into Seoul, and the
 972 emissions of primary species (CO and HOA) and photochemical production of secondary species
 973 (SOA, pNO₃, O_x, and CH₂O) impacting Seoul.



974 **5. Summary**

975 A suite of aerosol- and gas-phase measurements were made over Seoul and the West Sea
976 during May and June, 2016, as part of the KORUS-AQ campaign. The results from this study are
977 summarized below.

978 (1) Using a combination of a Lagrangian backtrajectory model (FLEXPART) and
979 observations, the hemispheric CO background was estimated to be 140 ppbv, the CO foreign
980 background over Seoul was estimated to be 60 ppbv, and the remainder of the CO over Seoul was
981 due to South Korean emissions. The CO background analysis allows estimating background values
982 for other species used throughout this study. In particular, the OA background was estimated to be
983 between 1 – 3 $\mu\text{g sm}^{-3}$.

984 (2) FLEXPART was also used for source analysis of NO₂, as a surrogate for SOA
985 precursors. NO₂ has a photochemical lifetime of less than 1 day (similar to the dominant urban
986 SOA precursors). Results from FLEXPART indicate that greater than 90% of NO₂ originates from
987 South Korea, consistent with most of the important SOA and pNO₃ precursors also originating
988 there.

989 (3) Factor analysis of OA showed that the OA growth over Seoul was dominated by OOA
990 (surrogate for SOA). This OOA (background subtracted) was low at low photochemical ages and
991 rapidly increased throughout the day as photochemistry occurred. This points to local emissions
992 controlling SOA production over Seoul.

993 (4) OOA was correlated with secondary gas-phase species, including O_x (O₃ + NO₂),
994 formaldehyde, peroxy acetyl nitrates, sum of acyl peroxy nitrates, dihydroxy toluene, and pNO₃.
995 Correlation with these species indicates that the SOA was produced from local emissions and



996 photochemistry since some of these compounds (CH_2O and PAN) had photochemical lifetimes of
997 less than three daytime hours during KORUS-AQ.

998 (5) Using an airborne OFR for the first time, the amount of potential SOA produced from
999 air sampled over Seoul was a factor of three higher than for air sampled over the West Sea (a
1000 background inflow location). This points to local SOA precursor emissions from Seoul, and
1001 subsequent rapid photochemistry, causing the increase in SOA observed over Seoul. The air
1002 sampled over West Sea did not have enough SOA precursors to cause the SOA production
1003 observed over Seoul.

1004 (6) A simple box model showed good agreement with the measured SOA growth. This
1005 allows an estimation of the contribution of various precursors to SOA over Seoul. Hydrocarbons
1006 with a photochemical lifetime of less than one day dominate the production of SOA. Specifically,
1007 short lived aromatic compounds (i.e., ethyltoluenes, xylenes, trimethylbenzenes) and S/IVOC are
1008 the main precursors to SOA, accounting for 70% of the calculated SOA. Toluene was found to
1009 contribute 9% of the calculated SOA.

1010 (7) Over Seoul, a large megacity with numerous sources of emissions, local emissions and
1011 their photochemical products overwhelm the foreign influence during KORUS-AQ. However, for
1012 smaller cities or more rural areas in South Korea that are not downwind of Seoul or other large
1013 sources, the foreign influence can more easily overwhelm the smaller local emissions. Thus,
1014 outside of the Seoul Metropolitan Area, the foreign influence has a greater impact on the air
1015 quality. During periods in which the foreign influence is larger than during KORUS-AQ (due to
1016 more favorable transport conditions), it will be more comparable to the importance of the Seoul
1017 emissions. However, given the apparently stronger emissions of SOA precursors than in other
1018 megacities, reducing South Korean emissions should improve air quality under all conditions.

**1019 Author Contribution**

1020 BAN, PCJ, DAD, JCS, and JLJ collected the AMS data; BA, AJB, CAC, and KLT collected the
1021 data from LARGE; DRB collected the WAS data; WHB collected the OH, HO₂, and OHR
1022 data; YC and JPD collected the CO measurements from Picarro; JD and ES collected
1023 MC/IC and filter measurements; GD and SEP collected H₂O and ambient CO
1024 measurements; AF collected CH₂O measurements; LGH collected PAN, PPN, and SO₂
1025 measurements; MJK collected HNO₃, DHT, and HCN measurements; CK ran the
1026 FLEXPART analysis; KDL collected the BC measurements; TL and TP collected the
1027 KAMS data; and, JHW provided the emissions for the FLEXPART analysis. JAdG assisted
1028 in the analysis of the photochemical clocks and SOA production. BAN and JLJ prepared
1029 the original manuscript, and all authors contributed to the review and editing of the
1030 manuscript.

1031

1032 Acknowledgements

1033 This study was supported by NASA grants NNX15AT96G & 80NSSC18K0630, and EPA STAR
1034 83587701-0. It has not been formally reviewed by EPA. The views expressed in this
1035 document are solely those of the authors and do not necessarily reflect those of EPA. EPA
1036 does not endorse any products or commercial services mentioned in this publication. Joost
1037 de Gouw worked as a part-time consultant for Aerodyne Research Inc during the
1038 preparation phase of this manuscript. The authors acknowledge Joshua Schwarz and Anne
1039 Perring for the use of their black carbon data, Ronald Cohen, Paul Wooldridge, and Paul
1040 Romer for use of their ΣRONO₂ and ΣROONO₂ data, Paul Wennberg and John Crounse
1041 for the use of their HCN, DHT, and HNO₃ data, Armin Wisthaler for the use of their PTR-
1042 MS data, and Andrew Weinheimer and Denise Montzka for the use of their O₃, NO_x, and
1043 NO_y data. Finally, the authors acknowledge the NOAA ESRL GMD CCGG for the use of
1044 the CO measurements in Mongolia and China for the background measurements.

1045

1046 Data Availability

1047 Measurements and FLEXPART results from the KORUS-AQ campaign are available at
1048 <https://www-air.larc.nasa.gov/cgi-bin/ArcView/korusaq>. Measurements for the CO
1049 background are available at ftp://aftp.cmdl.noaa.gov/data/trace_gases/co/flask/surface/.

1050

1051 Competing Interests

1052 The authors declare that they have no conflict of interest.



1 References

- 2 Aiken, A. C., Salcedo, D., Cubison, M. J., Huffman, J. A., DeCarlo, P. F., Ulbrich, I. M., Docherty,
3 K. S., Sueper, D., Kimmel, J. R., Worsnop, D. R., Trimborn, A., Northway, M., Stone, E. A.,
4 Schauer, J. J., Volkamer, R. M., Fortner, E., de Foy, B., Wang, J., Laskin, A., Shutthanandan, V.,
5 Zheng, J., Zhang, R., Gaffney, J., Marley, N. A., Paredes-Miranda, G., Arnott, W. P., Molina, L.
6 T., Sosa, G. and Jimenez, J. L.: Mexico City aerosol analysis during MILAGRO using high
7 resolution aerosol mass spectrometry at the urban supersite (T0) – Part 1: Fine particle composition
8 and organic source apportionment, *Atmos. Chem. Phys.*, 9(9), 6633–6653, doi:10.5194/acpd-9-
9 8377-2009, 2009.
- 10 Ait-Helal, W., Borbon, A., Sauvage, S., De Gouw, J. A., Colomb, A., Gros, V., Freutel, F., Crippa,
11 M., Afif, C., Baltensperger, U., Beekmann, M., Doussin, J.-F. F., Durand-Jolibois, R., Fronval, I.,
12 Grand, N., Leonardis, T., Lopez, M., Michoud, V., Miet, K., Perrier, S., Prévôt, A. S. H.,
13 Schneider, J., Siour, G., Zapf, P. and Locoge, N.: Volatile and intermediate volatility organic
14 compounds in suburban Paris: Variability, origin and importance for SOA formation, *Atmos.*
15 *Chem. Phys.*, 14(19), 10439–10464, doi:10.5194/acp-14-10439-2014, 2014.
- 16 Akagi, S. K., Craven, J. S., Taylor, J. W., Mcmeeking, G. R., Yokelson, R. J., Burling, I. R.,
17 Urbanski, S. P., Wold, C. E., Seinfeld, J. H., Coe, H., Alvarado, M. J. and Weise, D. R.: Evolution
18 of trace gases and particles emitted by a chaparral fire in California, *Atmos. Chem. Phys.*, 12,
19 1397–1421, doi:10.5194/acp-12-1397-2012, 2012.
- 20 Aknan, A. and Chen, G.: KORUS-AQ DC-8 Aircraft Dataset, [online] Available from:
21 <https://www-air.larc.nasa.gov/cgi-bin/ArcView/korusaq> (Accessed 6 December 2018), 2018.
- 22 Al-Saadi, J., Carmichael, G., Crawford, J., Emmons, L., Korean, S. K., Group, S., Song, C.-K.,
23 Chang, L.-S., Lee, G., Kim, J. and Park, R.: NASA Contributions to KORUS-AQ: An International
24 Cooperative Air Quality Field Study in Korea, 2015.
- 25 Anderson, T. L. and Ogren, J. A.: Determining Aerosol Radiative Properties Using the TSI 3563
26 Integrating Nephelometer, *Aerosol Sci. Technol.*, 29(1), 57–69,
27 doi:10.1080/02786829808965551, 1998.
- 28 Arnold, S. R., Methven, J., Evans, M. J., Chipperfield, M. P., Lewis, A. C., Hopkins, J. R.,
29 Mcquaid, J. B., Watson, N., Purvis, R. M., Lee, J. D., Atlas, E. L., Blake, D. R. and Rappenglück,
30 B.: Statistical inference of OH concentrations and air mass dilution rates from successive
31 observations of nonmethane hydrocarbons in single air masses, *J. Geophys. Res. Atmos.*, 112,
32 D10S40, doi:10.1029/2006JD007594, 2007.
- 33 Bahreini, R., Dunlea, E. J., Matthew, B. M., Simons, C., Docherty, K. S., DeCarlo, P. F., Jimenez,
34 J. L., Brock, C. A. and Middlebrook, A. M.: Design and Operation of a Pressure-Controlled Inlet
35 for Airborne Sampling with an Aerodynamic Aerosol Lens, *Aerosol Sci. Technol.*, 42(6), 465–
36 471, doi:10.1080/02786820802178514, 2008.
- 37 Bahreini, R., Ervens, B., Middlebrook, A. M., Warneke, C., de Gouw, J. A., DeCarlo, P. F.,
38 Jimenez, J. L., Brock, C. A., Neuman, J. A., Ryerson, T. B., Stark, H., Atlas, E., Brioude, J., Fried,
39 A., Holloway, J. S., Peischl, J., Richter, D., Walega, J., Weibring, P., Wollny, A. G. and
40 Fehsenfeld, F. C.: Organic aerosol formation in urban and industrial plumes near Houston and
41 Dallas, Texas, *J. Geophys. Res.*, 114(16), D00F16, doi:10.1029/2008JD011493, 2009.
- 42 Baklanov, A., Molina, L. T. and Gauss, M.: Megacities, Air Quality and Climate, *Atmos. Environ.*,
43 126, 235–249, doi:10.1016/j.atmosenv.2015.11.059, 2016.



- 1 Blake, N. J., Blake, D. R., Sive, B. C., Katzenstein, A. S., Meinardi, S., Wingenter, O. W., Atlas,
2 E. L., Flocke, F., Ridley, B. A. and Rowland, F. S.: The seasonal evolution of NMHC's and light
3 alkyl nitrates at middle to northern latitudes during TOPSE, *J. Geophys. Res.*, 108(D4), 8359,
4 2003.
- 5 Campuzano-Jost, P., Day, D. A., Nault, B. A., Schroder, J. C. and Jimenez, J. L.: Temporal
6 Variability of the Pieber Effect and Some Notes on AMS Dection Limits, in 17th AMS Users'
7 Meeting, Portland. [online] Available from: [http://cires1.colorado.edu/jimenez-](http://cires1.colorado.edu/jimenez-group/UsrMtg/UsersMtg17/10-14-2016_PCJ_AMSUsersMtg_Prez.pdf)
8 [group/UsrMtg/UsersMtg17/10-14-2016_PCJ_AMSUsersMtg_Prez.pdf](http://cires1.colorado.edu/jimenez-group/UsrMtg/UsersMtg17/10-14-2016_PCJ_AMSUsersMtg_Prez.pdf) (Accessed 5 April 2018),
9 2016.
- 10 Canagaratna, M. R., Jayne, J. T., Jimenez, J. L., Allan, J. D., Alfarra, M. R., Zhang, Q., Onasch,
11 T. B., Drewnick, F., Coe, H., Middlebrook, A. M., Delia, A., Williams, L. R., Trimborn, A. M.,
12 Northway, M. J., DeCarlo, P. F., Kolb, C. E., Davidovits, P. and Worsnop, D. R.: Chemical and
13 microphysical characterization of ambient aerosols with the Aerodyne Aerosol Mass
14 Spectrometer, *Mass Spectrom. Rev.*, 26(2), 185–222, doi:10.1002/mas, 2007.
- 15 Canagaratna, M. R., Jimenez, J. L., Kroll, J. H., Chen, Q., Kessler, S. H., Massoli, P., Hildebrandt
16 Ruiz, L., Fortner, E., Williams, L. R., Wilson, K. R., Surratt, J. D., Donahue, N. M., Jayne, J. T.
17 and Worsnop, D. R.: Elemental ratio measurements of organic compounds using aerosol mass
18 spectrometry: characterization, improved calibration, and implications, *Atmos. Chem. Phys.*,
19 15(1), 253–272, doi:10.5194/acp-15-253-2015, 2015.
- 20 Cappa, C. D. and Jimenez, J. L.: Quantitative estimates of the volatility of ambient organic aerosol,
21 *Atmos. Chem. Phys.*, 10(12), 5409–5424, doi:10.5194/acp-10-5409-2010, 2010.
- 22 Cappa, C. D., Jathar, S. H., Kleeman, M. J., Docherty, K. S., Jimenez, J. L., Seinfeld, J. H. and
23 Wexler, A. S.: Simulating secondary organic aerosol in a regional air quality model using the
24 statistical oxidation model – Part 2: Assessing the influence of vapor wall losses, *Atmos. Chem.*
25 *Phys.*, 16(5), 3041–3059, doi:10.5194/acp-16-3041-2016, 2016.
- 26 Chen, Q., Heald, C. L., Jimenez, J. L., Canagaratna, M. R., He, L., Huang, X.-F., Campuzano-Jost,
27 P., Palm, B. B., Poulain, L., Kuwata, M., Martin, S. T., Abbatt, J. P. D., Lee, A. K. Y., Liggio, J.,
28 Zhang, Q., He, L. and Huang, X.-F.: Elemental composition of organic aerosol: The gap between
29 ambient and laboratory measurements, *Geophys. Res. Lett.*, 42(10), 4182–4189,
30 doi:10.1002/2015GL063693, 2015.
- 31 Choi, J. K., Heo, J. B., Ban, S. J., Yi, S. M. and Zoh, K. D.: Chemical characteristics of PM_{2.5}
32 aerosol in Incheon, Korea, *Atmos. Environ.*, 60, 583–592, doi:10.1016/j.atmosenv.2012.06.078,
33 2012.
- 34 Cohen, A. J., Brauer, M., Burnett, R., Anderson, H. R., Frostad, J., Estep, K., Balakrishnan, K.,
35 Brunekreef, B., Dandona, L., Dandona, R., Feigin, V., Freedman, G., Hubbell, B., Jobling, A.,
36 Kan, H., Knibbs, L., Liu, Y., Martin, R., Morawska, L., Pope, C. A., Shin, H., Straif, K., Shaddick,
37 G., Thomas, M., van Dingenen, R., van Donkelaar, A., Vos, T., Murray, C. J. L. and Forouzanfar,
38 M. H.: Estimates and 25-year trends of the global burden of disease attributable to ambient air
39 pollution: an analysis of data from the Global Burden of Diseases Study 2015., *Lancet* (London,
40 England), 389(10082), 1907–1918, doi:10.1016/S0140-6736(17)30505-6, 2017.
- 41 Collier, S., Zhou, S., Onasch, T. B., Jaffe, D. A., Kleinman, L., Sedlacek, A. J., Briggs, N. L., Hee,
42 J., Fortner, E., Shilling, J. E., Worsnop, D., Yokelson, R. J., Parworth, C., Ge, X., Xu, J.,
43 Butterfield, Z., Chand, D., Dubey, M. K., Pekour, M. S., Springston, S. and Zhang, Q.: Regional



- 1 Influence of Aerosol Emissions from Wildfires Driven by Combustion Efficiency: Insights from
2 the BBOP Campaign, *Environ. Sci. Technol.*, 50(16), 8613–8622, doi:10.1021/acs.est.6b01617,
3 2016.
- 4 Craven, J. S., Metcalf, A. R., Bahreini, R., Middlebrook, A., Hayes, P. L., Duong, H. T.,
5 Sorooshian, A., Jimenez, J. L., Flagan, R. C. and Seinfeld, J. H.: Los Angeles Basin airborne
6 organic aerosol characterization during CalNex, *J. Geophys. Res. Atmos.*, 118(19), 11,453–11,467,
7 doi:10.1002/jgrd.50853, 2013.
- 8 Crippa, M., Canonaco, F., Lanz, V. A., Äijälä, M., Allan, J. D., Carbone, S., Capes, G., Ceburnis,
9 D., Dall'Osto, M., Day, D. A., DeCarlo, P. F., Ehn, M., Eriksson, A., Freney, E., Hildebrandt Ruiz,
10 L. H., Hillamo, R., Jimenez, J. L., Junninen, H., Kiendler-Scharr, A., Kortelainen, A.-M., Kulmala,
11 M., Laaksonen, A., Mensah, A. A., Mohr, C., Nemitz, E., O'Dowd, C., Ovadnevaite, J., Pandis, S.
12 N., Petäjä, T., Poulain, L., Saarikoski, S., Sellegri, K., Swietlicki, E., Tiitta, P., Worsnop, D. R.,
13 Baltensperger, U. and Prévôt, A. S. H.: Organic aerosol components derived from 25 AMS data
14 sets across Europe using a consistent ME-2 based source apportionment approach, *Atmos. Chem.*
15 *Phys.*, 14(12), 6159–6176, doi:10.5194/acp-14-6159-2014, 2014.
- 16 Crouse, J., McKinney, K. A., Kwan, A. J. and Wennberg, P. O.: Measurement of gas-phase
17 hydroperoxides by chemical ionization mass spectrometry, *Anal. Chem.*, 78(19), 6726–6732,
18 doi:doi:10.1021/ac0604235, 2006.
- 19 Cubison, M. J., Ortega, A. M., Hayes, P. L., Farmer, D. K., Day, D. A., Lechner, M. J., Brune, W.
20 H., Apel, E., Diskin, G. S., Fisher, J. A., Fuelberg, H. E., Hecobian, A., Knapp, D. J., Mikoviny,
21 T., Riemer, D., Sachse, G. W., Sessions, W., Weber, R. J., Weinheimer, A. J., Wisthaler, A. and
22 Jimenez, J. L.: Effects of aging on organic aerosol from open biomass burning smoke in aircraft
23 and laboratory studies, *Atmos. Chem. Phys.*, 11(23), 12049–12064, doi:10.5194/acp-11-12049-
24 2011, 2011.
- 25 Day, D. A., Wooldridge, P. J., Dillon, M. B., Thornton, J. A. and Cohen, R. C.: A thermal
26 dissociation laser-induced fluorescence instrument for in situ detection of NO₂, peroxy nitrates,
27 alkyl nitrates, and HNO₃, *J. Geophys. Res.*, 107(D5-6), 4046, doi:10.1029/2001JD000779, 2002.
- 28 DeCarlo, P. F., Kimmel, J. R., Trimborn, A., Northway, M. J., Jayne, J. T., Aiken, A. C., Gonin,
29 M., Fuhrer, K., Horvath, T., Docherty, K. S., Worsnop, D. R. and Jimenez, J. L.: Field-Deployable,
30 High-Resolution, Time-of-Flight Aerosol Mass Spectrometer, *Anal. Chem.*, 78(24), 8281–8289,
31 doi:10.1021/ac061249n, 2006.
- 32 DeCarlo, P. F., Dunlea, E. J., Kimmel, J. R., Aiken, A. C., Sueper, D., Crouse, J., Wennberg, P.
33 O., Emmons, L., Shinozuka, Y., Clarke, A., Zhou, J., Tomlinson, J., Collins, D. R., Knapp, D.,
34 Weinheimer, A. J., Montzka, D. D., Campos, T. and Jimenez, J. L.: Fast airborne aerosol size and
35 chemistry measurements above Mexico City and Central Mexico during the MILAGRO campaign,
36 *Atmos. Chem. Phys.*, 8(14), 4027–4048, doi:10.5194/acp-8-4027-2008, 2008.
- 37 DeCarlo, P. F., Ulbrich, I. M., Crouse, J., de Foy, B., Dunlea, E. J., Aiken, A. C., Knapp, D.,
38 Weinheimer, A. J., Campos, T., Wennberg, P. O. and Jimenez, J. L.: Investigation of the sources
39 and processing of organic aerosol over the Central Mexican Plateau from aircraft measurements
40 during MILAGRO, *Atmos. Chem. Phys.*, 10(12), 5257–5280, doi:10.5194/acp-10-5257-2010,
41 2010.
- 42 Deming, B., Pagonis, D., Liu, X., Talukdar, R. K., Roberts, J. M., Veres, P. R., Krechmer, J. E.,
43 de Gouw, J. A., Jimenez, J. L. and Ziemann, P. J.: Measurements of Delays of Gas-Phase



- 1 Compounds in a Wide Variety of Tubing Materials due to Gas-Wall Partitioning, *Atmos. Meas.*
2 *Tech., In Prep.*, 2018.
- 3 Dibb, J. E., Talbot, R. W., Scheuer, E. M., Seid, G., Avery, M. A. and Singh, H. B.: Aerosol
4 chemical composition in Asian continental outflow during the TRACE-P campaign: Comparison
5 with PEM-West B, *J. Geophys. Res.*, 108(D21), 8815, doi:10.1029/2002JD003111, 2003.
- 6 Diskin, G. S., Podolske, J. R., Sachse, G. W. and Slate, T. A.: Open-path airborne tunable diode
7 laser hygrometer, vol. 4817, edited by A. Fried, p. 196, International Society for Optics and
8 Photonics., 2002.
- 9 Docherty, K. S., Aiken, A. C., Huffman, J. A., Ulbrich, I. M., DeCarlo, P. F., Sueper, D., Worsnop,
10 D. R., Snyder, D. C., Peltier, R. E., Weber, R. J., Grover, B. D., Eatough, D. J., Williams, B. J.,
11 Goldstein, A. H., Ziemann, P. J. and Jimenez, J. L.: The 2005 Study of Organic Aerosols at
12 Riverside (SOAR-1): instrumental intercomparisons and fine particle composition, *Atmos. Chem.*
13 *Phys.*, 11(23), 12387–12420, doi:DOI 10.5194/acp-11-12387-2011, 2011.
- 14 Drewnick, F., Hings, S. S., Alfarra, M. R., Prevot, A. S. H. and Borrmann, S.: Aerosol
15 quantification with the Aerodyne Aerosol Mass Spectrometer: detection limits and ionizer
16 background effects, *Atmos. Meas. Tech.*, 2(1), 33–46, doi:10.5194/amt-2-33-2009, 2009.
- 17 Dunlea, E. J., DeCarlo, P. F., Aiken, A. C., Kimmel, J. R., Peltier, R. E., Weber, R. J., Tomlison,
18 J., Collins, D. R., Shinozuka, Y., McNaughton, C. S., Howell, S. G., Clarke, A. D., Emmons, L.
19 K., Apel, E. C., Pfister, G. G., van Donkelaar, A., Martin, R. V., Millett, D. B., Heald, C. L. and
20 Jimenez, J. L.: Evolution of Asian aerosols during transpacific transport in INTEX-B, *Atmos.*
21 *Chem. Phys.*, 9(19), 7257–7287, doi:10.5194/acp-9-7257-2009, 2009.
- 22 Dzepina, K., Volkamer, R. M. R., Madronich, S., Tulet, P., Ulbrich, I. M., Zhang, Q., Cappa, C.
23 D., Ziemann, P. J. and Jimenez, J. L.: Evaluation of recently-proposed secondary organic aerosol
24 models for a case study in Mexico City, *Atmos. Chem. Phys.*, 9(15), 5681–5709, doi:10.5194/acp-
25 9-5681-2009, 2009.
- 26 Dzepina, K., Cappa, C. D., Volkamer, R. M., Madronich, S., DeCarlo, P. F., Zaveri, R. A. and
27 Jimenez, J. L.: Modeling the Multiday Evolution and Aging of Secondary Organic Aerosol During
28 MILAGRO 2006, *Environ. Sci. Technol.*, 45(8), 3496–3503, doi:10.1021/es103186, 2011.
- 29 Faloon, I. C., Tan, D., Leshner, R. L., Hazen, N. L., Frame, C. L., Simpas, J. B., Harder, H.,
30 Martinez, M., Di Carlo, P., Ren, X. and Brune, W. H.: A Laser-induced Fluorescence Instrument
31 for Detecting Tropospheric OH and HO₂: Characteristics and Calibration, *J. Atmos. Chem.*, 47(2),
32 139–167, doi:10.1023/B:JOCH.0000021036.53185.0e, 2004.
- 33 Farmer, D. K., Matsunaga, A., Docherty, K. S., Surratt, J. D., Seinfeld, J. H., Ziemann, P. J. and
34 Jimenez, J. L.: Response of an aerosol mass spectrometer to organonitrates and organosulfates and
35 implications for atmospheric chemistry, *Proc. Natl. Acad. Sci. U. S. A.*, 107(15), 6670–6675,
36 doi:10.1073/pnas.0912340107, 2010.
- 37 Freney, E. J., Sellegri, K., Canonaco, F., Colomb, A., Borbon, A., Michoud, V., Doussin, J.-F.,
38 Crumeyrolle, S., Amarouche, N., Pichon, J.-M., Bourianne, T., Gomes, L., Prevot, A. S. H.,
39 Beekmann, M. and Schwarzenböck, A.: Characterizing the impact of urban emissions on regional
40 aerosol particles: airborne measurements during the MEGAPOLI experiment, *Atmos. Chem.*
41 *Phys.*, 14(3), 1397–1412, doi:10.5194/acp-14-1397-2014, 2014.
- 42 Fried, A., Cantrell, C., Olson, J., Crawford, J. H., Weibring, P., Walega, J., Richter, D.,



- 1 Junkermann, W., Volkamer, R., Sinreich, R., Heikes, B. G., O'Sullivan, D., Blake, D. R., Blake,
2 N., Meinardi, S., Apel, E., Weinheimer, A., Knapp, D., Perring, A., Cohen, R. C., Fuelberg, H.,
3 Shetter, R. E., Hall, S. R., Ullmann, K., Brune, W. H., Mao, J., Ren, X., Huey, L. G., Singh, H. B.,
4 Hair, J. W., Riemer, D., Diskin, G. and Sachse, G.: Detailed comparisons of airborne formaldehyde
5 measurements with box models during the 2006 INTEX-B and MILAGRO campaigns: Potential
6 evidence for significant impacts of unmeasured and multi-generation volatile organic carbon
7 compounds, *Atmos. Chem. Phys.*, 11(22), 11867–11894, doi:10.5194/acp-11-11867-2011, 2011.
- 8 Ge, X., Setyan, A., Sun, Y. and Zhang, Q.: Primary and secondary organic aerosols in Fresno,
9 California during wintertime: Results from high resolution aerosol mass spectrometry, *J. Geophys.*
10 *Res. Atmos.*, 117(D19), n/a-n/a, doi:10.1029/2012JD018026, 2012.
- 11 George, I. J., Slowik, J. and Abbatt, J. P. D.: Chemical aging of ambient organic aerosol from
12 heterogeneous reaction with hydroxyl radicals, *Geophys. Res. Lett.*, 35(13), L13811,
13 doi:10.1029/2008GL033884, 2008.
- 14 Goldberg, D. L., Vinciguerra, T. P., Hosley, K. M., Loughner, C. P., Canty, T. C., Salawitch, R. .
15 and Dickerson, R. R.: Evidence for an increase in the ozone photochemical lifetime in the eastern
16 United States using a regional air quality model, *J. Geophys. Res. Atmos.*, 120, 12,778-12,793,
17 doi:10.1002/2015JD02390, 2015.
- 18 Gordon, T. D., Tkacik, D. S., Presto, A. A., Zhang, M., Jathar, S. H., Nguyen, N. T., Massetti, J.,
19 Truong, T., Cicero-Fernandez, P., Maddox, C., Rieger, P., Chattopadhyay, S., Maldonado, H.,
20 Maricq, M. M. and Robinson, A. L.: Primary Gas- and Particle-Phase Emissions and Secondary
21 Organic Aerosol Production from Gasoline and Diesel Off-Road Engines, *Environ. Sci. Technol.*,
22 47(24), 14137–14146, doi:10.1021/es403556e, 2013.
- 23 de Gouw, J. A., Middlebrook, A. M., Warneke, C., Goldan, P. D., Kuster, W. C., Roberts, J. M.,
24 Fehsenfeld, F. C., Worsnop, D. R., Canagaratna, M. R., Pszenny, A. A. P., Keene, W. C.,
25 Marchewka, M. L., Bertman, S. B. and Bates, T. S.: Budget of organic carbon in a polluted
26 atmosphere: Results from the New England Air Quality Study in 2002, *J. Geophys. Res.*, 110(16),
27 D16305, doi:10.1029/2004JD005623, 2005.
- 28 de Gouw, J. A., Brock, C. A., Atlas, E. L., Bates, T. S., Fehsenfeld, F. C., Goldan, P. D., Holloway,
29 J. S., Kuster, W. C., Lerner, B. M., Matthew, B. M., Middlebrook, A. M., Onasch, T. B., Peltier,
30 R. E., Quinn, P. K., Senff, C. J., Stohl, A., Sullivan, A. P., Trainer, M., Warneke, C., Weber, R. J.
31 and Williams, E. J.: Sources of particulate matter in the northeastern United States in summer: 1.
32 Direct emissions and secondary formation of organic matter in urban plumes, *J. Geophys. Res.*,
33 113(8), D08301, doi:10.1029/2007JD009243, 2008.
- 34 de Gouw, J. A., Welsh-Bon, D., Warneke, C., Kuster, W. C., Alexander, L., Baker, A. K.,
35 Beyersdorf, A. J., Blake, D. R., Canagaratna, M., Celada, a. T., Huey, L. G., Junkermann, W.,
36 Onasch, T. B., Salcido, A., Sjostedt, S. J., Sullivan, A. P., Tanner, D. J., Vargas, O., Weber, R. J.,
37 Worsnop, D. R., Yu, X. Y. and Zaveri, R.: Emission and chemistry of organic carbon in the gas
38 and aerosol phase at a sub-urban site near Mexico City in March 2006 during the MILAGRO
39 study, *Atmos. Chem. Phys.*, 9(10), 3425–3442, doi:10.5194/acp-9-3425-2009, 2009.
- 40 Grieshop, A. P., Miracolo, M. A., Donahue, N. M. and Robinson, A. L.: Constraining the Volatility
41 Distribution and Gas-Particle Partitioning of Combustion Aerosols Using Isothermal Dilution and
42 Thermodenuder Measurements, *Environ. Sci. Technol.*, 43(13), 4750–4756,
43 doi:10.1021/Es8032378, 2009.



- 1 Griffin, R. J., Chen, J., Carmody, K., Vutukuru, S. and Dabdub, D.: Contribution of gas phase
2 oxidation of volatile organic compounds to atmospheric carbon monoxide levels in two areas of
3 the United States, *J. Geophys. Res. Atmos.*, 112(D10), doi:10.1029/2006JD007602, 2007.
- 4 Hallquist, M., Wenger, J. C., Baltensperger, U., Rudich, Y., Simpson, D., Claeys, M., Dommen,
5 J., Donahue, N. M., George, C., Goldstein, A. H., Hamilton, J. F., Herrmann, H., Hoffmann, T.,
6 Iinuma, Y., Jang, M., Jenkin, M. E., Jimenez, J. L., Kiendler-Scharr, A., Maenhaut, W.,
7 McFiggans, G., Mentel, T. F., Monod, A., Prévôt, A. S. H., Seinfeld, J. H., Surratt, J. D.,
8 Szmigielski, R. and Wildt, J.: The formation, properties and impact of secondary organic aerosol:
9 current and emerging issues, *Atmos. Chem. Phys.*, 9(14), 5155–5236, doi:10.5194/acp-9-5155-
10 2009, 2009.
- 11 Hayes, P. L., Ortega, A. M., Cubison, M. J., Froyd, K. D., Zhao, Y., Cliff, S. S., Hu, W. W.,
12 Toohey, D. W., Flynn, J. H., Lefer, B. L., Grossberg, N., Alvarez, S., Rappenglück, B., Taylor, J.
13 W., Allan, J. D., Holloway, J. S., Gilman, J. B., Kuster, W. C., de Gouw, J. A., Massoli, P., Zhang,
14 X., Liu, J., Weber, R. J., Corrigan, A. L., Russell, L. M., Isaacman, G., Worton, D. R., Kreisberg,
15 N. M., Goldstein, A. H., Thalman, R., Waxman, E. M., Volkamer, R., Lin, Y. H., Surratt, J. D.,
16 Kleindienst, T. E., Offenberg, J. H., Dusanter, S., Griffith, S., Stevens, P. S., Brioude, J., Angevine,
17 W. M. and Jimenez, J. L.: Organic aerosol composition and sources in Pasadena, California, during
18 the 2010 CalNex campaign, *J. Geophys. Res.*, 118(16), 9233–9257, doi:10.1002/jgrd.50530, 2013.
- 19 Hayes, P. L., Carlton, A. G., Baker, K. R., Ahmadov, R., Washenfelder, R. A., Alvarez, S.,
20 Rappenglück, B., Gilman, J. B., Kuster, W. C., de Gouw, J. A., Zotter, P., Prévôt, A. S. H., Szidat,
21 S., Kleindienst, T. E., Ma, P. K. and Jimenez, J. L.: Modeling the formation and aging of secondary
22 organic aerosols in Los Angeles during CalNex 2010, *Atmos. Chem. Phys.*, 15(10), 5773–5801,
23 doi:10.5194/acp-15-5773-2015, 2015.
- 24 Heald, C. L., Kroll, J. H., Jimenez, J. L., Docherty, K. S., Decarlo, P. F., Aiken, A. C., Chen, Q.,
25 Martin, S. T., Farmer, D. K. and Artaxo, P.: A simplified description of the evolution of organic
26 aerosol composition in the atmosphere, *Geophys. Res. Lett.*, 37(8), L08803,
27 doi:10.1029/2010GL042737, 2010.
- 28 Heim, E., Dibb, J., Scheuer, E., Campuzano-Jost, P., Nault, B. A., Jimenez, J. L., Peterson, D.,
29 Knote, C., Fenn, M., Hair, J., Beyersdorf, A. J. and Anderson, B. E.: Asian Dust Observed during
30 KORUS-AQ Facilitates the Uptake and Incorporation of Soluble Pollutants during Transport to
31 South Korea: The Hwangsa Anthropogenic Model, *J. Geophys. Res. Atmos.*, submitted, 2018.
- 32 Hennigan, C. J., Sullivan, A. P., Fountoukis, C. I., Nenes, A., Hecobian, A., Vargas, O., Peltier,
33 R. E., Hanks, A. T. C., Huey, L. G., Lefer, B. L., Russell, A. G. and Weber, R. J.: On the volatility
34 and production mechanisms of newly formed nitrate and water soluble organic aerosol in Mexico
35 City, *Atmos. Chem. Phys.*, 8(14), 3761–3768, doi:10.5194/acp-8-3761-2008, 2008.
- 36 Heo, J.-B., Hopke, P. K. and Yi, S.-M.: Source apportionment of PM_{2.5} in Seoul, Korea, *Atmos.*
37 *Chem. Phys.*, 9(14), 4957–4971, doi:10.5194/acp-9-4957-2009, 2009.
- 38 Herndon, S. C., Onasch, T. B., Wood, E. C., Kroll, J. H., Canagaratna, M. R., Jayne, J. T., Zavala,
39 M. A., Knighton, W. B., Mazzoleni, C., Dubey, M. K., Ulbrich, I. M., Jimenez, J. L., Seila, R., de
40 Gouw, J. A., de Foy, B., Fast, J., Molina, L. T., Kolb, C. E. and Worsnop, D. R.: Correlation of
41 secondary organic aerosol with odd oxygen in Mexico City, *Geophys. Res. Lett.*, 35(15),
42 doi:10.1029/2008GL034058, 2008.
- 43 Hersey, S. P., Craven, J. S., Metcalf, A. R., Lin, J., Lathem, T., Suski, K. J., Cahill, J. F., Duong,



- 1 H. T., Sorooshian, A., Jonsson, H. H., Shiraiwa, M., Zuend, A., Nenes, A., Prather, K. A., Flagan,
2 R. C. and Seinfeld, J. H.: Composition and hygroscopicity of the Los Angeles Aerosol: CalNex, J.
3 Geophys. Res. Atmos., 118(7), 3016–3036, doi:10.1002/jgrd.50307, 2013.
- 4 Hildebrandt Ruiz, L., Paciga, A. L., Cerully, K. M., Nenes, A., Donahue, N. M. and Pandis, S. N.:
5 Formation and aging of secondary organic aerosol from toluene: changes in chemical composition,
6 volatility, and hygroscopicity, Atmos. Chem. Phys., 15(14), 8301–8313, doi:10.5194/acp-15-
7 8301-2015, 2015.
- 8 Hodzic, A. and Jimenez, J. L.: Modeling anthropogenically controlled secondary organic aerosols
9 in a megacity: A simplified framework for global and climate models, Geosci. Model Dev., 4(4),
10 901–917, doi:10.5194/gmd-4-901-2011, 2011.
- 11 Hodzic, A., Jimenez, J. L., Madronich, S., Canagaratna, M. R., DeCarlo, P. F., Kleinman, L. and
12 Fast, J.: Modeling organic aerosols in a megacity: Potential contribution of semi-volatile and
13 intermediate volatility primary organic compounds to secondary organic aerosol formation,
14 Atmos. Chem. Phys., 10(12), 5491–5514, doi:10.5194/acp-10-5491-2010, 2010.
- 15 Hodzic, A., Madronich, S., Kasibhatla, P. S., Tyndall, G., Aumont, B., Jimenez, J. L., Lee-Taylor,
16 J. and Orlando, J.: Organic photolysis reactions in tropospheric aerosols: effect on secondary
17 organic aerosol formation and lifetime, Atmos. Chem. Phys., 15(16), 9253–9269, doi:10.5194/acp-
18 15-9253-2015, 2015.
- 19 Hong, J.-W. and Hong, J.: Changes in the Seoul Metropolitan Area Urban Heat Environment with
20 Residential Redevelopment, J. Appl. Meteorol. Climatol., 55, 1091–1106, doi:10.1175/JAMC-D-
21 15-0321.1, 2016.
- 22 Hu, W., Hu, M., Hu, W., Jimenez, J. L., Yuan, B., Chen, W., Wang, M., Wu, Y., Chen, C., Wang,
23 Z., Peng, J., Zeng, L. and Shao, M.: Chemical composition, sources and aging process of sub-
24 micron aerosols in Beijing: contrast between summer and winter, J. Geophys. Res. Atmos.,
25 doi:10.1002/2015JD024020, 2016.
- 26 Hu, W., Campuzano-Jost, P., Day, D. A., Croteau, P., Canagaratna, M. R., Jayne, J. T., Worsnop,
27 D. R. and Jimenez, J. L.: Evaluation of the new capture vaporizer for aerosol mass spectrometers
28 (AMS) through field studies of inorganic species, , doi:10.1080/02786826.2017.1296104, 2017a.
- 29 Hu, W., Campuzano-Jost, P., Day, D. A., Croteau, P., Canagaratna, M. R., Jayne, J. T., Worsnop,
30 D. R. and Jimenez, J. L.: Evaluation of the new capture vapourizer for aerosol mass spectrometers
31 (AMS) through laboratory studies of inorganic species, Atmos. Meas. Tech., 10(6), 2897–2921,
32 doi:10.5194/amt-10-2897-2017, 2017b.
- 33 Hu, W., Day, D. A., Campuzano-Jost, P., Nault, B. A., Park, T., Lee, T., Croteau, P., Canagaratna,
34 M. R., Jayne, J. T., Worsnop, D. R. and Jimenez, J. L.: Evaluation of the new capture vaporizer
35 for Aerosol Mass Spectrometers: Characterization of organic aerosol mass spectra, Aerosol Sci.
36 Technol., 52(7), 752–739, doi:10.1080/02786826.2018.1454584, 2018a.
- 37 Hu, W., Day, D. A., Campuzano-Jost, P., Nault, B. A., Park, T., Lee, T., Croteau, P., Canagaratna,
38 M. R., Jayne, J. T., Worsnop, D. R. and Jimenez, J. L.: Evaluation of the New Capture Vaporizer
39 for Aerosol Mass Spectrometers (AMS): Elemental Composition and Source Apportionment of
40 Organic Aerosols (OA), ACS Earth Sp. Chem., 2(4), 410–421,
41 doi:10.1021/acsearthspacechem.8b00002, 2018b.
- 42 Hu, W. W., Hu, M., Yuan, B., Jimenez, J. L., Tang, Q., Peng, J. F., Hu, W., Shao, M., Wang, M.,



- 1 Zeng, L. M., Wu, Y. S., Gong, Z. H., Huang, X. F. and He, L. Y.: Insights on organic aerosol aging
2 and the influence of coal combustion at a regional receptor site of central eastern China, *Atmos.*
3 *Chem. Phys.*, 13(19), 10095–10112, doi:10.5194/acp-13-10095-2013, 2013.
- 4 Huang, C., Wang, H. L., Li, L., Wang, Q., Lu, Q., de Gouw, J. A., Zhou, M., Jing, S. A., Lu, J.
5 and Chen, C. H.: VOC species and emission inventory from vehicles and their SOA formation
6 potentials estimation in Shanghai, China, *Atmos. Chem. Phys.*, 15(19), 11081–11096,
7 doi:10.5194/acp-15-11081-2015, 2015.
- 8 Huey, L. G., Tanner, D. J., Slusher, D. L., Dibb, J. E., Arimoto, R., Chen, G., Davis, D., Buhr, M.
9 P., Nowak, J. B., Mauldin III, R. L., Eisele, F. L. and Kosciuch, E.: CIMS measurements of HNO₃
10 and SO₂ at the South Pole during ISCAT 2000, *Atmos. Environ.*, 38(32), 5411–5421,
11 doi:10.1016/J.ATMOSENV.2004.04.037, 2004.
- 12 Huffman, J. A., Docherty, K. S., Aiken, A. C., Cubison, M. J., Ulbrich, I. M., DeCarlo, P. F.,
13 Sueper, D., Jayne, J. T., Worsnop, D. R., Ziemann, P. J. and Jimenez, J. L.: Chemically-resolved
14 aerosol volatility measurements from two megacity field studies, *Atmos. Chem. Phys.*, 9(1), 7161–
15 7182, doi:doi:10.5194/acp-9-7161-2009, 2009.
- 16 Hunter, J. F., Day, D. A., Palm, B. B., Yatavelli, R. L. N., Chan, A. W. H., Kaser, L., Cappellin,
17 L., Hayes, P. L., Cross, E. S., Carrasquillo, A. J., Campuzano-Jost, P., Stark, H., Zhao, Y., Hohaus,
18 T., Smith, J. N., Hansel, A., Karl, T., Goldstein, A. H., Guenther, A., Worsnop, D. R., Thornton,
19 J. A., Heald, C. L., Jimenez, J. L. and Kroll, J. H.: Comprehensive characterization of atmospheric
20 organic carbon at a forested site, *Nat. Geosci.*, 10(10), 748–753, doi:10.1038/ngeo3018, 2017.
- 21 Jacob, D. J.: Heterogeneous chemistry and tropospheric ozone, *Atmos. Environ.*, 34, 2131–2159,
22 doi:10.1016/S1352-2310(99)00462-8, 2000.
- 23 Janssen, R. H. H., Tsimpidi, A. P., Karydis, V. A., Pozzer, A., Lelieveld, J., Crippa, M., Prévôt,
24 A. S. H., Ait-Helal, W., Borbon, A., Sauvage, S. and Locoge, N.: Influence of local production
25 and vertical transport on the organic aerosol budget over Paris, *J. Geophys. Res. Atmos.*, 1–21,
26 doi:10.1002/2016JD026402, 2017.
- 27 Jathar, S. H., Miracolo, M. A., Tkacik, D. S., Donahue, N. M., Adams, P. J. and Robinson, A. L.:
28 Secondary Organic Aerosol Formation from Photo-Oxidation of Unburned Fuel: Experimental
29 Results and Implications for Aerosol Formation from Combustion Emissions, *Environ. Sci.*
30 *Technol.*, 47(22), 12886–12893, doi:10.1021/es403445q, 2013.
- 31 Jathar, S. H., Gordon, T. D., Hennigan, C. J., Pye, H. O. T., Pouliot, G., Adams, P. J., Donahue,
32 N. M. and Robinson, A. L.: Unspeciated organic emissions from combustion sources and their
33 influence on the secondary organic aerosol budget in the United States., *Proc. Natl. Acad. Sci. U.*
34 *S. A.*, 111(29), 10473–10478, doi:10.1073/pnas.1323740111, 2014.
- 35 Jayne, J. T. and Worsnop, D. R.: Particle Capture Device Aerodyne Research, 2015.
- 36 Jeong, U., Kim, J., Lee, H. and Lee, Y. G.: Assessing the effect of long-range pollutant
37 transportation on air quality in Seoul using the conditional potential source contribution function
38 method, *Atmos. Environ.*, 150, 33–44, doi:10.1016/j.atmosenv.2016.11.017, 2017.
- 39 Jimenez, J. L., Canagaratna, M. R., Donahue, N. M., Prévôt, A. S. H., Zhang, Q., Kroll, J. H.,
40 DeCarlo, P. F., Allan, J. D., Coe, H., Ng, N. L., Aiken, A. C., Docherty, K. S., Ulbrich, I. M.,
41 Grieshop, A. P., Robinson, A. L., Duplissy, J., Smith, J. D., Wilson, K. R., Lanz, V. A., Hueglin,
42 C., Sun, Y. L., Tian, J., Laaksonen, A., Raatikainen, T., Rautiainen, J., Vaattovaara, P., Ehn, M.,



- 1 Kulmala, M., Tomlinson, J. M., Collins, D. R., Cubison, M. J., Dunlea, E. J., Huffman, J. A.,
2 Onasch, T. B., Alfarra, M. R., Williams, P. I., Bower, K., Kondo, Y., Schneider, J., Drewnick, F.,
3 Borrmann, S., Weimer, S., Demerjian, K., Salcedo, D., Cottrell, L., Griffin, R., Takami, A.,
4 Miyoshi, T., Hatakeyama, S., Shimono, A., Sun, J. Y., Zhang, Y. M., Dzepina, K., Kimmel, J. R.,
5 Sueper, D., Jayne, J. T., Herndon, S. C., Trimborn, A. M., Williams, L. R., Wood, E. C.,
6 Middlebrook, A. M., Kolb, C. E., Baltensperger, U. and Worsnop, D. R.: Evolution of Organic
7 Aerosols in the Atmosphere, *Science* (80-.), 326(5959), 1525–1529,
8 doi:10.1126/science.1180353, 2009.
- 9 Jimenez, J. L., Campuzano-Jost, P., Day, D. A., Nault, B. A., Schroder, J. C. and Cubison, M. J.:
10 Frequently Asked Questions for AMS Data Users, [online] Available from:
11 http://cires.colorado.edu/jimenez-group/wiki/index.php?title=FAQ_for_AMS_Data_Users,
12 accessed month-year (Accessed 6 December 2018), 2018.
- 13 Kang, E., Root, M. J., Toohey, D. W. and Brune, W. H.: Introducing the concept of Potential
14 Aerosol Mass (PAM), *Atmos. Chem. Phys.*, 7(22), 5727–5744, doi:10.5194/acp-7-5727-2007,
15 2007.
- 16 Kang, E., Lee, M., Brune, W. H., Lee, T., Park, T., Ahn, J. and Shang, X.: Photochemical aging
17 of aerosol particles in different air masses arriving at Baengnyeong Island, Korea, *Atmos. Chem.*
18 *Phys.*, 18(9), 6661–6677, doi:10.5194/acp-18-6661-2018, 2018.
- 19 Khare, P. and Gentner, D. R.: Considering the future of anthropogenic gas-phase organic
20 compound emissions and the increasing influence of non-combustion sources on urban air quality,
21 *Atmos. Chem. Phys.*, 18(8), 5391–5413, doi:10.5194/acp-18-5391-2018, 2018.
- 22 Kim, B. M., Seo, J., Kim, J. Y., Lee, J. Y. and Kim, Y.: Transported vs. local contributions from
23 secondary and biomass burning sources to PM_{2.5}, *Atmos. Environ.*, 144, 24–36,
24 doi:10.1016/j.atmosenv.2016.08.072, 2016.
- 25 Kim, H., Zhang, Q., Bae, G.-N., Kim, J. Y. and Lee, S. B.: Sources and atmospheric processing of
26 wintertime aerosols in Seoul, Korea: Insights from real-time measurements using a high-resolution
27 aerosol mass spectrometer, *Atmos. Chem. Phys. Discuss.*, 17(3), 2009–2003, doi:10.5194/acp-17-
28 2009-2017, 2017.
- 29 Kim, H., Zhang, Q. and Heo, J.: Influence of Intense secondary aerosol formation and long-range
30 transport on aerosol chemistry and properties in the Seoul Metropolitan Area during spring time :
31 Results from KORUS-AQ, *Atmos. Chem. Phys.*, 18, 7149–7168, doi:10.5194/acp-2017-947,
32 2018.
- 33 Kim, H. C., Kim, E. H., Kim, B. U. and Kim, S.: Regional Contributions to the Particulate Matter
34 Concentration in the Seoul Metropolitan Area, Korea: Seasonal Variation and Sensitivity to
35 Meteorology, *Atmos. Chem. Phys.*, 17(17), 10315–10332, doi:10.5194/acp-17-10315-2017, 2017.
- 36 Kim, H. S., Huh, J. B., Hopke, P. K., Holsen, T. M. and Yi, S. M.: Characteristics of the major
37 chemical constituents of PM_{2.5} and smog events in Seoul, Korea in 2003 and 2004, *Atmos.*
38 *Environ.*, 41(32), 6762–6770, doi:10.1016/j.atmosenv.2007.04.060, 2007.
- 39 Kim, S., Huey, L. G., Stickel, R. E., Tanner, D. J., Crawford, J. H., Olson, J. R., Chen, G., Brune,
40 W. H., Ren, X., Leshner, R., Wooldridge, P. J., Bertram, T. H., Perring, A., Cohen, R. C., Lefer, B.
41 L., Shetter, R. E., Avery, M., Diskin, G. and Sokolik, I.: Measurement of HO₂ NO₂ in the free
42 troposphere during the Intercontinental Chemical Transport Experiment–North America 2004, J.



- 1 Geophys. Res., 112, D12S01, doi:10.1029/2006JD007676, 2007.
- 2 Kim, Y. J., Woo, J. H., Ma, Y. Il, Kim, S., Nam, J. S., Sung, H., Choi, K. C., Seo, J., Kim, J. S.,
3 Kang, C. H., Lee, G., Ro, C. U., Chang, D. and Sunwoo, Y.: Chemical characteristics of long-
4 range transport aerosol at background sites in Korea, Atmos. Environ., 43(34), 5556–5566,
5 doi:10.1016/j.atmosenv.2009.03.062, 2009.
- 6 Kimmel, J. R., Farmer, D. K., Cubison, M. J., Sueper, D., Tanner, C., Nemitz, E., Worsnop, D. R.,
7 Gonin, M. and Jimenez, J. L.: Real-time aerosol mass spectrometry with millisecond resolution,
8 Int. J. Mass Spectrom., 303(1), 15–26, doi:10.1016/j.ijms.2010.12.004, 2011.
- 9 Kleinman, L., Kuang, C., Sedlacek, A., Senum, G., Springston, S., Wang, J., Zhang, Q., Jayne, J.,
10 Fast, J., Hubbe, J., Shilling, J. and Zaveri, R.: What do correlations tell us about anthropogenic-
11 biogenic interactions and SOA formation in the Sacramento plume during CARES?, Atmos.
12 Chem. Phys., 16(3), 1729–1746, doi:10.5194/acp-16-1729-2016, 2016.
- 13 Kleinman, L. I., Daum, P. H., Lee, Y.-N., Senum, G. I., Springston, S. R., Wang, J., Berkowitz,
14 C., Hubbe, J., Zaveri, R. A., Brechtel, F. J., Jayne, J., Onasch, T. B. and Worsnop, D.: Aircraft
15 observations of aerosol composition and ageing in New England and Mid-Atlantic States during
16 the summer 2002 New England Air Quality Study field campaign, J. Geophys. Res., 112(D9),
17 D09310, doi:10.1029/2006JD007786, 2007.
- 18 Kleinman, L. I., Springston, S. R., Daum, P. H., Lee, Y.-N., Nunnermacker, L. J., Senum, G. I.,
19 Wang, J., Weinstein-Lloyd, J., Alexander, M. L., Hubbe, J., Ortega, J., Canagaratna, M. R. and
20 Jayne, J.: The time evolution of aerosol composition over the Mexico City plateau, Atmos. Chem.
21 Phys., 8(6), 1559–1575, doi:10.5194/acp-8-1559-2008, 2008.
- 22 Kleinman, L. I., Springston, S. R., Wang, J., Daum, P. H., Lee, Y.-N. N., Nunnermacker, L. J.,
23 Senum, G. I., Weinstein-Lloyd, J., Alexander, M. L., Hubbe, J., Ortega, J., Zaveri, R. A.,
24 Canagaratna, M. R. and Jayne, J.: The time evolution of aerosol size distribution over the Mexico
25 City plateau, Atmos. Chem. Phys., 9(13), 4261–4278, doi:10.5194/acpd-9-1621-2009, 2009.
- 26 Knote, C., Hodzic, A., Jimenez, J. L., Volkamer, R., Orlando, J. J., Baidar, S., Brioude, J., Fast, J.,
27 Gentner, D. R., Goldstein, A. H., Hayes, P. L., Knighton, W. B., Oetjen, H., Setyan, A., Stark, H.,
28 Thalman, R., Tyndall, G., Washenfelder, R., Waxman, E. and Zhang, Q.: Simulation of semi-
29 explicit mechanisms of SOA formation from glyoxal in aerosol in a 3-D model, Atmos. Chem.
30 Phys., 14(12), 6213–6239, doi:10.5194/acp-14-6213-2014, 2014.
- 31 Krechmer, J. E., Pagonis, D., Ziemann, P. J. and Jimenez, J. L.: Quantification of Gas-Wall
32 Partitioning in Teflon Environmental Chambers Using Rapid Bursts of Low-Volatility Oxidized
33 Species Generated in Situ, Environ. Sci. Technol., 50(11), 5757–5765,
34 doi:10.1021/acs.est.6b00606, 2016.
- 35 Krechmer, J. E., Day, D. A., Ziemann, P. J. and Jimenez, J. L.: Direct Measurements of
36 Gas/Particle Partitioning and Mass Accommodation Coefficients in Environmental Chambers,
37 Environ. Sci. Technol., 51(20), 11867–11875, doi:10.1021/acs.est.7b02144, 2017.
- 38 Kroll, J. H. and Seinfeld, J. H.: Chemistry of secondary organic aerosol: Formation and evolution
39 of low-volatility organics in the atmosphere, Atmos. Environ., 42(16), 3593–3624,
40 doi:10.1016/J.ATMOSENV.2008.01.003, 2008.
- 41 Kroll, J. H., Donahue, N. M., Jimenez, J. L., Kessler, S. H., Canagaratna, M. R., Wilson, K. R.,
42 Altieri, K. E., Mazzoleni, L. R., Wozniak, A. S., Bluhm, H., Mysak, E. R., Smith, J. D., Kolb, C.



- 1 E. and Worsnop, D. R.: Carbon oxidation state as a metric for describing the chemistry of
2 atmospheric organic aerosol., *Nat. Chem.*, 3(2), 133–139, doi:10.1038/nchem.948, 2011.
- 3 Kupc, A., Williamson, C., Wagner, N. L., Richardson, M. and Brock, C. A.: Modification,
4 calibration, and performance of the Ultra-High Sensitivity Aerosol Spectrometer for particle size
5 distribution and volatility measurements during the Atmospheric Tomography Mission (ATom)
6 airborne campaign, *Atmos. Meas. Tech.*, 11(1), 369–383, doi:10.5194/amt-11-369-2018, 2018.
- 7 Lambe, A. T., Ahern, A. T., Williams, L. R., Slowik, J. G., Wong, J. P. S., Abbatt, J. P. D., Brune,
8 W. H., Ng, N. L., Wright, J. P., Croasdale, D. R., Worsnop, D. R., Davidovits, P. and Onasch, T.
9 B.: Characterization of aerosol photooxidation flow reactors: heterogeneous oxidation, secondary
10 organic aerosol formation and cloud condensation nuclei activity measurements, *Atmos. Meas.*
11 *Tech.*, 4(3), 445–461, doi:10.5194/amt-4-445-2011, 2011.
- 12 Lambe, A. T., Onasch, T. B., Croasdale, D. R., Wright, J. P., Martin, A. T., Franklin, J. P., Massoli,
13 P., Kroll, J. H., Canagaratna, M. R., Brune, W. H., Worsnop, D. R. and Davidovits, P.: Transitions
14 from Functionalization to Fragmentation Reactions of Laboratory Secondary Organic Aerosol
15 (SOA) Generated from the OH Oxidation of Alkane Precursors, *Environ. Sci. Technol.*, 46(10),
16 5430–5437, doi:10.1021/Es300274t, 2012.
- 17 Landrigan, P. J., Fuller, R., Acosta, N. J. R., Adeyi, O., Arnold, R., Basu, N., Baldé, A. B.,
18 Bertollini, R., Bose-O'Reilly, S., Boufford, J. I., Breysse, P. N., Chiles, T., Mahidol, C., Coll-Seck,
19 A. M., Cropper, M. L., Fobil, J., Fuster, V., Greenstone, M., Haines, A., Hanrahan, D., Hunter, D.,
20 Khare, M., Krupnick, A., Lanphear, B., Lohani, B., Martin, K., Mathiasen, K. V., McTeer, M. A.,
21 Murray, C. J. L., Ndahimananjara, J. D., Perera, F., Potočnik, J., Preker, A. S., Ramesh, J.,
22 Rockström, J., Salinas, C., Samson, L. D., Sandilya, K., Sly, P. D., Smith, K. R., Steiner, A.,
23 Stewart, R. B., Suk, W. A., van Schayck, O. C. P., Yadama, G. N., Yumkella, K. and Zhong, M.:
24 The Lancet Commission on pollution and health, *Lancet*, 391(10119), 462–512,
25 doi:10.1016/S0140-6736(17)32345-0, 2018.
- 26 Lee, G., Choi, H. S., Lee, T., Choi, J., Park, J. S. and Ahn, J. Y.: Variations of regional background
27 peroxyacetyl nitrate in marine boundary layer over Baengyeong Island, South Korea, *Atmos.*
28 *Environ.*, 61, 533–541, doi:10.1016/j.atmosenv.2012.07.075, 2012.
- 29 Lee, H. M., Park, R. J., Henze, D. K., Lee, S., Shim, C., Shin, H. J., Moon, K. J. and Woo, J. H.:
30 PM_{2.5} source attribution for Seoul in May from 2009 to 2013 using GEOS-Chem and its adjoint
31 model, *Environ. Pollut.*, 221, 377–384, doi:10.1016/j.envpol.2016.11.088, 2017.
- 32 Lee, S., Ho, C.-H., Lee, Y. G., Choi, H.-J. and Song, C.-K.: Influence of transboundary air
33 pollutants from China on the high-PM₁₀ episode in Seoul, Korea for the period October 16–20,
34 2008, *Atmos. Environ.*, 77, 430–439, doi:10.1016/J.ATMOSENV.2013.05.006, 2013.
- 35 Lee, T., Choi, J., Lee, G., Ahn, J., Park, J. S., Atwood, S. A., Schurman, M., Choi, Y., Chung, Y.
36 and Collett, J. L.: Characterization of aerosol composition, concentrations, and sources at
37 Baengyeong Island, Korea using an aerosol mass spectrometer, *Atmos. Environ.*, 120, 297–306,
38 doi:10.1016/j.atmosenv.2015.08.038, 2015.
- 39 Lelieveld, J., Evans, J. S., Fnais, M., Giannadaki, D. and Pozzer, A.: The contribution of outdoor
40 air pollution sources to premature mortality on a global scale, *Nature*, 525(7569), 367–371,
41 doi:10.1038/nature15371, 2015.
- 42 Li, R., Palm, B. B., Ortega, A. M., Hlywiak, J., Hu, W., Peng, Z., Day, D. A., Knote, C., Brune,



- 1 W. H., de Gouw, J. A. and Jimenez, J. L.: Modeling the radical chemistry in an oxidation flow
2 reactor: radical formation and recycling, sensitivities, and the OH exposure estimation equation.,
3 *J. Phys. Chem. A*, 119(19), 4418–4432, doi:10.1021/jp509534k, 2015.
- 4 Liu, T., Wang, X., Deng, W., Hu, Q., Ding, X., Zhang, Y., He, Q., Zhang, Z., Lü, S., Bi, X., Chen,
5 J. and Yu, J.: Secondary organic aerosol formation from photochemical aging of light-duty
6 gasoline vehicle exhausts in a smog chamber, *Atmos. Chem. Phys.*, 15(15), 9049–9062,
7 doi:10.5194/acp-15-9049-2015, 2015.
- 8 Liu, X., Huey, L. G., Yokelson, R. J., Selimovic, V., Simpson, I. J., Müller, M., Jimenez, J. L.,
9 Campuzano-Jost, P., Beyersdorf, A. J., Blake, D. R., Butterfield, Z., Choi, Y., Crouse, J. D., Day,
10 D. A., Diskin, G. S., Dubey, M. K., Fortner, E., Hanisco, T. F., Hu, W., King, L. E., Kleinman, L.,
11 Meinardi, S., Mikoviny, T., Onasch, T. B., Palm, B. B., Peischl, J., Pollack, I. B., Ryerson, T. B.,
12 Sachse, G. W., Sedlacek, A. J., Shilling, J. E., Springston, S., St. Clair, J. M., Tanner, D. J., Teng,
13 A. P., Wennberg, P. O., Wisthaler, A. and Wolfe, G. M.: Airborne measurements of western U.S.
14 wildfire emissions: Comparison with prescribed burning and air quality implications, *J. Geophys.*
15 *Res.*, 122(11), 6108–6129, doi:10.1002/2016JD026315, 2017.
- 16 Ma, P. K., Zhao, Y., Robinson, A. L., Worton, D. R., Goldstein, A. H., Ortega, A. M., Jimenez, J.-
17 L., Zotter, P., Prévôt, A. S. H., Szidat, S. and Hayes, P. L.: Evaluating the impact of new
18 observational constraints on P-S/IVOC emissions, multi-generation oxidation, and chamber wall
19 losses on SOA modeling for Los Angeles, CA, *Atmos. Chem. Phys.*, 17(15), 9237–9259,
20 doi:10.5194/acp-17-9237-2017, 2017.
- 21 Mao, J., Ren, X., Brune, W. H., Olson, J. R., Crawford, J. H., Fried, a., Huey, L. G., Cohen, R.
22 C., Heikes, B., Singh, H. B., Blake, D. R., Sachse, G. W., Diskin, G. S., Hall, S. R. and Shetter, R.
23 E.: Airborne measurement of OH reactivity during INTEX-B, *Atmos. Chem. Phys.*, 9(1), 163–
24 173, doi:10.5194/acp-9-163-2009, 2009.
- 25 Matsunaga, A. and Ziemann, P. J.: Gas-Wall Partitioning of Organic Compounds in a Teflon Film
26 Chamber and Potential Effects on Reaction Product and Aerosol Yield Measurements, *Aerosol*
27 *Sci. Technol.*, 44(10), 881–892, doi:10.1080/02786826.2010.501044, 2010.
- 28 McDonald, B. C., de Gouw, J. A., Gilman, J. B., Jathar, S. H., Akherati, A., Cappa, C. D., Jimenez,
29 J. L., Lee-Taylor, J., Hayes, P. L., McKeen, S. A., Cui, Y. Y., Kim, S.-W., Gentner, D. R.,
30 Isaacman-VanWertz, G., Goldstein, A. H., Harley, R. A., Frost, G. J., Roberts, J. M., Ryerson, T.
31 B. and Trainer, M.: Volatile chemical products emerging as largest petrochemical source of urban
32 organic emissions., *Science*, 359(6377), 760–764, doi:10.1126/science.aag0524, 2018.
- 33 McKeen, S. A., Liu, S. C., Hsie, E.-Y., Lin, X., Bradshaw, J. D., Smyth, S., Gregory, G. L. and
34 Blake, D. R.: Hydrocarbon ratios during PEM-WEST A: A model perspective, *J. Geophys. Res.*
35 *Atmos.*, 101(D1), 2087–2109, doi:10.1029/95JD02733, 1996.
- 36 McMeeking, G. R., Bart, M., Chazette, P., Haywood, J. M., Hopkins, J. R., McQuaid, J. B.,
37 Morgan, W. T., Raut, J.-C., Ryder, C. L., Savage, N., Turnbull, K. and Coe, H.: Airborne
38 measurements of trace gases and aerosols over the London metropolitan region, *Atmos. Chem.*
39 *Phys.*, 12(11), 5163–5187, doi:10.5194/acp-12-5163-2012, 2012.
- 40 McNaughton, C. S., Clarke, A. D., Howell, S. G., Pinkerton, M., Anderson, B., Thornhill, L.,
41 Hudgins, C., Winstead, E., Dibb, J. E., Scheuer, E. and Maring, H.: Results from the DC-8 Inlet
42 Characterization Experiment (DICE): Airborne versus surface sampling of mineral dust and sea
43 salt aerosols, *Aerosol Sci. Technol.*, 41(2), 136–159, doi:10.1080/02786820601118406, 2007.



- 1 Middlebrook, A. M., Bahreini, R., Jimenez, J. L. and Canagaratna, M. R.: Evaluation of
2 Composition-Dependent Collection Efficiencies for the Aerodyne Aerosol Mass Spectrometer
3 using Field Data, *Aerosol Sci. Technol.*, 46(3), 258–271, doi:10.1080/02786826.2011.620041,
4 2012.
- 5 Miracolo, M. A., Presto, A. A., Lambe, A. T., Hennigan, C. J., Donahue, N. M., Kroll, J. H.,
6 Worsnop, D. R. and Robinson, A. L.: Photo-Oxidation of Low-Volatility Organics Found in Motor
7 Vehicle Emissions: Production and Chemical Evolution of Organic Aerosol Mass, *Environ. Sci.*
8 *Technol.*, 44(5), 1638–1643, doi:10.1021/es902635c, 2010.
- 9 Mitroo, D., Sun, Y., Combet, D. P., Kumar, P. and Williams, B. J.: Assessing the degree of plug
10 flow in oxidation flow reactors (OFRs): a study on a potential aerosol mass (PAM) reactor, *Atmos.*
11 *Meas. Tech.*, 11, 1741–1756, doi:10.5194/amt-11-1741-2018, 2018.
- 12 Monks, P. S., Granier, C., Fuzzi, S., Stohl, A., Williams, M. L., Akimoto, H., Amann, M.,
13 Baklanov, A., Baltensperger, U., Bey, I., Blake, N., Blake, R. S., Carslaw, K., Cooper, O. R.,
14 Dentener, F., Fowler, D., Fragkou, E., Frost, G. J., Generoso, S., Ginoux, P., Grewe, V., Guenther,
15 A., Hansson, H. C., Henne, S., Hjorth, J., Hofzumahaus, A., Huntrieser, H., Isaksen, I. S. A.,
16 Jenkin, M. E., Kaiser, J., Kanakidou, M., Klimont, Z., Kulmala, M., Laj, P., Lawrence, M. G., Lee,
17 J. D., Liousse, C., Maione, M., McFiggans, G., Metzger, A., Mieville, A., Moussiopoulos, N.,
18 Orlando, J. J., O'Dowd, C. D., Palmer, P. I. I., Parrish, D. D., Petzold, A., Platt, U., Pöschl, U.,
19 Prévôt, A. S. H., Reeves, C. E., Reimann, S., Rudich, Y., Sellegri, K., Steinbrecher, R., Simpson,
20 D., ten Brink, H., Theloke, J., van der Werf, G. R., Vautard, R., Vestreng, V., Vlachokostas, C.
21 and von Glasow, R.: Atmospheric composition change - global and regional air quality, *Atmos.*
22 *Environ.*, 43(33), 5268–5350, doi:10.1016/j.atmosenv.2009.08.021, 2009.
- 23 Morino, Y., Tanabe, K., Sato, K. and Ohara, T.: Secondary organic aerosol model intercomparison
24 based on secondary organic aerosol to odd oxygen ratio in Tokyo, *J. Geophys. Res. Atmos.*,
25 119(23), 13,489–13,505, doi:10.1002/2014JD021937, 2014.
- 26 Müller, M., Mikoviny, T., Feil, S., Haidacher, S., Hanel, G., Hartungen, E., Jordan, A., Märk, L.,
27 Mutschlechner, P., Schotchkowsky, R., Sulzer, P., Crawford, J. H. and Wisthaler, A.: A compact
28 PTR-ToF-MS instrument for airborne measurements of volatile organic compounds at high
29 spatiotemporal resolution, *Atmos. Meas. Tech.*, 7(11), 3763–3772, doi:10.5194/amt-7-3763-2014,
30 2014.
- 31 Murphy, B. N., Donahue, N. M., Fountoukis, C. and Pandis, S. N.: Simulating the oxygen content
32 of ambient organic aerosol with the 2D volatility basis set, *Atmos. Chem. Phys.*, 11(15), 7859–
33 7873, doi:10.5194/acp-11-7859-2011, 2011.
- 34 Murphy, B. N., Woody, M. C., Jimenez, J. L., Carlton, A. M. G., Hayes, P. L., Liu, S., Ng, N. L.,
35 Russell, L. M., Setyan, A., Xu, L., Young, J., Zaveri, R. A., Zhang, Q. and Pye, H. O. T.:
36 Semivolatile POA and parameterized total combustion SOA in CMAQv5.2: impacts on source
37 strength and partitioning, *Atmos. Chem. Phys.*, 17(18), 11107–11133, doi:10.5194/acp-17-11107-
38 2017, 2017.
- 39 Myhre, G., Shindell, D., Bréon, F.-M., Collins, W., Fuglestedt, J., Huang, J., Koch, D., Lamarque,
40 J.-F., Lee, D., Mendoza, B., Nakajima, T., Robock, A., Stephens, G., Takemura, T. and Zhang, H.:
41 Anthropogenic and Natural Radiative Forcing, in *Climate Change 2013: The Physical Science*
42 *Basis. Contribution of Working Group I to the Fifth Assessment Report of the Intergovernmental*
43 *Panel on Climate Change*, edited by T. F. Stocker, D. Qin, G.-K. Plattner, M. Tignor, S. K. Allen,



- 1 J. Boschung, A. Nauels, Y. Xia, V. Bex, and P. M. Midgley, p. 659, Cambridge University Press,
2 Cambridge, United Kingdom and New York, NY, USA, United Kingdom and New York, NY,
3 USA. [online] Available from: <https://www.ipcc.ch/report/ar5/wg1/>, 2013.
- 4 Novelli, P. C., Crotwell, A., Lang, P. M. and Mund, J.: Atmospheric Carbon Monoxide Dry Air
5 Mole Fractions from the NOAA ESRL Carbon Cycle Cooperative Global Air Sampling Network,
6 1988-2016, Version: 2017-07-28, [online] Available from:
7 ftp://aftp.cmdl.noaa.gov/data/trace_gases/co/flask/surface/, 2017.
- 8 OECD: Exposure to PM_{2.5} in countries and regions : Exposure to PM_{2.5} in macroregions, [online]
9 Available from: <https://stats.oecd.org/index.aspx?queryid=72722> (Accessed 1 August 2018),
10 2018.
- 11 Ortega, A. M., Hayes, P. L., Peng, Z., Palm, B. B., Hu, W., Day, D. A., Li, R., Cubison, M. J.,
12 Brune, W. H., Graus, M., Warneke, C., Gilman, J. B., Kuster, W. C., de Gouw, J. A., Gutiérrez-
13 Montes, C. and Jimenez, J. L.: Real-time measurements of secondary organic aerosol formation
14 and aging from ambient air in an oxidation flow reactor in the Los Angeles area, *Atmos. Chem.*
15 *Phys.*, 16(11), 7411–7433, doi:10.5194/acp-16-7411-2016, 2016.
- 16 Ots, R., Vieno, M., Allan, J. D., Reis, S., Nemitz, E., Young, D. E., Coe, H., Di Marco, C.,
17 Detournay, A., Mackenzie, I. A., Green, D. C. and Heal, M. R.: Model simulations of cooking
18 organic aerosol (COA) over the UK using estimates of emissions based on measurements at two
19 sites in London, *Atmos. Chem. Phys.*, 16(21), 13773–13789, doi:10.5194/acp-16-13773-2016,
20 2016.
- 21 Pagonis, D., Krechmer, J. E., de Gouw, J., Jimenez, J. L. and Ziemann, P. J.: Effects of gas–wall
22 partitioning in Teflon tubing and instrumentation on time-resolved measurements of gas-phase
23 organic compounds, *Atmos. Meas. Tech.*, 10(12), 4687–4696, doi:10.5194/amt-10-4687-2017,
24 2017.
- 25 Palm, B. B., Campuzano-Jost, P., Ortega, A. M., Day, D. A., Kaser, L., Jud, W., Karl, T., Hansel,
26 A., Hunter, J. F., Cross, E. S., Kroll, J. H., Peng, Z., Brune, W. H. and Jimenez, J. L.: In situ
27 secondary organic aerosol formation from ambient pine forest air using an oxidation flow reactor,
28 *Atmos. Chem. Phys.*, 16(5), 2943–2970, doi:10.5194/acp-16-2943-2016, 2016.
- 29 Palm, B. B., Campuzano-Jost, P., Day, D. A., Ortega, A. M., Fry, J. L., Brown, S. S., Zarzana, K.
30 J., Dube, W., Wagner, N. L., Draper, D. C., Kaser, L., Jud, W., Karl, T., Hansel, A., Gutiérrez-
31 Montes, C. and Jimenez, J. L.: Secondary organic aerosol formation from in situ OH, O₃, and NO₃
32 oxidation of ambient forest air in an oxidation flow reactor, *Atmos. Chem. Phys.*, 17(8), 5331–
33 5354, doi:10.5194/acp-17-5331-2017, 2017.
- 34 Palm, B. B., de Sá, S. S., Day, D. A., Campuzano-Jost, P., Hu, W., Seco, R., Sjøstedt, S. J., Park,
35 J.-H., Guenther, A. B., Kim, S., Brito, J., Wurm, F., Artaxo, P., Thalman, R., Wang, J., Yee, L. D.,
36 Wernis, R., Isaacman-VanWertz, G., Goldstein, A. H., Liu, Y., Springston, S. R., Souza, R.,
37 Newburn, M. K., Alexander, M. L., Martin, S. T. and Jimenez, J. L.: Secondary organic aerosol
38 formation from ambient air in an oxidation flow reactor in central Amazonia, *Atmos. Chem. Phys.*,
39 18(1), 467–493, doi:10.5194/acp-18-467-2018, 2018.
- 40 Park, M.-S., Park, S.-H., Chae, J.-H., Choi, M.-H., Song, Y., Kang, M. and Roh, J.-W.: High-
41 resolution urban observation network for user-specific meteorological information service in the
42 Seoul Metropolitan Area, South Korea, *Atmos. Meas. Tech.*, 10, 1575–1594, doi:10.5194/amt-10-
43 1575-2017, 2017.



- 1 Park, M. E., Song, C. H., Park, R. S., Lee, J., Kim, J., Lee, S., Woo, J.-H., Carmichael, G. R., Eck,
2 T. F., Holben, B. N., Lee, S.-S., Song, C. K. and Hong, Y. D.: New approach to monitor
3 transboundary particulate pollution over Northeast Asia, *Atmos. Chem. Phys.*, 14, 659–674,
4 doi:10.5194/acp-14-659-2014, 2014.
- 5 Park, S. S., Kim, J.-H. and Jeong, J.-U.: Abundance and sources of hydrophilic and hydrophobic
6 water-soluble organic carbon at an urban site in Korea in summer., *J. Environ. Monit.*, 14(1), 224–
7 32, doi:10.1039/c1em10617a, 2012.
- 8 Parrish, D. D., Stohl, A., Forster, C., Atlas, E. L., Blake, D. R., Goldan, P. D., Kuster, W. C. and
9 de Gouw, J. A.: Effects of mixing on evolution of hydrocarbon ratios in the troposphere, *J.*
10 *Geophys. Res.*, 112(D10), D10S34, doi:10.1029/2006JD007583, 2007.
- 11 Parrish, D. D., Ryerson, T. B., Mellqvist, J., Johansson, J., Fried, A., Richter, D., Walega, J. G.,
12 Washenfelder, R. A., de Gouw, J. A., Peischl, J., Aikin, K. C., McKeen, S. A., Frost, G. J.,
13 Fehsenfeld, F. C. and Herndon, S. C.: Primary and secondary sources of formaldehyde in urban
14 atmospheres: Houston Texas region, *Atmos. Chem. Phys.*, 12(7), 3273–3288, doi:10.5194/acp-12-
15 3273-2012, 2012.
- 16 Peischl, J., Ryerson, T. B., Brioude, J., Aikin, K. C., Andrews, A. E., Atlas, E., Blake, D., Daube,
17 B. C., de Gouw, J. A., Dlugokencky, E., Frost, G. J., Gentner, D. R., Gilman, J. B., Goldstein, A.
18 H., Harley, R. A., Holloway, J. S., Kofler, J., Kuster, W. C., Lang, P. M., Novelli, P. C., Santoni,
19 G. W., Trainer, M., Wofsy, S. C. and Parrish, D. D.: Quantifying sources of methane using light
20 alkanes in the Los Angeles basin, California, *J. Geophys. Res. Atmos.*, 118(10), 4974–4990,
21 doi:10.1002/jgrd.50413, 2013.
- 22 Peng, J. F., Hu, M., Wang, Z. B., Huang, X. F., Kumar, P., Wu, Z. J., Guo, S., Yue, D. L., Shang,
23 D. J., Zheng, Z. and He, L. Y.: Submicron aerosols at thirteen diversified sites in China: size
24 distribution, new particle formation and corresponding contribution to cloud condensation nuclei
25 production, *Atmos. Chem. Phys.*, 14(18), 10249–10265, doi:10.5194/acp-14-10249-2014, 2014.
- 26 Peng, Z., Day, D. A., Stark, H., Li, R., Lee-Taylor, J., Palm, B. B., Brune, W. H. and Jimenez, J.
27 L.: HO_x radical chemistry in oxidation flow reactors with low-pressure mercury lamps
28 systematically examined by modeling, *Atmos. Meas. Tech.*, 8(11), 4863–4890, doi:10.5194/amt-
29 8-4863-2015, 2015.
- 30 Peng, Z., Day, D. A., Ortega, A. M., Palm, B. B., Hu, W., Stark, H., Li, R., Tsigaridis, K., Brune,
31 W. H. and Jimenez, J. L.: Non-OH chemistry in oxidation flow reactors for the study of
32 atmospheric chemistry systematically examined by modeling, *Atmos. Chem. Phys.*, 16(7), 4283–
33 4305, doi:10.5194/acp-16-4283-2016, 2016.
- 34 Perring, A. E., Bertram, T. H., Farmer, D. K., Wooldridge, P. J., Dibb, J., Blake, N. J., Blake, D.
35 R., Singh, H. B., Fuelberg, H., Diskin, G., Sachse, G. and Cohen, R. C.: The production and
36 persistence of ΣRONO_2 in the Mexico City plume, *Atmos. Chem. Phys.*, 10(15), 7215–7229,
37 doi:10.5194/acp-10-7215-2010, 2010.
- 38 Platt, S. M., El Haddad, I., Zardini, A. A., Clairotte, M., Astorga, C., Wolf, R., Slowik, J. G.,
39 Temime-Roussel, B., Marchand, N., Ježek, I., Drinovec, L., Močnik, G., Möhler, O., Richter, R.,
40 Barmet, P., Bianchi, F., Baltensperger, U. and Prévôt, A. S. H.: Secondary organic aerosol
41 formation from gasoline vehicle emissions in a new mobile environmental reaction chamber,
42 *Atmos. Chem. Phys.*, 13(18), 9141–9158, doi:10.5194/acp-13-9141-2013, 2013.



- 1 Platt, S. M., El Haddad, I., Pieber, S. M., Zardini, A. A., Suarez-Bertoa, R., Clairotte, M.,
2 Daellenbach, K. R., Huang, R.-J., Slowik, J. G., Hellebust, S., Temime-Roussel, B., Marchand,
3 N., de Gouw, J., Jimenez, J. L., Hayes, P. L., Robinson, A. L., Baltensperger, U., Astorga, C. and
4 Prévôt, A. S. H.: Gasoline cars produce more carbonaceous particulate matter than modern filter-
5 equipped diesel cars, *Sci. Rep.*, 7(1), 4926, doi:10.1038/s41598-017-03714-9, 2017.
- 6 Presto, A. A., Gordon, T. D. and Robinson, A. L.: Primary to secondary organic aerosol: Evolution
7 of organic emissions from mobile combustion sources, *Atmos. Chem. Phys.*, 14(10), 5015–5036,
8 doi:10.5194/acp-14-5015-2014, 2014.
- 9 Price, H. U., Jaffe, D. A., Cooper, O. R. and Doskey, P. V.: Photochemistry, ozone production, and
10 dilution during long-range transport episodes from Eurasia to the northwest United States, *J.*
11 *Geophys. Res. Atmos.*, 109, D23S13, doi:10.1029/2003JD004400, 2004.
- 12 Pye, H. O. T. and Seinfeld, J. H.: A global perspective on aerosol from low-volatility organic
13 compounds, *Atmos. Chem. Phys. Atmos. Chem. Phys.*, 10(9), 4377–4401, doi:10.5194/acp-10-
14 4377-2010, 2010.
- 15 Richter, D., Weibring, P., Walega, J. G., Fried, A., Spuler, S. M. and Taubman, M. S.: Compact
16 highly sensitive multi-species airborne mid-IR spectrometer, *Appl. Phys. B*, 119(1), 119–131,
17 doi:10.1007/s00340-015-6038-8, 2015.
- 18 Robinson, A. L., Donahue, N. M., Shrivastava, M. K., Weitkamp, E. A., Sage, A. M., Grieshop,
19 A. P., Lane, T. E., Pierce, J. R. and Pandis, S. N.: Rethinking Organic Aerosols: Semivolatile
20 Emissions and Photochemical Aging, *Science* (80-.), 315(5816), 1259–1262,
21 doi:10.1126/science.1133061, 2007.
- 22 Sachse, G. W., Hill, G. F., Wade, L. O. and Perry, M. G.: Fast-Response, High-Precision Carbon
23 Monoxide Sensor using a Tunable Diode Laser Absorption Technique, *J. Geophys. Res.*, 92(D2),
24 2071–2081, doi:doi:10.1029/JD092iD02p02071, 1987.
- 25 Sato, K., Nakashima, Y., Morino, Y., Imamura, T., Kurokawa, J. and Kajii, Y.: Total OH reactivity
26 measurements for the OH-initiated oxidation of aromatic hydrocarbons in the presence of NO_x,
27 *Atmos. Environ.*, 171, 272–278, doi:10.1016/j.atmosenv.2017.10.036, 2017.
- 28 Schroder, J. C., Campuzano-Jost, P., Day, D. A., Shah, V., Larson, K., Sommers, J. M., Sullivan,
29 A. P., Campos, T., Reeves, J. M., Hills, A., Hornbrook, R. S., Blake, N. J., Scheuer, E., Guo, H.,
30 Fibiger, D. L., McDuffie, E. E., Hayes, P. L., Weber, R. J., Dibb, J. E., Apel, E. C., Jaeglé, L.,
31 Brown, S. S., Thornton, J. A. and Jimenez, J. L.: Sources and Secondary Production of Organic
32 Aerosols in the Northeastern US during WINTER, *J. Geophys. Res. Atmos.*,
33 doi:10.1029/2018JD028475, 2018.
- 34 Schwantes, R. H., Schilling, K. A., McVay, R. C., Lignell, H., Coggon, M. M., Zhang, X.,
35 Wennberg, P. O. and Seinfeld, J. H.: Formation of Highly Oxygenated Low-Volatility Products
36 from Cresol Oxidation, *Atmos. Chem. Phys.*, 7(5), 3453–3474, doi:10.5194/acp-17-3453-2017,
37 2017.
- 38 Schwarz, J. P., Samset, B. H., Perring, A. E., Spackman, J. R., Gao, R. S., Stier, P., Schulz, M.,
39 Moore, F. L., Ray, E. A. and Fahey, D. W.: Global-scale seasonally resolved black carbon vertical
40 profiles over the Pacific, *Geophys. Res. Lett.*, 40(20), 5542–5547, doi:10.1002/2013GL057775,
41 2013.
- 42 Seo, J., Kim, J. Y., Youn, D., Lee, J. Y., Kim, H., Lim, Y. Bin, Kim, Y. and Jin, H. C.: On the



- 1 multi-day haze in the Asian continental outflow: An important role of synoptic condition combined
2 with regional and local sources, *Atmos. Chem. Phys.*, 17(15), 9311–9332, doi:10.5194/acp-17-
3 9311-2017, 2017.
- 4 Shrivastava, M., Cappa, C. D., Fan, J., Goldstein, A. H., Guenther, A. B., Jimenez, J. L., Kuang,
5 C., Laskin, A., Martin, S. T., Ng, N. L., Petaja, T., Pierce, J. R., Rasch, P. J., Roldin, P., Seinfeld,
6 J. H., Shilling, J., Smith, J. N., Thornton, J. A., Volkamer, R., Wang, J., Worsnop, D. R., Zaveri,
7 R. A., Zelenyuk, A. and Zhang, Q.: Recent advances in understanding secondary organic aerosol:
8 Implications for global climate forcing, *Rev. Geophys.*, 55(2), 509–559,
9 doi:10.1002/2016RG000540, 2017.
- 10 Shrivastava, M. K., Lane, T. E., Donahue, N. M., Pandis, S. N. and Robinson, A. L.: Effects of
11 gas particle partitioning and aging of primary emissions on urban and regional organic aerosol
12 concentrations, *J. Geophys. Res.*, 113(D18), D18301, doi:10.1029/2007JD009735, 2008.
- 13 Silva, S. J., Arellano, A. F. and Worden, H. M.: Toward anthropogenic combustion emission
14 constraints from space-based analysis of urban CO₂/CO sensitivity, *Geophys. Res. Lett.*, 40(18),
15 4971–4976, doi:10.1002/grl.50954, 2013.
- 16 Slusher, D. L., Huey, L. G., Tanner, D. J., Flocke, F. M. and Roberts, J. M.: A thermal dissociation–
17 chemical ionization mass spectrometry (TD-CIMS) technique for the simultaneous measurement
18 of peroxyacyl nitrates and dinitrogen pentoxide, *J. Geophys. Res.*, 109(D19), D19315,
19 doi:10.1029/2004JD004670, 2004.
- 20 Stith, J. L., Ramanathan, V., Cooper, W. A., Roberts, G. C., DeMott, P. J., Carmichael, G., Hatch,
21 C. D., Adhikary, B., Twohy, C. H., Rogers, D. C., Baumgardner, D., Prenni, A. J., Campos, T.,
22 Gao, R., Anderson, J. and Feng, Y.: An overview of aircraft observations from the Pacific Dust
23 Experiment campaign, *J. Geophys. Res.*, 114(D5), D05207, doi:10.1029/2008JD010924, 2009.
- 24 Sueper, D.: ToF-AMS Data Analysis Software Webpage, [online] Available from:
25 http://cires1.colorado.edu/jimenez-group/wiki/index.php/ToF-AMS_Analysis_Software
26 (Accessed 4 January 2017), 2018.
- 27 Talbot, R. W., Dibb, J. E., Lefer, B. L., Scheuer, E. M., Bradshaw, J. D., Sandholm, S. T., Smyth,
28 S., Blake, D. R., Blake, N. J., Sachse, G. W., Collins, J. E. and Gregory, G. L.: Large-scale
29 distributions of tropospheric nitric, formic, and acetic acids over the western Pacific basin during
30 wintertime, *J. Geophys. Res.*, 102(D23), 28303–28313, 1997.
- 31 Tang, W., Arellano, A. F., DiGangi, J. P., Choi, Y., Diskin, G. S., Agustí-Panareda, A., Parrington,
32 M., Massart, S., Gaubert, B., Lee, Y., Kim, D., Jung, J., Hong, J., Hong, J.-W., Kanaya, Y., Lee,
33 M., Stauffer, R. M., Thompson, A. M., Flynn, J. H. and Woo, J.-H.: Evaluating High-Resolution
34 Forecasts of Atmospheric CO and CO₂ from a Global Prediction System during KORUS-AQ Field
35 Campaign, *Atmos. Chem. Phys. Discuss.*, 1–41, doi:10.5194/acp-2018-71, 2018.
- 36 Tkacik, D. S., Lambe, A. T., Jathar, S., Li, X., Presto, A. A., Zhao, Y., Blake, D., Meinardi, S.,
37 Jayne, J. T., Croteau, P. L. and Robinson, A. L.: Secondary Organic Aerosol Formation from in-
38 Use Motor Vehicle Emissions Using a Potential Aerosol Mass Reactor., *Environ. Sci. Technol.*,
39 48(19), 11235–42, doi:10.1021/es502239v, 2014.
- 40 Tohjima, Y., Kubo, M., Minejima, C., Mukai, H., Tanimoto, H., Ganshin, A., Maksyutov, S.,
41 Katsumata, K., Machida, T. and Kita, K.: Temporal changes in the emissions of CH₄ and CO from
42 China estimated from CH₄ / CO₂ and CO / CO₂ correlations observed at Hateruma Island, *Atmos.*



- 1 Chem. Phys., 14(3), 1663–1677, doi:10.5194/acp-14-1663-2014, 2014.
- 2 Tritscher, T., Dommen, J., DeCarlo, P. F., Gysel, M., Barmet, P. B., Praplan, A. P., Weingartner,
3 E., Prévôt, A. S. H., Riipinen, I., Donahue, N. M. and Baltensperger, U.: Volatility and
4 hygroscopicity of aging secondary organic aerosol in a smog chamber, Atmos. Chem. Phys.,
5 11(22), 11477–11496, doi:10.5194/acp-11-11477-2011, 2011.
- 6 Tsimpidi, A. P., Karydis, V. A., Zavala, M., Lei, W., Molina, L., Ulbrich, I. M., Jimenez, J. L. and
7 Pandis, S. N.: Evaluation of the volatility basis-set approach for the simulation of organic aerosol
8 formation in the Mexico City metropolitan area, Atmos. Chem. Phys., 10(2), 525–546,
9 doi:10.5194/acp-10-525-2010, 2010.
- 10 Tsimpidi, A. P., Karydis, V. A., Pandis, S. N. and Lelieveld, J.: Global-scale combustion sources
11 of organic aerosols: sensitivity to formation and removal mechanisms, Atmos. Chem. Phys.,
12 17(12), 7345–7364, doi:10.5194/acp-17-7345-2017, 2017.
- 13 Ulbrich, I. M., Canagaratna, M. R., Zhang, Q., Worsnop, D. R. and Jimenez, J. L.: Interpretation
14 of organic components from Positive Matrix Factorization of aerosol mass spectrometric data,
15 Atmos. Chem. Phys., 9(9), 2891–2918, doi:10.5194/acp-9-2891-2009, 2009.
- 16 UNDESA, P. D.: World Urbanization Prospects: The 2014 Revision., 2015.
- 17 Vay, S. A., Tyler, S. C., Choi, Y., Blake, D. R., Blake, N. J., Sachse, G. W., Diskin, G. S. and
18 Singh, H. B.: Sources and transport of $\Delta^{14}\text{C}$ in CO_2 within the Mexico City Basin and vicinity,
19 Atmos. Chem. Phys., 9, 4973–4985, doi:10.5194/acp-9-4973-2009, 2009.
- 20 Virkkula, A.: Correction of the Calibration of the 3-wavelength Particle Soot Absorption
21 Photometer (3λ PSAP), Aerosol Sci. Technol., 44, 706–712, doi:10.1080/02786826.2010.482110,
22 2010.
- 23 Volkamer, R., Jimenez, J. L., San Martini, F., Dzepina, K., Zhang, Q., Salcedo, D., Molina, L. T.,
24 Worsnop, D. R. and Molina, M. J.: Secondary organic aerosol formation from anthropogenic air
25 pollution: Rapid and higher than expected, Geophys. Res. Lett., 33(17), L17811,
26 doi:10.1029/2006GL026899, 2006.
- 27 Wang, Y., Munger, J. W., Xu, S., McElroy, M. B., Hao, J., Nielsen, C. P. and Ma, H.: CO_2 and its
28 correlation with CO at a rural site near Beijing: implications for combustion efficiency in China,
29 Atmos. Chem. Phys., 10(18), 8881–8897, doi:10.5194/acp-10-8881-2010, 2010.
- 30 Weibring, P., Richter, D., Walega, J. G., Rippe, L. and Fried, A.: Difference frequency generation
31 spectrometer for simultaneous multispecies detection, Opt. Express, 18(26), 27670,
32 doi:10.1364/OE.18.027670, 2010.
- 33 Weinheimer, A. J., Walega, J. G., Ridley, B. A., Gary, B. L., Blake, D. R., Blake, N. J., Rowland,
34 F. S., Sachse, G. W., Anderson, B. E. and Collins, J. E.: Meridional distributions of NO_x , NO_y ,
35 and other species in the lower stratosphere and upper troposphere during AASE II, Geophys. Res.
36 Lett., 21(23), 2583–2586, doi:10.1029/94GL01897, 1994.
- 37 WHO: Ambient air pollution: A global assessment of exposure and burden of disease, World
38 Health Organization., 2016.
- 39 Wisthaler, A., Hansel, A., Dickerson, R. R. and Crutzen, P. J.: Organic trace gas measurements by
40 PTR-MS during INDOEX 1999, J. Geophys. Res., 107(D19), 8024, doi:10.1029/2001JD000576,
41 2002.



- 1 Wood, E. C., Canagaratna, M. R., Herndon, S. C., Onasch, T. B., Kolb, C. E., Worsnop, D. R.,
2 Kroll, J. H., Knighton, W. B., Seila, R., Zavala, M., Molina, L. T., DeCarlo, P. F., Jimenez, J. L.,
3 Weinheimer, A. J., Knapp, D. J., Jobson, B. T., Stutz, J., Kuster, W. C. and Williams, E. J.:
4 Investigation of the correlation between odd oxygen and secondary organic aerosol in Mexico City
5 and Houston, *Atmos. Chem. Phys.*, 10(18), 8947–8968, doi:DOI 10.5194/acp-10-8947-2010,
6 2010.
- 7 Woody, M. C., Baker, K. R., Hayes, P. L., Jimenez, J. L., Koo, B. and Pye, H. O. T.: Understanding
8 sources of organic aerosol during CalNex-2010 using the CMAQ-VBS, *Atmos. Chem. Phys.*,
9 16(6), 4081–4100, doi:10.5194/acp-16-4081-2016, 2016.
- 10 Wooldridge, P. J., Perring, A. E., Bertram, T. H., Flocke, F. M., Roberts, J. M., Singh, H. B., Huey,
11 L. G., Thornton, J. A., Wolfe, G. M., Murphy, J. G., Fry, J. L., Rollins, A. W., LaFranchi, B. W.
12 and Cohen, R. C.: Total Peroxy Nitrates (Σ PNs) in the atmosphere: the Thermal Dissociation-Laser
13 Induced Fluorescence (TD-LIF) technique and comparisons to speciated PAN measurements,
14 *Atmos. Meas. Tech.*, 3(3), 593–607, doi:DOI 10.5194/amt-3-593-2010, 2010.
- 15 Wu, W., Zhao, B., Wang, S. and Hao, J.: Ozone and secondary organic aerosol formation potential
16 from anthropogenic volatile organic compounds emissions in China, *J. Environ. Sci.*, 53,
17 doi:10.1016/j.jes.2016.03.025, 2016.
- 18 Xu, W., Croteau, P., Williams, L., Canagaratna, M., Onasch, T., Cross, E., Zhang, X., Robinson,
19 W., Worsnop, D. and Jayne, J.: Laboratory characterization of an aerosol chemical speciation
20 monitor with $\text{PM}_{2.5}$ measurement capability, *Aerosol Sci. Technol.*, 51(1), 69–83,
21 doi:10.1080/02786826.2016.1241859, 2017.
- 22 Zhang, Q., Jimenez, J. L., Canagaratna, M. R., Allan, J. D., Coe, H., Ulbrich, I., Alfarra, M. R.,
23 Takami, A., Middlebrook, A. M., Sun, Y. L., Dzepina, K., Dunlea, E., Docherty, K., DeCarlo, P.
24 F., Salcedo, D., Onasch, T., Jayne, J. T., Miyoshi, T., Shimo, A., Hatakeyama, S., Takegawa,
25 N., Kondo, Y., Schneider, J., Drewnick, F., Borrmann, S., Weimer, S., Demerjian, K., Williams,
26 P., Bower, K., Bahreini, R., Cottrell, L., Griffin, R. J., Rautiainen, J., Sun, J. Y., Zhang, Y. M. and
27 Worsnop, D. R.: Ubiquity and dominance of oxygenated species in organic aerosols in
28 anthropogenically-influenced Northern Hemisphere midlatitudes, *Geophys. Res. Lett.*, 34(13),
29 L13801, doi:10.1029/2007gl029979, 2007.
- 30 Zhang, Q. J., Beekmann, M., Freney, E., Sellegri, K., Pichon, J. M., Schwarzenboeck, A., Colomb,
31 A., Bourriane, T., Michoud, V. and Borbon, A.: Formation of secondary organic aerosol in the
32 Paris pollution plume and its impact on surrounding regions, *Atmos. Chem. Phys.*, 15(24), 13973–
33 13992, doi:10.5194/acp-15-13973-2015, 2015.
- 34 Zhang, X., Smith, K. A., Worsnop, D. R., Jimenez, J., Jayne, J. T. and Kolb, C. E.: A Numerical
35 Characterization of Particle Beam Collimation by an Aerodynamic Lens-Nozzle System: Part I.
36 An Individual Lens or Nozzle, *Aerosol Sci. Technol.*, 36, 617–631,
37 doi:10.1080/02786820252883856, 2002.
- 38 Zhang, X., Smith, K. A., Worsnop, D. R., Jimenez, J. L., Jayne, J. T., Kolb, C. E., Morris, J. and
39 Davidovits, P.: Numerical Characterization of Particle Beam Collimation: Part II Integrated
40 Aerodynamic-Lens-Nozzle System, *Aerosol Sci. Technol.*, 38, 619–638,
41 doi:10.1080/02786820490479833, 2004.
- 42 Zhang, X., Cappa, C. D., Jathar, S. H., McVay, R. C., Ensberg, J. J., Kleeman, M. J., Seinfeld, J.
43 H. and Christopher D. Cappa: Influence of vapor wall loss in laboratory chambers on yields of



- 1 secondary organic aerosol., Proc. Natl. Acad. Sci. U. S. A., 111(16), 1–6,
2 doi:10.1073/pnas.1404727111, 2014.
- 3 Zhao, Y., Hennigan, C. J., May, A. A., Tkacik, D. S., de Gouw, J. A., Gilman, J. B., Kuster, W.
4 C., Borbon, A. and Robinson, A. L.: Intermediate-volatility organic compounds: a large source of
5 secondary organic aerosol, Environ. Sci. Technol., 48(23), 13743–50, doi:10.1021/es5035188,
6 2014.
- 7 Zhao, Y., Nguyen, N. T., Presto, A. A., Hennigan, C. J., May, A. A. and Robinson, A. L.:
8 Intermediate Volatility Organic Compound Emissions from On-Road Gasoline Vehicles and Small
9 Off-Road Gasoline Engines, Environ. Sci. Technol., 50(8), 4554–4563,
10 doi:10.1021/acs.est.5b06247, 2016.
- 11 Ziemba, L. D., Lee Thornhill, K., Ferrare, R., Barrick, J., Beyersdorf, A. J., Chen, G., Crumeyrolle,
12 S. N., Hair, J., Hostetler, C., Hudgins, C., Obland, M., Rogers, R., Scarino, A. J., Winstead, E. L.
13 and Anderson, B. E.: Airborne observations of aerosol extinction by in situ and remote-sensing
14 techniques: Evaluation of particle hygroscopicity, Geophys. Res. Lett., 40(2), 417–422,
15 doi:10.1029/2012GL054428, 2013.
- 16